NASA CR-66622

FINAL REPORT FOR NAS 1-7439 DEVELOPMENT OF AN ACOUSTIC FLOW TRANSITION DETECTOR FOR REENTRY SPACECRAFT

Distribution of this report is provided in the interest of information exchange. Responsibility for the contents resides in the author or organization that prepared it.

Prepared by

AVCO MISSILES, SPACE AND ELECTRONICS GROUP
MISSILE SYSTEMS DIVISION
201 Lowell Street
Wilmington, Massachusetts 01887

AVMSD-0294-68-CR
NAS 1-7439

GPO PRICE $ _____
CFSTI PRICE(S) $ _____
Hard copy (HC) 3.00
Microfiche (MF) .65
ff 653 July 65

MARCH 1968

Prepared for

NATIONAL AERONAUTICS AND SPACE ADMINISTRATION

Langley Research Center
Langley Station
Hampton, Virginia 23365

FACILITY FORM 602
N 68-27064 (ACCESSION NUMBER)
(THRU)
140 (PAGES)
(CODE)
CR-66622 (NASA CR OR TMX OR AD NUMBER)
14 (CATEGORY)

NASA CR-66622

FINAL REPORT FOR NAS 1-7439 DEVELOPMENT OF AN ACOUSTIC FLOW TRANSITION DETECTOR FOR REENTRY SPACECRAFT

Distribution of this report is provided in the interest of information exchange.
Responsibility for the contents resides in the author or organization
that prepared it.

Prepared by

AVCO MISSILES, SPACE AND ELECTRONICS GROUP
MISSILE SYSTEMS DIVISION
201 Lowell Street
Wilmington, Massachusetts 01887

AVMSD-0294-68-CR
NAS 1-7439

MARCH 1968

Approvals

R. H. Myers, Jr.

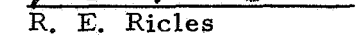

R. E. Ricles

Prepared for

NATIONAL AERONAUTICS AND SPACE ADMINISTRATION

Langley Research Center
Langley Station
Hampton, Virginia 23365

PRECEDING PAGE BLANK NOT FILMED.

ABSTRACT

The development of an acoustic flow transition detector for reentry spacecraft has been successfully completed. The sensor system has been developed to measure the occurrence and progression of turbulent flow over the surface of a vehicle during hypersonic reentry. Physical force is provided by the vorticity of the turbulent flow and transduction is accomplished by a miniature microphone. Electronics have been developed to condition the microphone output and provide a system compatible with typical flight test requirements. The concept and hardware have been evaluated in wind tunnel and arc facilities to ensure that the system will function successfully in the reentry environment.

A typical NASA reentry configuration has been selected to provide a reference for analytical work and to provide criteria for the sensor design effort. Estimates of the boundary layer fluctuating pressure spectra and associated shell response of the vehicle have been generated to provide criteria for microphone evaluation. Electrical characteristics of the system have been designed and tested to be compatible with the power source and data transmission subsystem of the reference vehicle. The design and hardware have been realized within a reliability and quality assurance framework that will facilitate production of flight qualified units.

CONTENTS

ILLUSTRATIONS

ILLUSTRATIONS (continued)

ILLUSTRATIONS (continued)

ILLUSTRATIONS (continued)

TABLES

SUMMARY

The occurrence and progression of turbulent flow over a reentering body is a prime measurement parameter required to allow understanding and eventual control of boundary layer transition. The importance of basic knowledge concerning transition must be emphasized since many factors such as heating, observables and dynamic stability are directly dependent on boundary layer flow characteristics. Consequently, a measurement concept based on the detection of vorticity is required to provide a very localized and quantitative assessment of the boundary layer. The development of a system specifically designed to detect the fluctuating pressure of the boundary layer has been completed under NASA Langley Contract NAS 1-7439.

The system consists basically of a miniature microphone and associated electronics to condition the signal so as to be compatible with the recording and/or data transmission system. The sensing element utilizes a barium-titanate crystal and field-effect transistor to provide high sensitivity and low output impedance. Modular layout and cordwood construction has been used for the electronics to provide a flexible design within a relatively small package. Active filtering has been incorporated to limit the output as required for compatibility with the data retrieval system.

The concept and hardware have been carefully evaluated to ensure the adequacy of the system to accomplish the intended measurement. Estimates of the fluctuating pressure levels associated with initial turbulence have been generated and the corresponding structural response of the vehicle has been calculated to ensure that the vibrational environment does not contaminate the measurement. The acoustic characteristics of the port which allows communication between the boundary layer and sensing element have been determined in terms of frequency response and possible generation of self noise. In addition, the hardware has been subjected to electrical and environmental tests to verify the design and establish the adequacy of the techniques used in fabricating the system.

The primary results of the contract include the analytical and experimental effort as documented throughout the program and compiled in this final report. The deliverable end item hardware consists of an engineering prototype and a packaged unit as illustrated on the facing page. The reliability and quality assurance aspects of the development program[1] have been structured to ensure delivery of satisfactory hardware under this contract and provide a basis for implementation of subsequent hardware procurement contracts.

Note: Superscripts indicate references were used in the text.

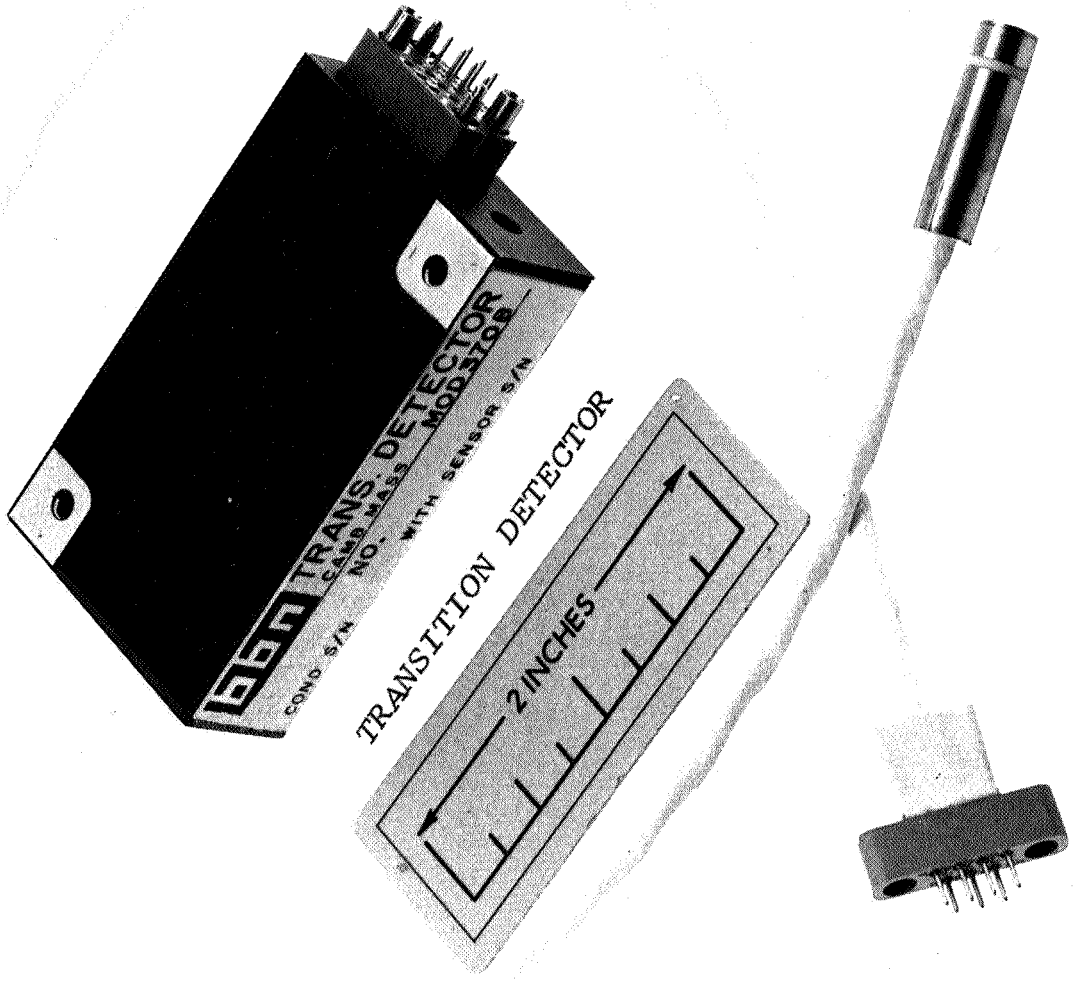
TRANS. DETECTOR
CAMS MASS MOD 370B
COND S/N NO. WITH SENSOR S/N
TRANSITION DETECTOR
2 INCHES

I. INTRODUCTION

The development of the acoustic transition detector as described herein has been accomplished under NASA Langley Contract NAS 1-7439 by the Avco Missiles, Space and Electronics Group together with Bolt, Beranek and Newman (BBN). The effort was facilitated by the basic acoustic technology developed under the RVTO Phase 1A Contract [AF04(694)-913] and was extended under the Endo-Decoy Contract [AF04(694)-932] to include the packaging of the system into a flight worthy configuration. The interrelation of these contracts and their complementary requirements has fortuitously allowed the Avco/BBN team that has worked across the several contracts to provide a significantly greater contribution to individual areas than would have otherwise been possible. Consequently this report contains and/or references technology derived from all of the contracts without detailing the sponsor throughout the text. Therefore, it seems appropriate to identify the specific contracts in chronological order and summarize the effort required and accomplished under each.

The Reentry Vehicle Technology and Observables (RVTO) Phase 1A Contract, AF04(694)-913, required via CCN No. 3 the development of a ported microphone to monitor boundary layer pressure fluctuations deep into reentry. The severe environment associated with the very high performance RVTO vehicles and the lack of knowledge of environmental attenuation (primarily gas temperature) caused by the blocked port resulted in a very sophisticated acoustic porting arrangement. This factor coupled with the relatively large size of the microphone complicated the acoustic response of the system and as a result considerable theoretical and experimental effort was expended in understanding the characteristics of the system. A primary contribution of this effort was the application of piston theory to describe port dynamics in the hypersonic flow environment and establish the proper relationships between theory, anechoic chamber experiments and supersonic flow tests. In addition, tests were accomplished to assess the effect of ablation (shortening and aggravation of the port) on acoustic response and the possibility of port blockage by ablation products.

The transition detector development sponsored under NAS 1-7439 was required to provide a system considerably smaller than the RVTO acoustic environmental sensor and study the problems specifically associated with measurement of initial transition. Consequently the primary effort was directed toward developing a miniature microphone with low vibration sensitivity and compatible electronics that could be packaged into a small flight worthy unit. The validity of a port concept for a transition detection system was evaluated in terms of frequency response and possible initiation of turbulence due to the port itself. Thermal testing of the candidate nylon-phenolic heat shield and measurements of gas temperature within the port were also accomplished. Development testing of an engineering prototype was completed, including electrical performance and limited environmental tests.

The Endo-Decoy Program, AF04(694)-932, extended the development effort into a flight hardware procurement including complete packaging of the system into a flight worthy configuration. The miniaturization and quality assurance aspects of the hardware fabrication also benefitted greatly from the Endo-Decoy requirements. In addition, complete environmental testing will be accomplished to qualify the system for flight.

This report has been structured to provide a maximum of information to the various sponsors without presenting repetitious or excessive data. Consequently, data has been extracted from various sources for inclusion into this report and the source has been referenced. Reports generated under the contracts described above and referenced herein will be provided to the project sponsors under separate cover. In addition, a bibliography of pertinent documents used in a general sense throughout the development effort is included at the end of this report.

II. DEVELOPMENT OBJECTIVES

A. Measurement Requirements

The occurrence and progression of turbulent flow over a reentering body is of fundamental concern for several reasons; 1) the effect of boundary layer transition on heating and the attendant design of heat shields, 2) the understanding of transition and its effect on observables as related to the defense discrimination problem, 3) the requirement for ever increasing reentry guidance accuracy and the effect that transition might have in producing asymmetrical ablation and boundary layer mass addition. The obvious importance of understanding the basic phenomena has resulted in many laboratory and flight experiments either partially or wholly designed to study boundary layer transition. Unfortunately, the measurement systems devised to detect transition have, particularly in the flight case, been based on effects of the change from laminar to turbulent flow such as surface temperature, structural vibration, etc., rather than the fundamental change in vorticity of the boundary layer. This has resulted in flight data that cannot be precisely correlated (~ 15 Kft data scatter) probably largely as a result of deficiencies in the sensors used to gather the raw data. A pertinent example of the problem is illustrated by the use of "surface" thermocouples to detect transition on ablating vehicles. The thermocouples are typically recessed a few mils below the heat shield surface with the result that a significant response lag is created. It should also be noted that this type of measurement is not adequate to detect the cyclic transition that may be caused by angle of attack effects. Consequently, a significant improvement in terms of a flight-worthy sensor is required to allow a precise measurement of the transition to turbulence, including the possibility of cyclic transition, during reentry.

B. Sensor Concept

The measurement requirements indicate the need for a device with rapid response that is in direct communication with the boundary layer and senses the increased vorticity associated with turbulent flow. A technique that satisfies these criteria but is relatively untried for reentry flight is the ported microphone that senses turbulent pressure fluctuations in the boundary layer. This approach is somewhat related to the measurement of structural vibration as a means of transition detection but the problems of spatial averaging and structural transmission associated with vibration measurements are eliminated. The ported microphone will yield a very localized indication of turbulence as long as the sensing element is not overly sensitive to vibration. The response of a typical system is sufficiently rapid to be thought of in terms of milliseconds. In addition, the acoustic spectrum and associated sensor output are sufficiently understood so that the data can be handled by wide band or sampled data acquisition techniques depending on technical requirements.

The role of the acoustic transition detector can easily be expanded to include acquisition of valuable environmental data by adding a structural vibration sensor to the vehicle instrumentation. The spectra of the excitation and response data is then analyzed to determine the structural response of the vehicle to turbulent pressure fluctuations and establish environmental criteria for on-board systems and components.

III. DESIGN CRITERIA

A. Parameter to be Measured

The phenomena of boundary layer transition and the various problems associated with measuring its occurrence as well as theoretical developments to date are provided in references 2 through 5, and will not be repeated here. It is sufficient to say that the estimates currently available, although crude, are considered adequate to provide reasonable confidence that the design of the acoustic transition detector and its associated sensitivity adjustment within the 25-30 db dynamic range provided by typical data transmission systems will be valid for initial flights. The techniques used to estimate the boundary layer parameters and corresponding fluctuating pressure levels will be illustrated using a typical NASA reentry vehicle and reference reentry mission as a basis for the calculations. The configuration selected was a 26 degree (half-angle) cone with a 0.1 inch nose radius. The reference vehicle was approximately 5 feet long with a 30 inch base diameter and utilized low density nylon phenolic as the thermal protection material.

The boundary layer analysis was performed to determine the altitude of transition and attendant parameters at both the 1 and 2.85 foot (referenced to vehicle tip) stations of the typical NASA reentry vehicle. The basic trajectory and vehicle performance characteristics were provided by NASA/LRC as summarized in reference 6. The relevant parameters associated with the free-stream and edge-of-boundary-layer flow obtained from NASA calculated data are shown in figures III-1 through III-8.

With local properties thus established, the Reynolds number based on displacement thickness ($Re_{\delta *}$)* was calculated from

$$Re_{\delta *} = (Re_x)\left(\frac{\theta}{x}\right)\left(\frac{\delta^*}{\theta}\right)$$

1. The local Reynolds number based on wetted length (Re_x) was obtained directly from the local flow properties.

2. The momentum thickness term (θ/x) was developed from the Von Karman momentum integral equation for the case of steady, compressible, axisymmetric flow including mass injection:

$$\frac{d\theta}{dx} + (H+2)\frac{\theta}{v} + \frac{\theta}{\rho}\frac{d\rho}{dx} + \frac{\theta}{r}\frac{dr}{dx} - \frac{(\rho v)_w}{\rho v} = \frac{C_f}{2}$$

*Nomenclature are defined on p. III–30.

The momentum thickness factor (θ/x) is calculated using the above and assuming zero pressure gradients along the surface for a sharp cone in conjunction with the Blasius incompressible laminar flat plate solution for the skin friction coefficient.

$$\frac{\theta}{x} = \frac{0.664}{3} (Re_x)^{-1/2} \left(\frac{\rho^* \mu^*}{\rho_e \mu_e}\right)^{-1/2} \quad (F)$$

(Corrected for axisymmetric flow and compressibility using the Mangler transformation and Eckert's reference enthalpy analysis respectively)

The effect of mass injection into the boundary layer upon the momentum thickness, expressed by the parameter (F), is a function of both the reduction in skin friction due to blowing C_f/C_{f_o} and the injection parameter

$$(2\dot{m}/\rho_e \mu_e C_{f_o}).$$

Experimental data (references 7 and 8) have been used as a basis for the empirical expression of C_f/C_{f_o} in terms of $2\dot{m}/\rho_e \mu_e C_{f_o}$, resulting in $C_f/C_{f_o} = \dfrac{1}{1 + \dfrac{2m}{\rho_e \mu_e C_{f_o}}}$

Therefore, the mass transfer effect $\left(F = C_f/C_{f_o} + \dfrac{2\dot{m}}{\rho_e \mu_e C_{f_o}}\right)$ becomes a function only of the injection parameters

$$2\dot{m}/\rho_e \mu_e C_{f_o}$$

3. The displacement thickness (δ^*) is incorporated into the solution by utilizing the shape factor ($H = \delta^*/\theta$) from the work by Andrews[9] wherein a curve-fit of similar solutions for laminar equilibrium air boundary layers resulted in the relationship:

$$\frac{\delta^*}{\theta} = (3.34 - 2.73\ gw) + (1.39\ gw - 1.43)\ M_e + 0.212\ M_e^2 + 0.0113\ gw\ M_e^2$$

Utilizing the method developed above and recent correlations of boundary layer transition data the boundary layer parameters at both the 1 and 2.85 foot station have been calculated and are presented in Table III-1. The referenced correlations by Zavasky and Malone[10] demonstrate the advantage of using a Reynolds number based on boundary layer displacement thickness that has been corrected to account for mass addition resulting from ablation. The application of the improved correlation technique to a

large number of experimental measurements provides the empirical transition criterion shown in figure III-9. The transition time/altitude for a given vehicle reentry is estimated by calculating the variation of laminar Reynolds number based on displacement thickness and edge of boundary layer Mach number over that portion of the trajectory necessary to define the intersection with the transition correlation curve.

The above discussion of boundary layer transition is predicated on a zero angle of attack. This zero condition is frequently not achieved during flight. Consequently, an analysis of the effect of vehicle angle of attack on transition altitude for a typical case was accomplished. A reentry angle of attack of 25 degrees at 300,000 ft was selected as the initial condition. Nominal convergence to 6 degrees at 150,000 ft was assumed. The general analysis using the preceding conditions as steady state values indicates that transition will occur 10,000 to 15,000 ft higher on the leeward side of the vehicle as compared with the zero angle of attack case.

Since the actual case is not steady state but oscillatory, the leeward flow will probably tend to return toward the laminar condition as the vehicle moves toward zero angle of attack. Calculation of the non-steady case in terms of both vehicle and flow field oscillations is extremely complex. Consequently, we must generalize by stating that the highest altitude of transition occurs on the leeward side of the vehicle and the lowest on the windward side. The steady state zero case provides altitudes midway between these two extremes. Therefore, an oscillatory calculation (if such a calculation were possible) might indicate transition at an altitude somewhat higher than the steady state zero case because of the oscillatory character of the flow field and its greater instability especially on the leeward side.

The primary criterion for design and flight use of the acoustic transition detector is the spectra of the boundary layer pressure fluctuations. Estimates of these spectra can be generated using the boundary layer edge parameters as calculated by the methods previously discussed. The boundary layer variables most significant for the acoustic estimation procedure are the turbulent displacement thickness, dynamic pressure and edge velocity. These parameters provide the input for a relatively straightforward procedure for determination of the FPL-spectrum for subsonic flow speeds has been developed by Bies [11] utilizing the above parameters at the point of interest. This empirical prediction scheme is based on a large number of actual flight and experimental wind tunnel data. The general shape of the 1/3 octave band fluctuating pressure spectrum versus the center frequency of each 1/3 octave band is provided in figure III-10. The spectrum

rises at a rate of 3 db/octave up to a peak level and drops at a rate of 9 db/octave thereafter. The location of the peak frequency is obtained from

$$f_{peak} = \frac{1}{6} \cdot U/\delta^*$$

The overall level can be calculated from

$$FPL_{OA} = 20 \log q + 84 \text{ db}$$

with q in lb/ft^2.

The actual peak of the spectrum is then established by fairing a smooth curve as illustrated (figure III-10) with a maximum value 6 db down from the point calculated by the above equations.

It was quite clear that these estimation procedures, valid for the subsonic case could not readily be applied to the case of hypersonic flow speeds associated with reentry. It was expected that the levels under hypersonic flow would be lower as compared to the subsonic case due to compressibility effects. The question of how much the levels would drop and whether the general shape of the spectrum would change could only be resolved by a test of a conical model in a well understood supersonic wind tunnel.

The urgent requirement to provide a high confidence estimate for use in adjusting the sensitivity of the Endo-Decoy, AF04(694)-932, transition detectors resulted in a Mach 3 test in the MIT wind tunnel[12]. A slender conical (8 degrees half angle) model of essentially the same scale as the flight vehicles (28 inches long and 6-inch base diameter) was installed in the tunnel and the fluctuating pressures measured by flush microphones on the cone and base. The test installation is shown in figure III-11. Figure III-12 is a Schlieren-optical visualization of the flow along the cone and the base of the model. Figure III-13 shows FPL-spectra for various tunnel stagnation pressures obtained from a microphone 17 inches downstream of the tip. The RMS-fluctuating-pressures are normalized with the dynamic head q. At a stagnation pressure of 25 psi, the boundary layer at the 17-inch location on the model was fully turbulent for the test section conditions.

The right hand ordinate of figure III-13 gives the fluctuating pressure levels for the "25 psi-spectrum" in db re $2.10^{-4}\mu$ bar. If we were to apply the subsonic estimates, utilizing the flow and boundary layer data for the test section in the MIT wind tunnel, curve A would be obtained. The following parameters and flow data in the test section and on the model surface were used:

$U = 2000$ ft/sec

$\delta^* = 0.06$ inch

$q = 610$ lb/ft^2

It is obvious that the extrapolated subsonic estimates are too high by about 15 db in the frequency range of interest.

Supersonic wind tunnel tests[13] of flow transition on a flat test plate in a Mach 3 flow revealed that during the transitional flow regime the fluctuating pressure levels increase quite rapidly and then decrease after turbulent flow is established. The experimental data show that the levels drop by approximately 10 db (see figure V-19). We would, therefore, estimate that the FPL-spectrum under transitional flow lies approximately 5 db under the "subsonic estimates." The estimated transitional spectrum for the transition-ablation vehicle is shown in figure III-14.

In conclusion, it is recommended that the transitional spectra for the flight environment be obtained as follows:

1) perform the "subsonic estimation procedure" using the relevant aerodynamic parameters δ^*, V and q for the flight conditions,

2) lower the levels by 15 db, in order to obtain the FPL-spectrum for a turbulent boundary layer on the surface of a cone; and,

3) increase the turbulent levels by 10 db to obtain the estimate for the transitional regime.

B. Contaminating Environments

Intuitive consideration of the reentry environment, particularly until and during the transition event, together with general knowledge of the transition detector characteristics indicates that vibration is the most critical environment. The vibration is caused by the turbulent boundary layer and its interaction with the structural shell of the vehicle. It is apparent that, if the vehicle is sufficiently responsive so that the vibration induced output of the transducer would mask the output resulting from fluctuating boundary layer pressure, then localized measurement would be impossible. Consequently, the response of the transition-ablation vehicle to the previously estimated fluctuating pressure spectra was estimated as described in the subsequent discussion.

The first step in estimating the shell vibration levels was to determine the mechanical properties of the low density nylon phenolic-aluminum laminate. Toward this end two experiments were conducted using the test setup illustrated in figure III-15. In the first, a beam sample of the laminate was excited with a point drive shaker and the resonance frequencies of the beam were measured. The n-th resonance frequency is related to the bending wavespeed by the equation:

$$f_n = \frac{C_b}{\lambda_n}$$

where f_n is the nth resonance frequency, C_b is the bending wavespeed, and λ_n is the wavelength of the nth mode. For the beam sample used in the experiment,

$$\lambda_n = \frac{4}{2n + 1} \quad L$$

where L is the length of the beam. Bending wavespeeds obtained by this procedure are shown in figure III-16. The bending wavespeed of the phenolic-aluminum laminate follows that of an aluminum beam 0.42 inches thick.

The damping of the phenolic-aluminum laminate was found experimentally by measuring the 3 db bandwidths of the beam sample resonances. The damping loss factor of the laminate is given by

$$\eta = \frac{\Delta f}{f_n}$$

where η is the damping loss factor (η is twice the ratio of damping to critical damping), f_n is the nth resonance frequency, and Δf is the 3 db bandwidth. The damping loss factor for the laminate is shown in figure III-17. It is significantly higher than that of a typical aluminum shell without a heat shield.

Estimates of the shell vibration level were obtained using the experimentally determined bending wavespeed and damping and an estimation technique developed under the RVTO Phase 1A contract (AF04(694)-913). This technique is outlined in reference 14. The prediction technique has been used to generate an upper and lower bound for the vibration levels and a best estimate for two locations on the shell. Predicted levels normalized by the exciting pressure field level are shown in figure III-18. This prediction was combined with the expected pressure levels during transition to give the response mean-square acceleration spectral density shown in figure III-19.

The predicted levels are low relative to the exciting pressure field and provide a margin of approximately 15 db for the acoustic output as compared with the vibration induced output (see figure IV-3). This can be improved by mounting the transducer so that its most critical axis, in terms of vibration sensitivity, is parallel to the vehicle surface. This improvement is realized as a result of the shell response being on the order of 10 db higher in the direction perpendicular to the skin as compared with the other orthogonal axes.

C. Contractual Requirements

The statement of work associated with Contract NAS 1-7439 indicated a number of general and specific criteria that were considered during the development of the measurement system. The primary requirement was that the sensor be capable of measuring the change in sound power level in the boundary layer as a result of developing turbulent flow over the reentering spacecraft. In addition, the system was to be designed so as to be relatively insensitive to other environmental effects such as ambient temperature, pressure and both sustained and vibrational accelerations. The primary consideration being that the environmental conditions expected during reentry of the spacecraft (contractual reference vehicle) must not interfere with the measurement of sound power indicative of the initiation of the transition from laminar to turbulent flow. The sensor design was predicated on the system being able to respond to the threshold level of sound power indicative of the initiation of the transition from laminar to turbulent for the typical NASA configuration that served as the analytical reference vehicle. The system was further designed to be capable of transducing sound power level linearly within 5 percent to 60 db or more above its established threshold level of sensitivity (this latter threshold is taken as the microphone noise floor - approximately 85 db SPL in the 4 KHz measurement bandwidth). Sensor elements were to be selected to provide a flat frequency response to within 20 percent from less than 10 Hz to at least 10 KHz.

The design of the port through which the acoustic energy is coupled from the boundary environment to the sensor element was to permit adequate acoustic coupling to the environment and also affort protection of the sensor element from the hot boundary layer gas. The port design could incorporate acoustic damping as required. The port design was to minimize the effects of undesirable acoustic perturbations arising within the port structure, such as self resonance of the port, upon the environmental data of interest.

The sensor element output signal was to be treated by an electronic signal conditioning process, which could also provide filtering of the signal to restrict information transfer to those frequency bands having significance to the environmental conditions under investigation. The information content of the sensor output signal was to be restricted to approximately a 4 Kilohertz passband, by appropriate filtering in the electronic circuitry. The electronic circuit must also provide whatever impedance matching, amplification, or other signal processing required to make the sensor output

signal compatible with a typical reentry spacecraft telemetry system incorporating telemetry or tape recorders.

Small size, low weight and low power consumption were design objectives. The design configuration was to be as small and lightweight as possible consistent with satisfactory operation of the sensor. Mounting hardware and interconnecting cabling were considered a part of the sensor design and subject to the same small size and lightweight design objectives. Direct current power of 28 volts ± 10 percent was to be considered available for sensor power in the typical reentry spacecraft power supply system. A design objective was to keep power consumption of the sensor system including its electronic circuitry to a minimum, consistent with adequate functional performance and reliability.

The sensor system, including its electronic circuitry, mounting hardware and interconnecting cabling was to be capable of performing adequately and obtaining valid data under the environmental conditions specified in Table V-4. The sensor system performance characteristics were to remain unchanged after exposure to the ambient environmental conditions of Table V-4.

TABLE III-I FLOW FIELD PROPERTIES AT TRANSITION

FREE STREAM PROPERTIES	1 FOOT STA.		2.85 FOOT STA.	
TRANSITION ALTITUDE, KFT	110		135	
MACH NUMBER, M_∞	18.2		24.5	
VELOCITY, V_∞, KFT/SEC	18.0		25.8	
DYNAMIC PRESSURE, q_∞, LBS/FT^2	3450		2000	
LOCAL FLOW PROPERTIES				
DYNAMIC PRESSURE, q_e, LBS/FT^2	19.84×10^3		14.14×10^3	
DENSITY, ρ_e, SLUGS/FT^3	15.5×10^{-5}		23.1×10^{-5}	
VELOCITY, V_e, KFT/SEC	16.0		23.1	
MACH NUMBER, M_e	4.90		5.52	
STATIC PRESSURE, ρ_e, ATM	.661		.383	
STATIC TEMP., T_e, °R	4140		3580	
BOUNDARY LAYER PROPERTIES	LAM.	TURB.	LAM.	TURB.
MOMENTUM THICKNESS, θ INCHES	.019	.064	.020	.117
DISPLACEMENT THICKNESS, δ^*, INCHES	.042	.365	.048	.702
SHAPE FACTOR, $H = \delta^*/\theta$	2.26	5.70	2.38	6.00
BLOWING CORRECTION, F	1.13	1.13	1.30	1.30

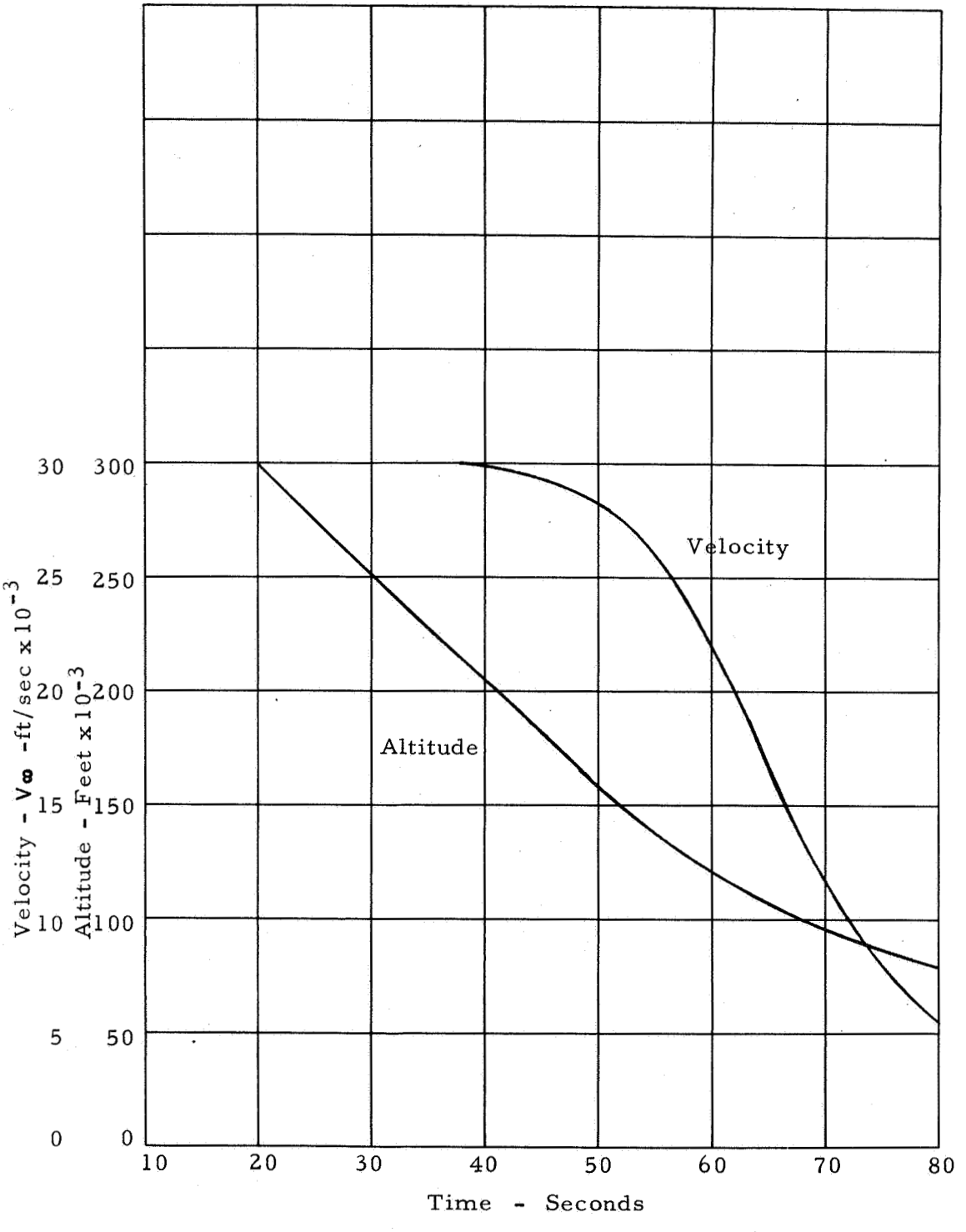

Figure III-1 TRAJECTORY PARAMETERS

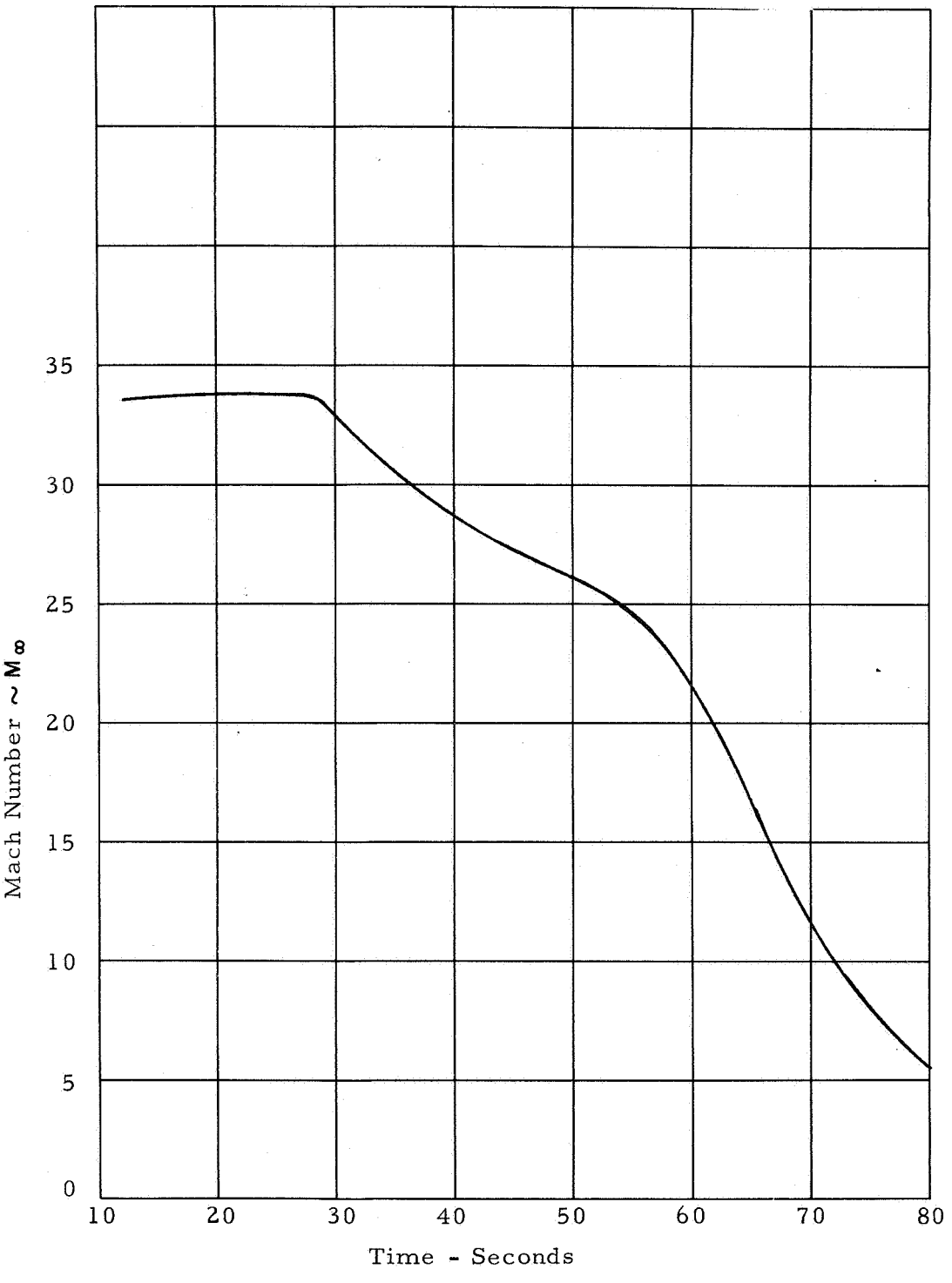

Figure III-2 FREE STREAM MACH NUMBER

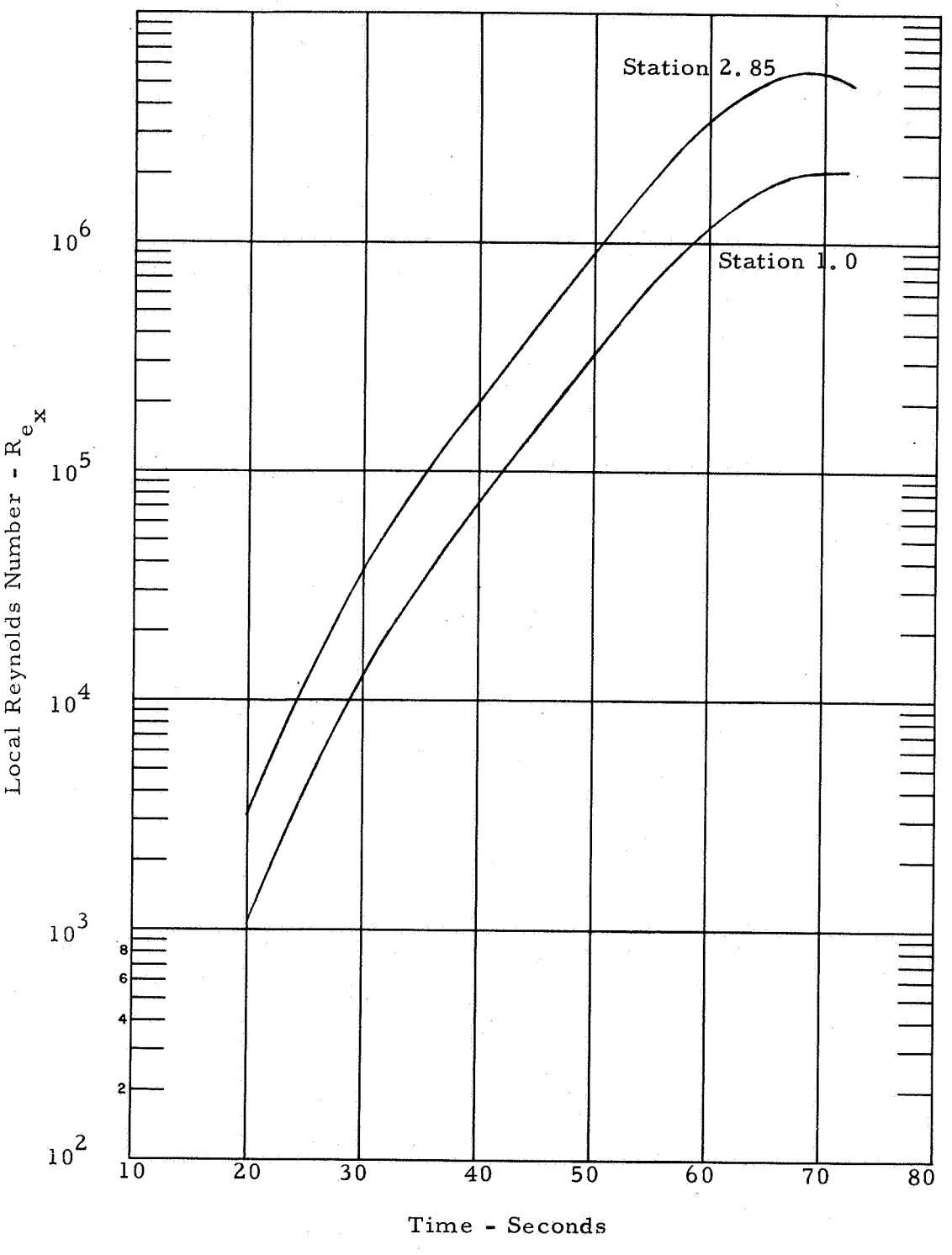

Figure III-3 EDGE REYNOLDS NUMBER

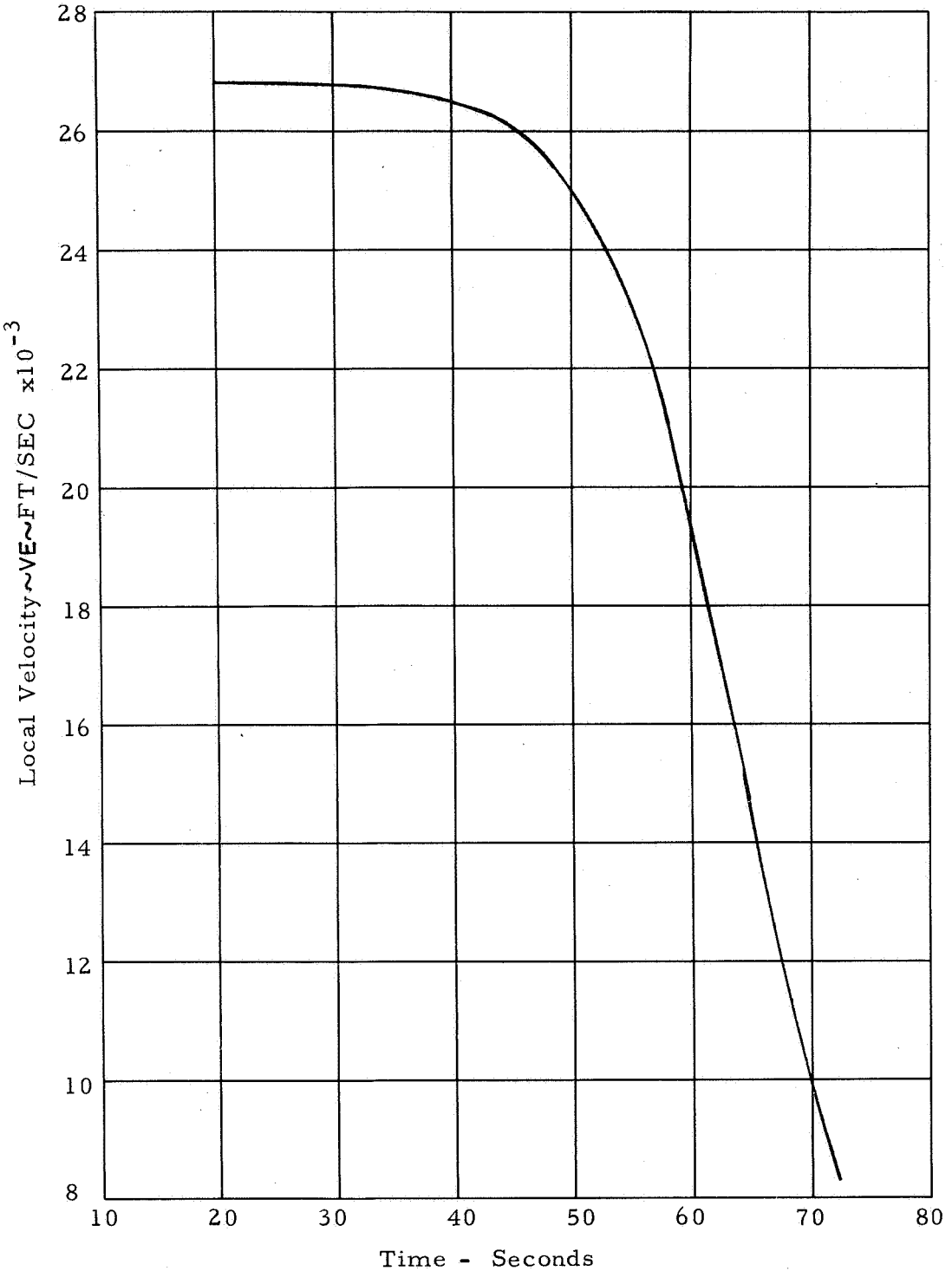

Figure III-4 EDGE VELOCITY

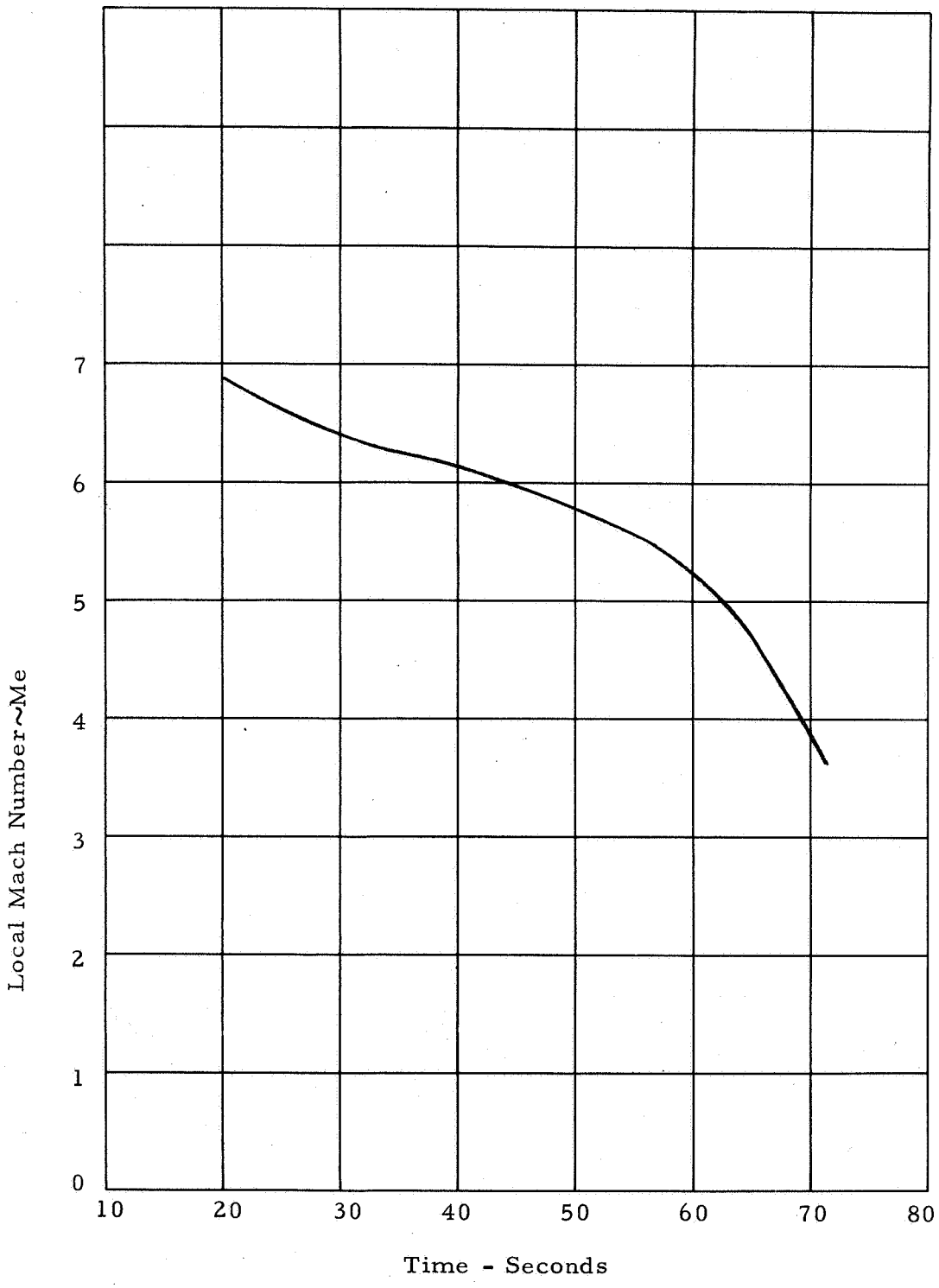

Figure III-5 EDGE MACH NUMBER

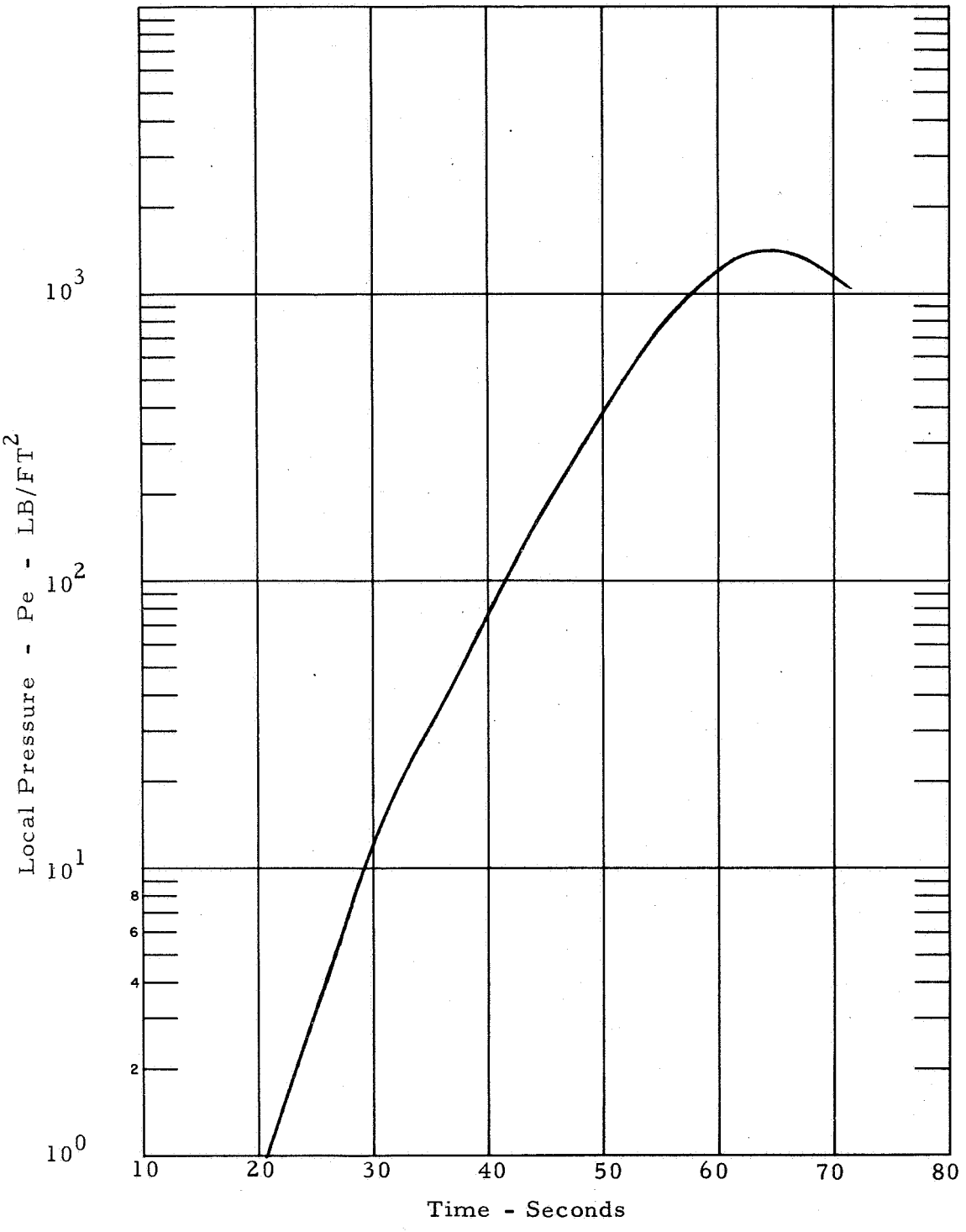

Figure III-6 LOCAL STATIC PRESSURE

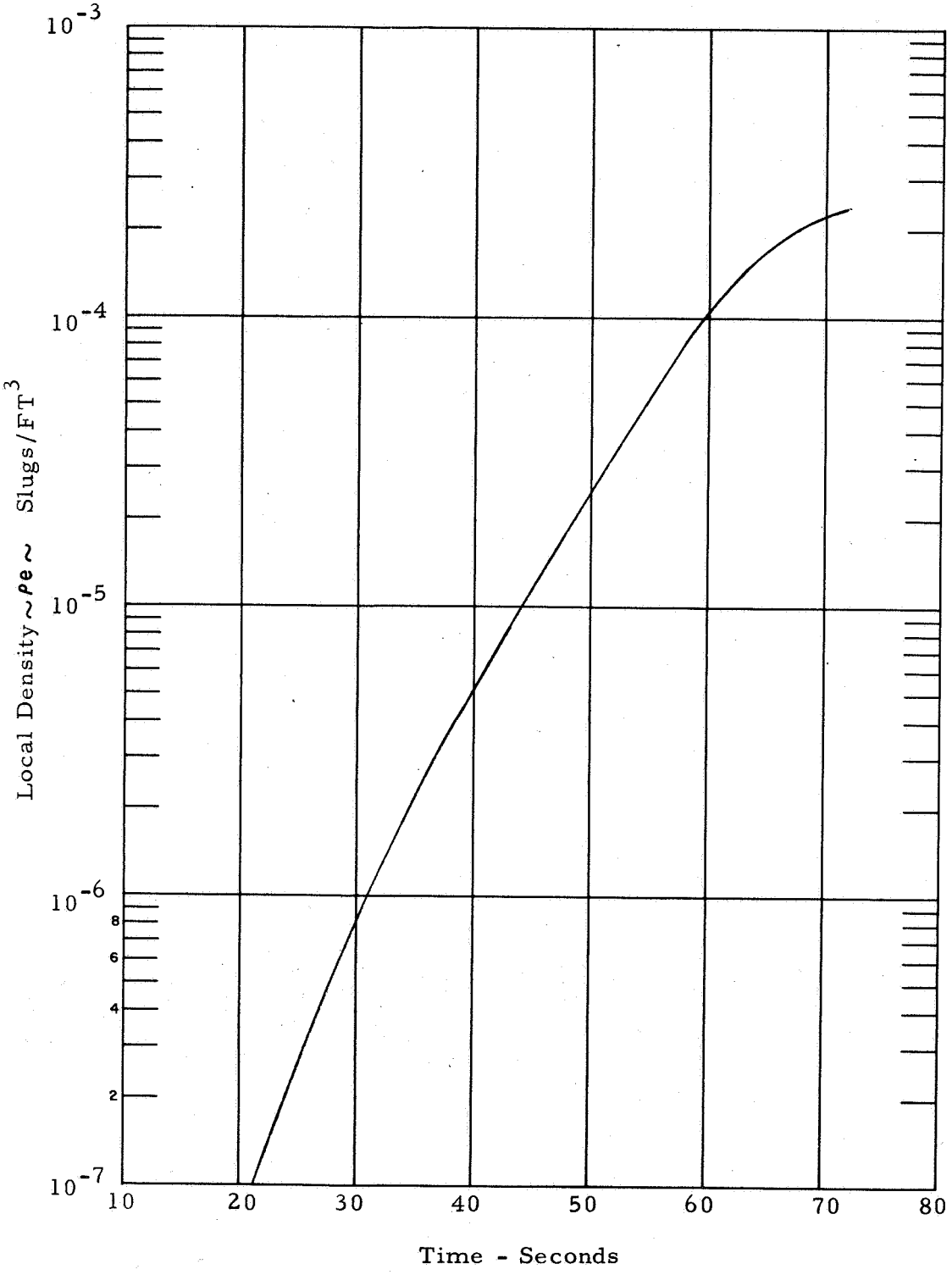

Figure III-7 EDGE DENSITY

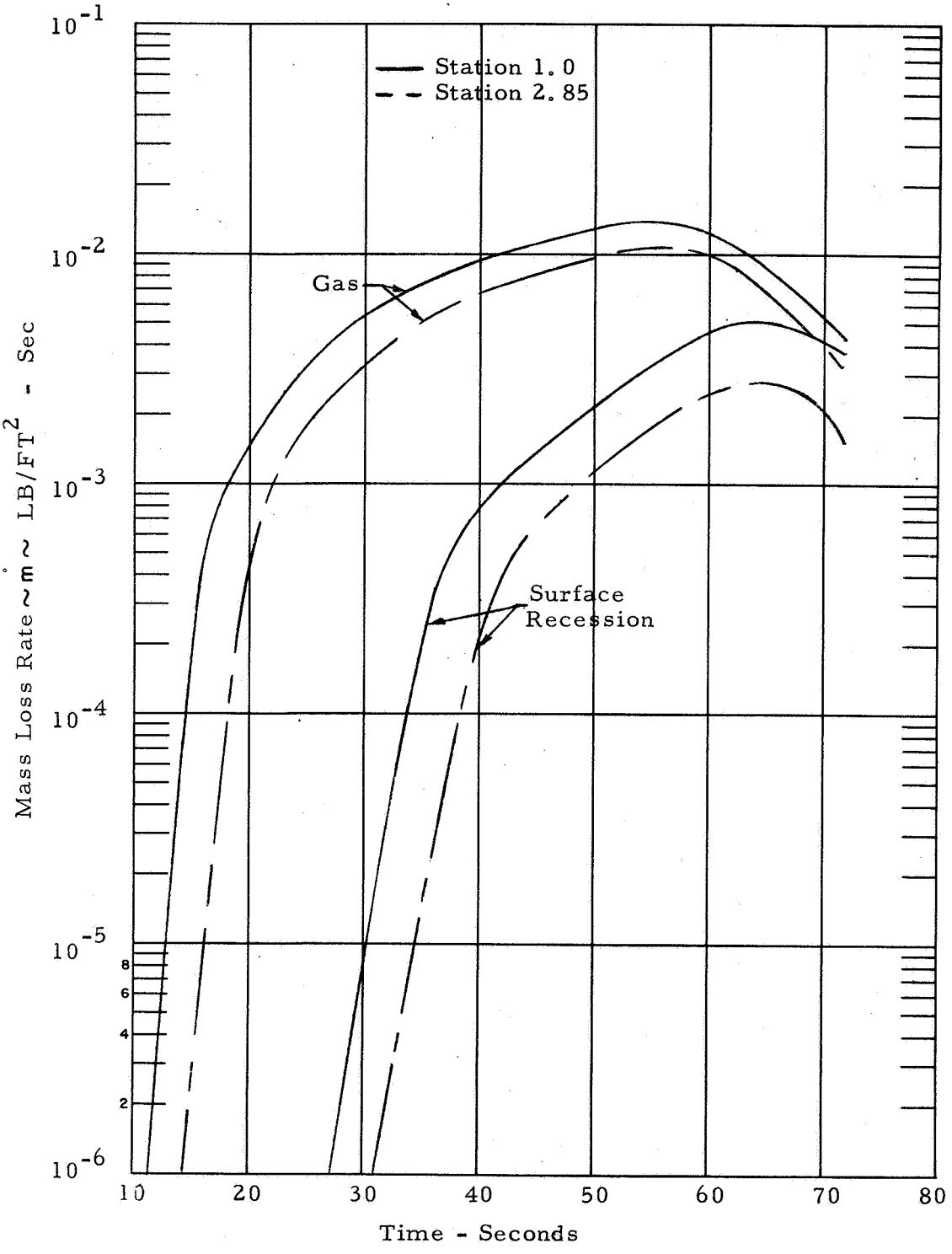

Figure III-8 MASS LOSS RATE

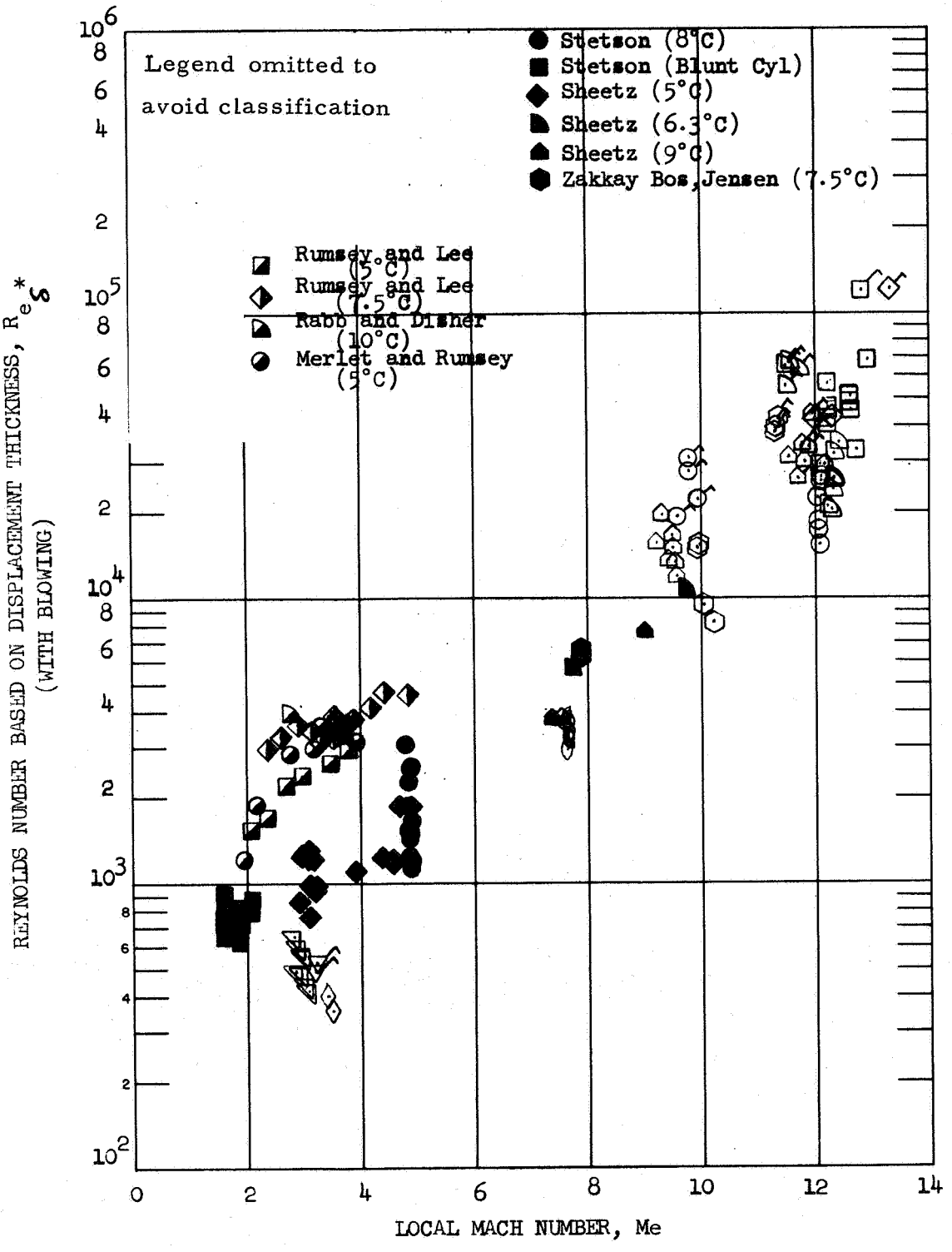

Figure III-9 TRANSITION CORRELATIONS

Subsonic

$$L_p^{OA} = 20 \log q + 84$$

after Bies

$$f_o = \frac{1}{6} \frac{U}{\delta^*}, \text{ or } \frac{1}{6} \frac{U}{D}$$

δ^* - displacement thickness, (attached flow)

D - vehicle diameter (separated flow)

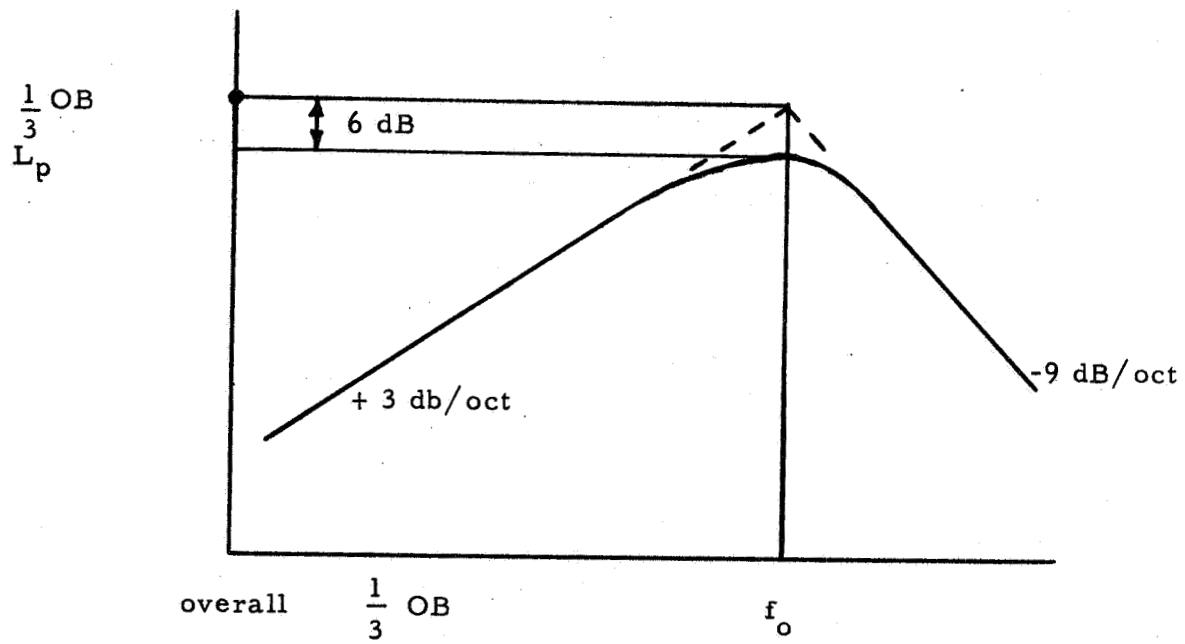

For M = 3 or greater, reduce levels by 15 dB on conical vehicles

Figure III-10 ACOUSTIC ESTIMATION PROCEDURE

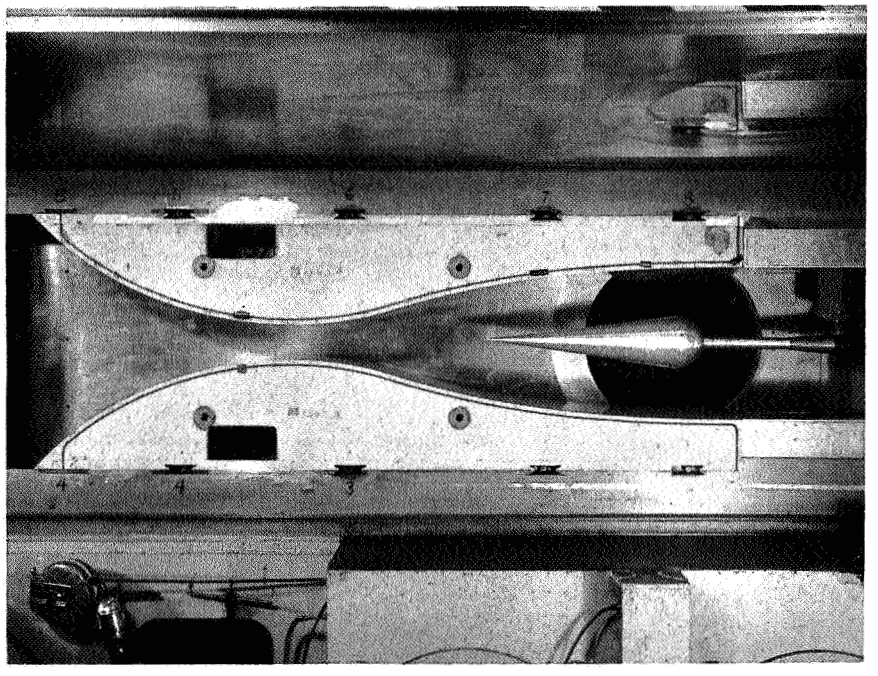

Figure III-11 SLENDER CONE TEST

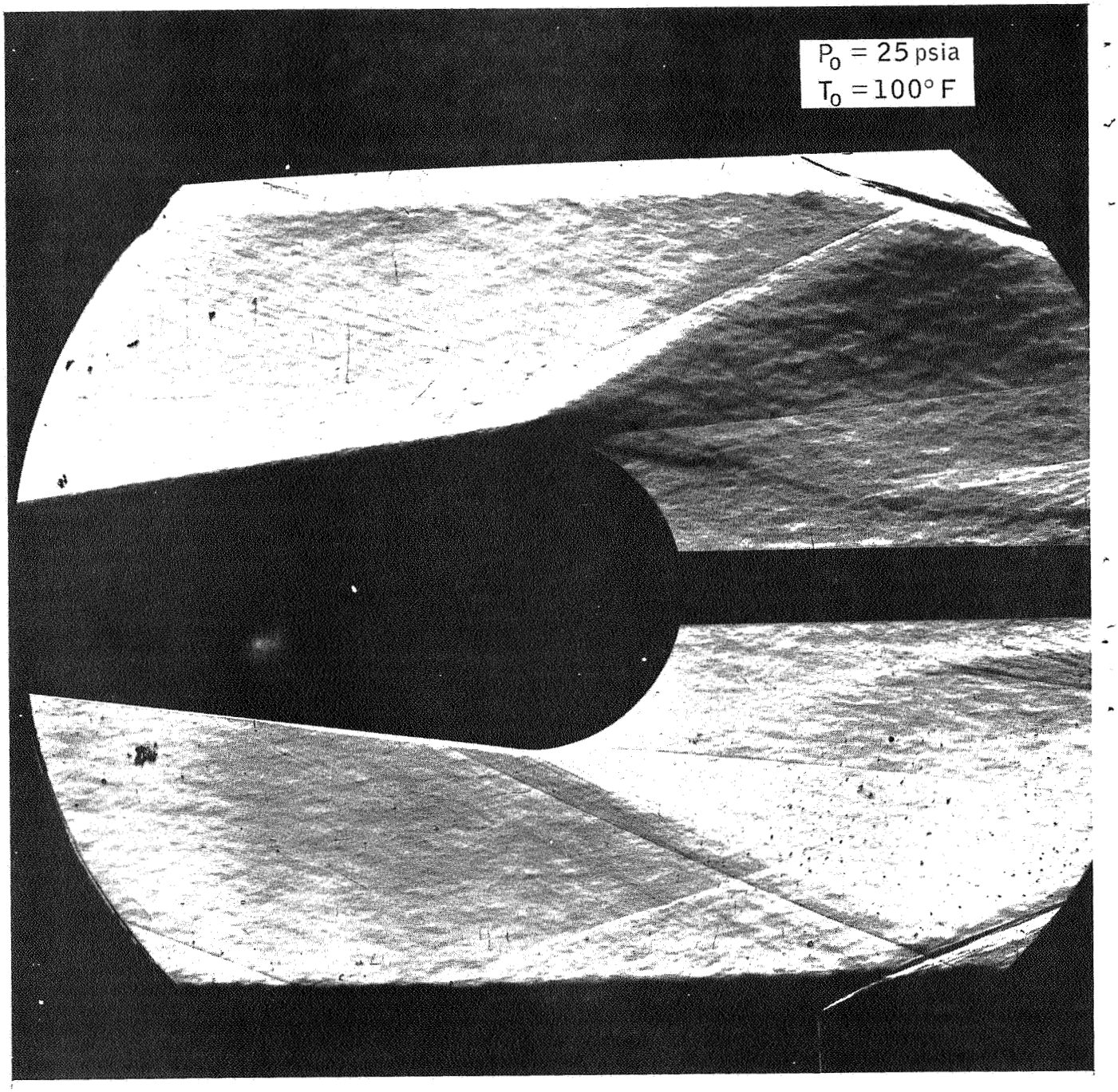

Figure III-12 CONE TEST SCHLIEREN PHOTO

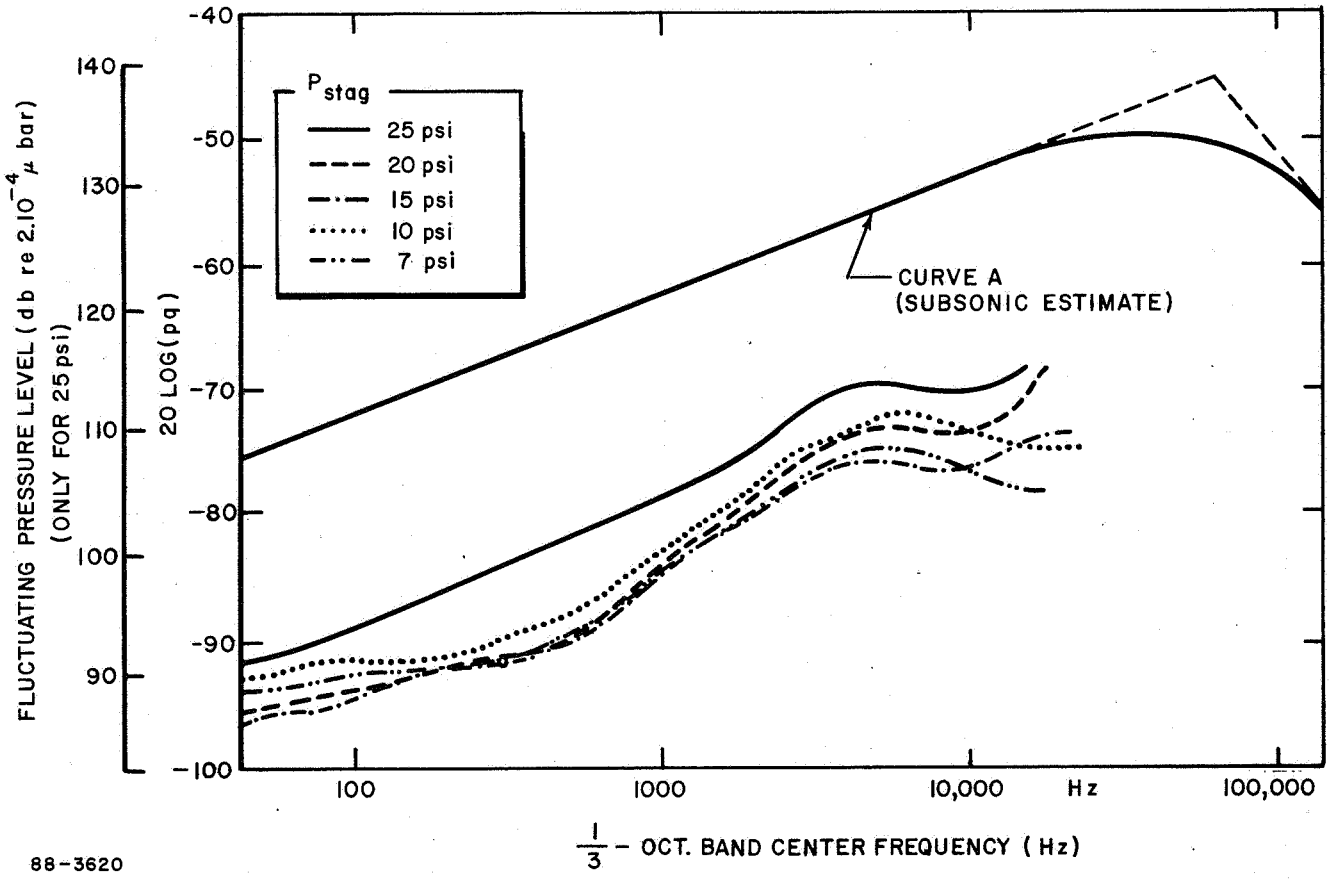

Figure III-13 CONE FLUCTUATING PRESSURE SPECTRA

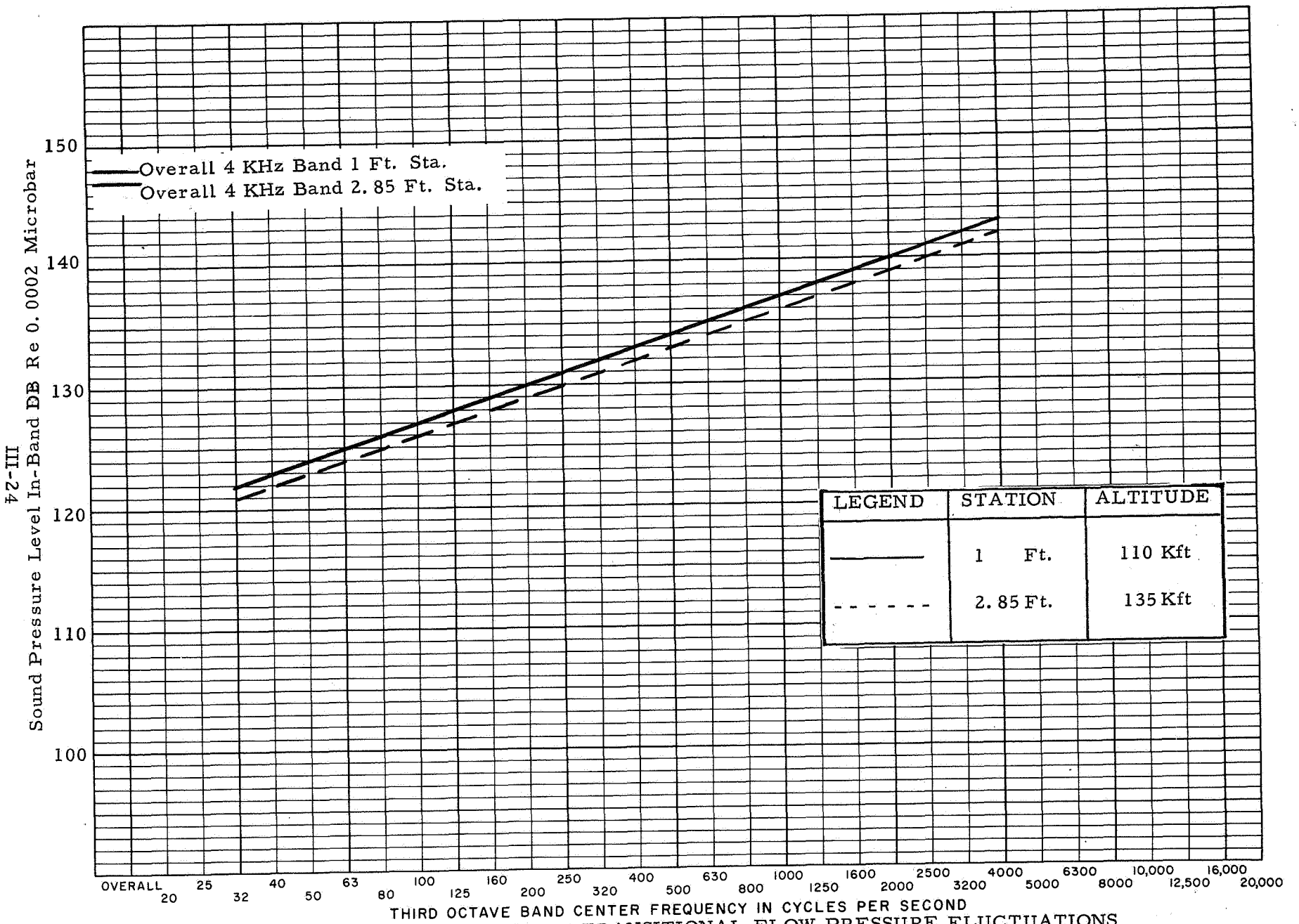

Figure III-14 ESTIMATE OF TRANSITIONAL FLOW PRESSURE FLUCTUATIONS

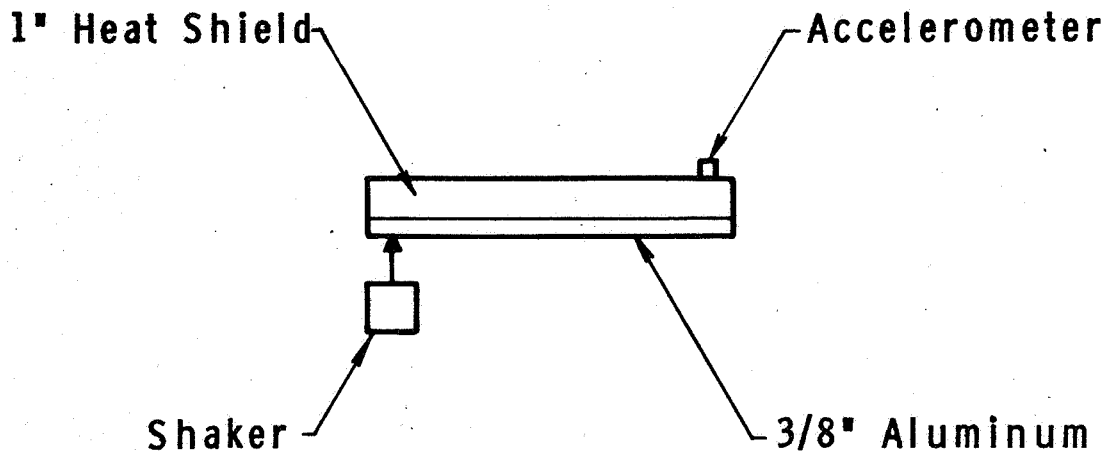

1. By measuring resonance frequencies we can estimate bending wavespeed
2. By measuring resonance 3dB bandwidth we can estimate damping loss factor

Figure III-15 EXPERIMENTAL ESTIMATION OF ALUMINUM-HEAT SHIELD LAMINATE VIBRATION PROPERTIES

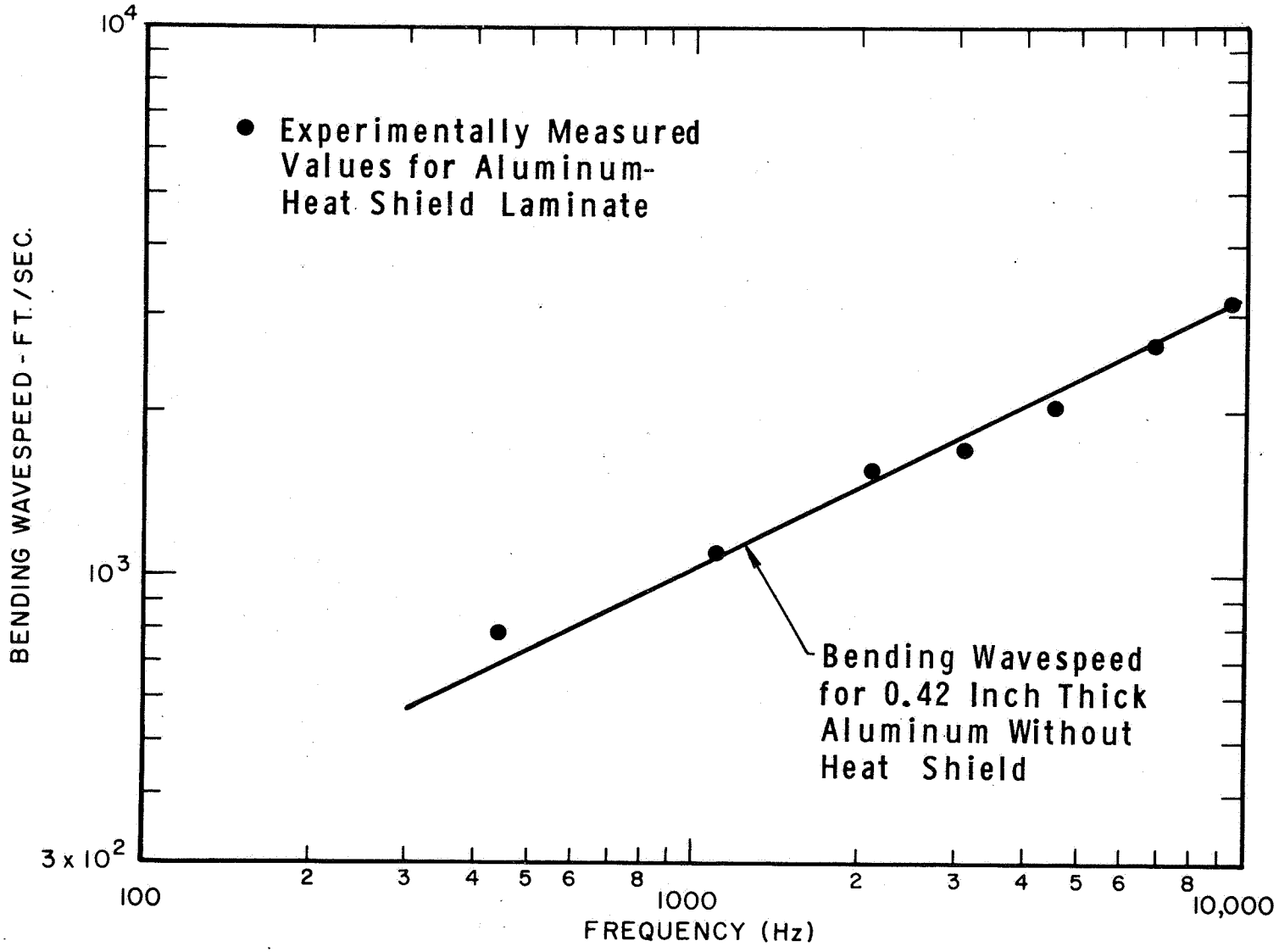

Figure III-16 BENDING WAVESPEED FOR ALUMINUM-HEAT SHIELD LAMINATE

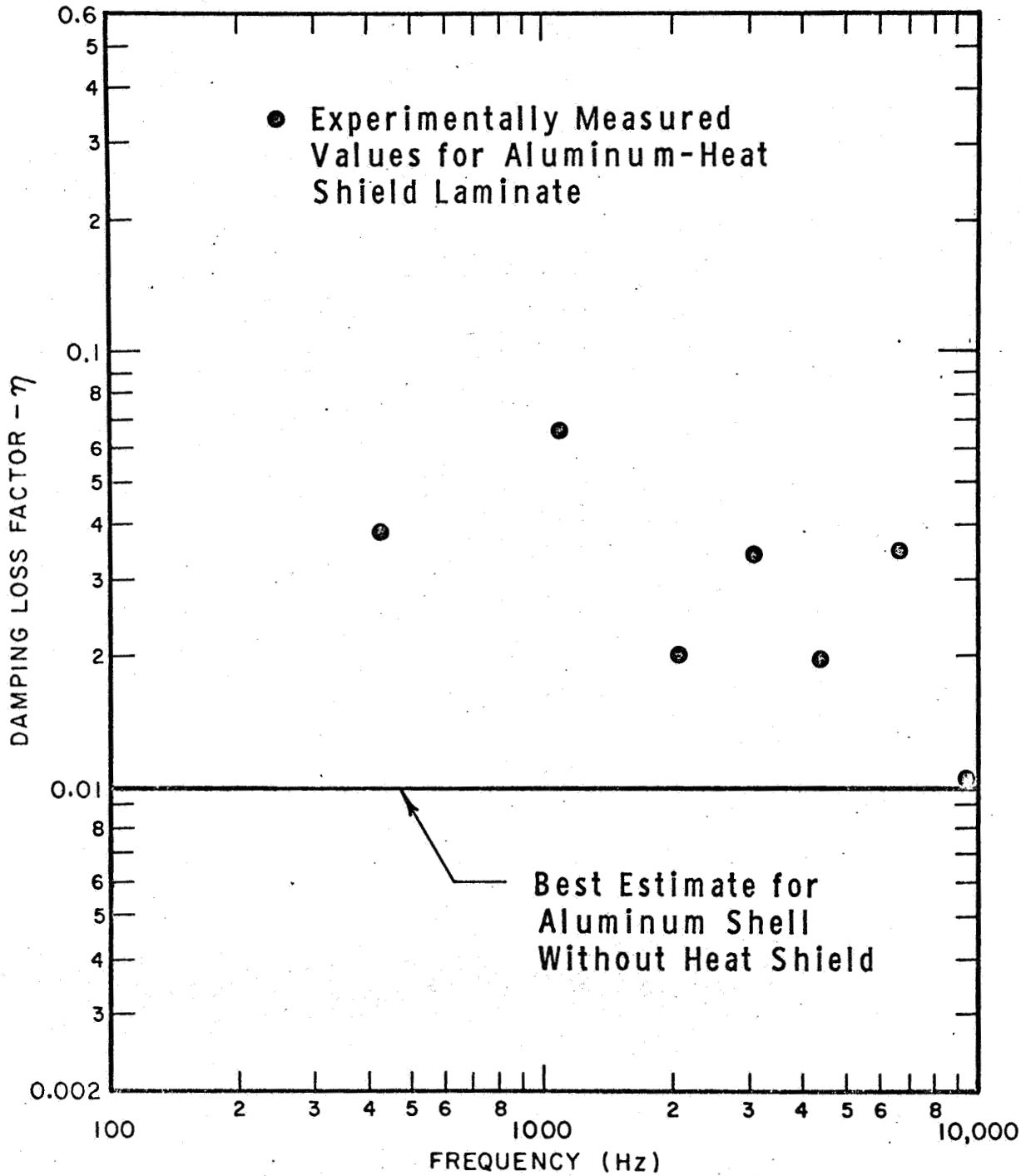

Figure III-17 DAMPING LOSS FACTOR FOR ALUMINUM-HEAT SHIELD LAMINATE

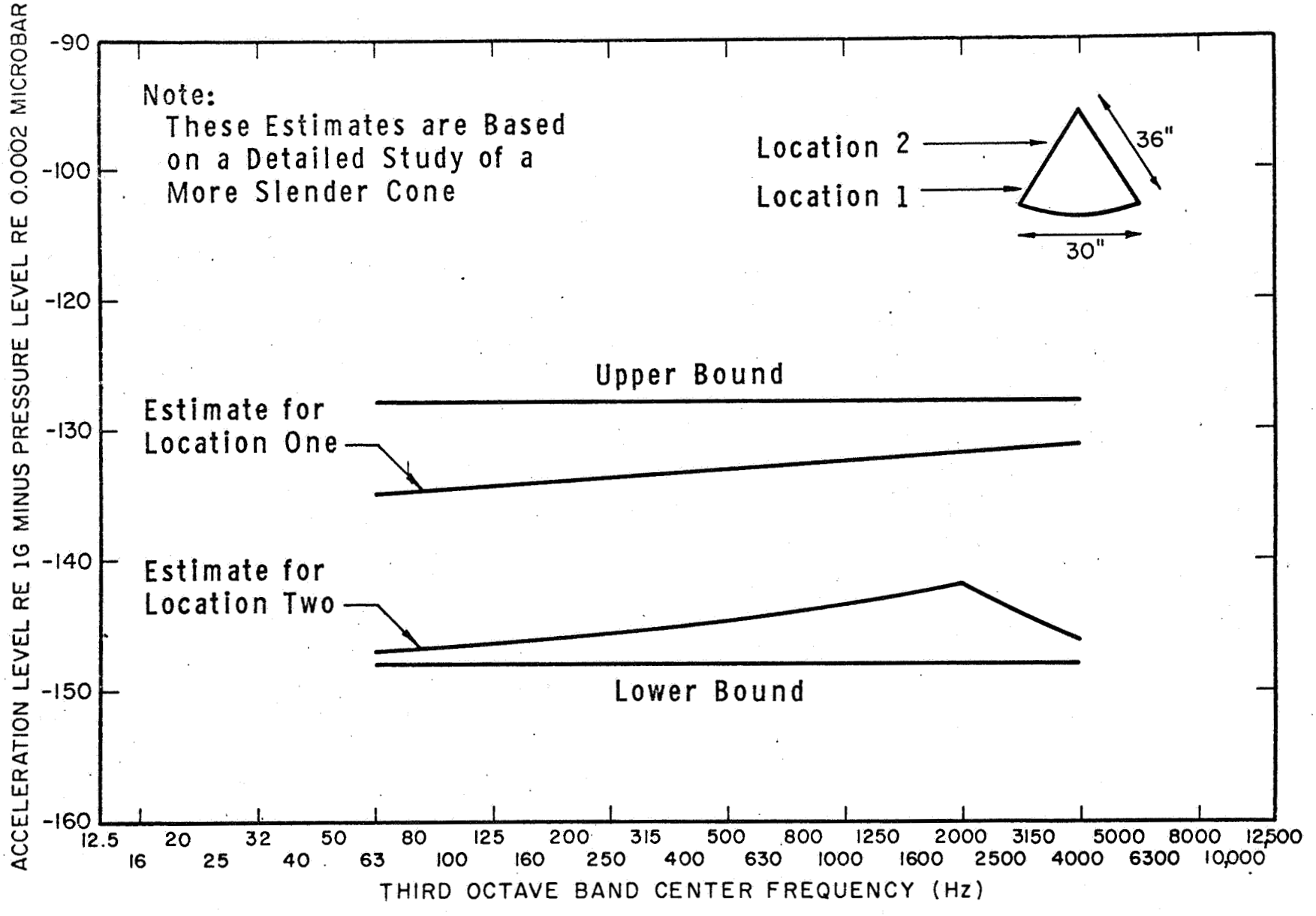

Figure III-18 ESTIMATED VEHICLE RESPONSE TO TURBULENT BOUNDARY LAYER EXCITATION

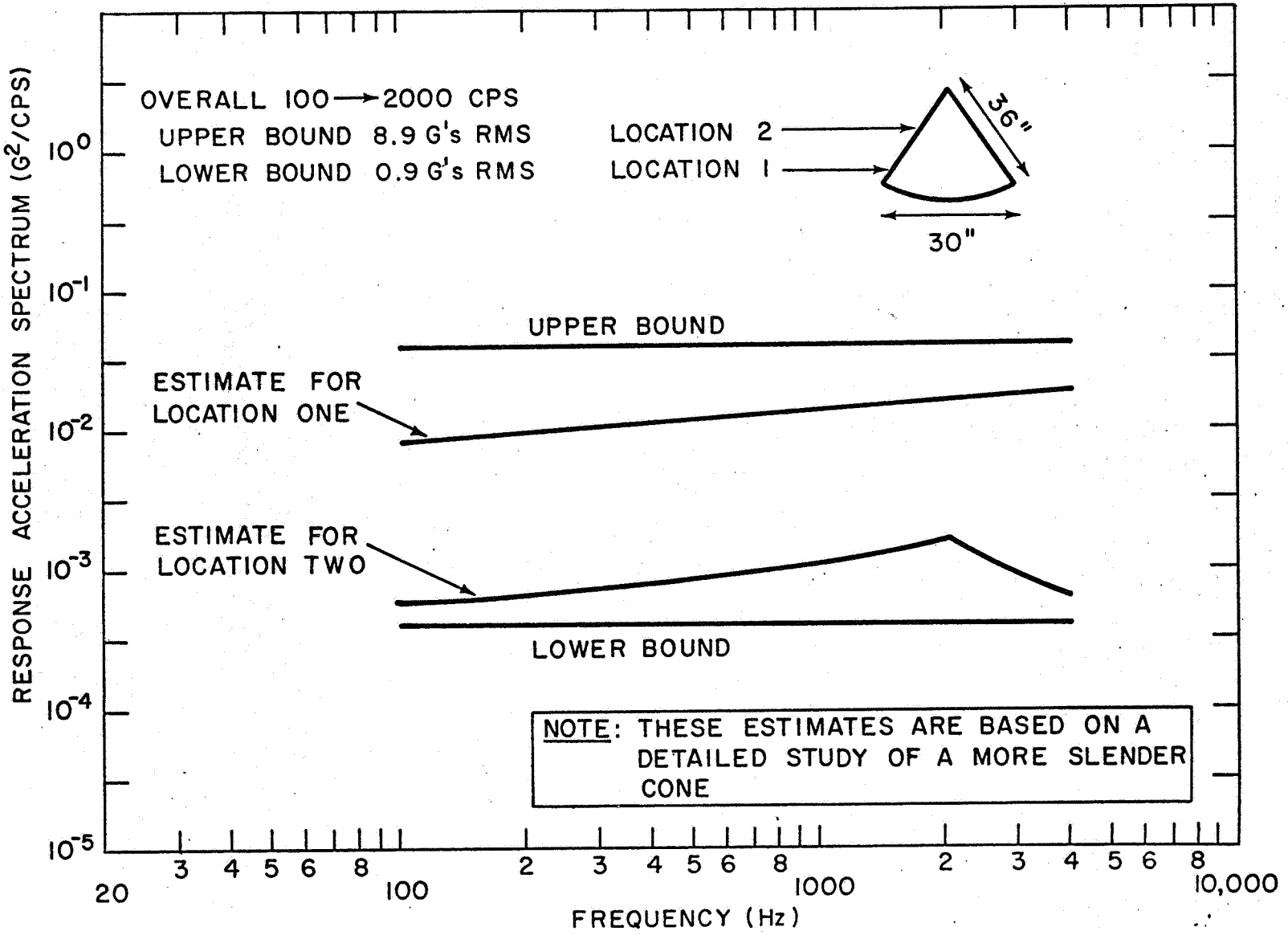

Figure III-19 ESTIMATED VEHICLE RESPONSE TO TURBULENT BOUNDARY LAYER EXCITATION AT TRANSITION (110 KFT)

NOMENCLATURE

C_f	local skin friction coefficient
F	blowing parameter
g_w	ratio of wall enthalpy to stagnation enthalpy
H	shape factor, δ^*/θ
$\dot{m}$	mass injection rate
M	Mach number
Re_x	Reynolds number based upon whetted length
Re_θ	Reynolds number based upon momentum thickness
Re_{δ^*}	Reynolds number based upon displacement thickness
U-V	flow velocity
X	surface distance from tip
δ^*	displacement thickness
θ	momentum thickness
ρ	density
μ	viscosity

Subscripts:

$_e$ ~ edge of boundary layer conditions

$_w$ ~ wall conditions

$_o$ ~ reference conditions (i.e., no blowing)

Superscript $( )^*$ ~ evaluated at Eckert reference enthalpy.

Note: U & V are used interchangeably throughout the text to indicate flow velocity.

IV. SYSTEM DESIGN AND DEVELOPMENT

Pressure fluctuations associated with boundary layer turbulence during and after transition provide the mechanical stimulus to be measured. The initial task is to provide a porting arrangement to couple the pressure fluctuations to the transducer which, in turn, converts the mechanical energy to an electrical signal. The requirement then becomes one of conditioning the signal generated by the transducer to the desired input to the data retrieval system. A goal of the hardware development was that of relatively small size and weight with an attendant reduction in current drawn from the primary source. Consequently, we can isolate several areas within the system such as the acoustic coupler, transducer and signal conditioner that are integral parts of the whole and merit separate treatment in the following discussion.

A. Acoustic Coupler

The basic function of the acoustic coupler is to provide communication between the boundary layer at the surface of the vehicle and the diaphragm of the transducer. The porting arrangement must protect the transducer from the severe environment that exists at the surface during reentry and must not distort the mechanical input to the sensing element over the frequency range of interest. In addition, the port as it intersects the outer surface of the vehicle cannot disturb the flow and hence generate self-noise or premature turbulence.

The conceptual design of the porting arrangement recognized the desire for a simple acoustic configuration to allow predictions of its characteristics to be made with confidence. It also seemed logical to limit the tube diameter to avoid possible disturbance of the laminar flow. This combination when considered in conjunction with the dynamics of porting systems (see Appendix) under the influence of supersonic flow dictated the smallest practicable microphone. This is brought about by the fact that the best port response is obtained with a tube of essentially constant cross-section that does not incorporate increases in diameter since these represent acoustic compliances that degrade the upper limit of the system frequency response. Consequently, we can see that the optimum would be a transducer with the same diameter as the tube to avoid the small cavity required at the tube/transducer interface if the microphone is larger than the tube diameter.

A typical coupler configuration is illustrated in figure IV-1 which is, in fact, very representative of the flight arrangement for the Endo-Decoy vehicles. The basic design includes a 1/16 inch diameter tube with a right angle bend leading to the 1/4 inch diameter transducer. Two small cavities are allowed to facilitate physical requirements such as alignment of holes

during assembly. The performance of this porting arrangement was evaluated in both an anechoic chamber (acoustic excitation) and in the MIT Wind Tunnel at Mach 3 (fluctuating pressure excitation). The response to acoustic excitation is characterized by the expected tube resonances as shown in figure IV-2. The radically modified response of the system under Mach 3 flow is also provided and indicates that the port now behaves as a highly damped second order system. Considered in the most simple terms, the acoustic resistance associated with the port has been greatly increased by the supersonic flow over the tube opening. This phenomena is described in detail in the appendix. The essentially flat response of the coupling arrangment to approximately 2,000 Hz is considered completely adequate especially since the upper limit of the flat response varies as a function of gas temperature. Estimates of the increased frequency response provided by the hot flow over the vehicle during reentry indicate an increase in flat response to approximately 5000 Hz. The performance of the porting arrangement is not affected by ablation (tube shortening) as shown in the appendix analytically and demonstrated experimentally in the MIT Wind Tunnel.

B. Transducer

The criteria used to evaluate available microphones for use as the transducing element were derived from the estimated pressure fluctuations, the anticipated vibration environment and the desire for small physical size. The search for suitable units was restricted to strain gage and crystal elements since they provide the desired rugged construction and do not require venting of the diaphragm. Figure IV-3 is a composite illustration providing the anticipated signal to noise ratio for the measurement based on the estimates presented in section III. Comparison of the boundary layer excitation with the vibration induced output of the transducer (115 db SPL/g sensitivity) yields a signal to vibration margin of 15 db. This margin is adequate to accomplish the measurement especially if the transducer is mounted as shown in figure IV-1 with the most sensitive axis parallel to the vehicle surface. This arrangement lowers the vibration environment as described in section III-B.

Data for a number of microphones are presented in Table IV-I and a photograph of four typical units is shown in figure IV-4. The primary criterion is the ratio of acoustic to vibration sensitivity shown as a Figure of Merit (FOM) in Table IV-I. The larger the absolute FOM the more suited the transducer to provide the desired measurement in a vibration environment. Five of the transducers of Table IV-I have FOM's of approximately -220 db. Two of these, the 2510 and the MA299507 employ vibration cancelling crystals and are quite large. The other three are all quite similar and are equally suitable, with the two 1/4 inch diameter units pre-

ferred. Other parameters such as frequency response, temperature range, etc. could have been included in Table IV-I but since these parameters were adequate for all transducers cited, they were omitted.
In conclusion, the Avco CT-4S or the BBN 370 transducers are considered most appropriate for the transition detection system. The two units preferred above are both commercially available and, consequently, the minute details of their design and fabrication are not presented in this report. An exploded view of the BBN Model 370 microphone is provided in figure IV-5. The diaphragm is constructed from .001 inch brass backed by a barium titanate crystal with 150 pfd of capacity. An insulated-gate field effect transitor is used immediately following the crystal to lower the impedance.

A physical resistor of about 10^9 ohms is placed in parallel with the crystal to control the low frequency response of the unit, and to allow transients to decay rapidly. The time constant for the device is of the order of 0.1 seconds. A .015 inch coating of black heat shield material is placed over the brass diaphragm to prevent direct radiation to the diaphragm and crystal.

C. Signal Conditioner

The signal conditioner must accomplish all functions needed between the transducer and the telemetry equipment to ensure compatibility. These functions are:

- provide stable bias current to the transducer,
- amplify the transducer signal without contributing to the noise,
- limit the data bandwidth to be consistent with the subcarrier modulation,
- provide a stable output bias,
- provide clipping of the signal above approximately 5 volts and below 0 volts,
- convert battery voltage to isolated, regulated voltages for the circuits and transducer.

The design of the conditioning electronics has been accomplished to satisfy the above functions without undue circuit complexity. The goal consequently has been to simplify the circuit without sacrificing performance. The final circuits, for example, have significantly fewer components than the original design, but maintain the performance of the original breadboard. The engineering prototype fabricated after the breadboard optimization is illustrated in figure IV-6.

The signal conditioner contains two amplifiers, a low-pass filter and a DC to DC converter. Figure IV-7 is a simplified schematic of the transition detector electronics. Since the transducer contains an insulated-gate field effect transistor source follower amplifier, the signal conditioner contains a current source diode (A3CR1)* to provide power for the transducer.

The first amplifier consists of integrated-circuit operational amplifier (A3AR1), and a feedback network providing adjustable gain from 20 to 40 db. The circuit has one low frequency roll-off at about 10 Hz due to A3C1 and A3R2 (the input coupling network), and a second roll-off due to A3C5 and the feedback resistor network. This second roll-off stops at unity gain, i.e. the DC voltage gain is unity for bias stability.

The gain determining network, consisting of A3R3 through A3R6, appears somewhat complex. The reason is that subminiature trimmer potentiometers are linear; for a wide gain adjustment, a linear control would lack resolution at one end. A3R3 and A3R5 load the arm of linear pot A3R4 to approximate the more desirable logarithmic function.

Following the first amplifier is an RC low pass network which, with the second amplifier, forms an active filter. The filter network consists of three cascaded RC low pass sections: A4R1-A4C1, A4R2-A4C2, and A4R3-A5C3. The second section, A4C2, has positive feedback from the second amplifier, A5AR1, output through the voltage divider A4R5 and A4R4. The positive feedback permits realization of complex poles in the filter response without using inductors.

The second amplifier consists of an integrated circuit operational amplifier (A5AR1) and a feedback network (A5R3, A5C5, and A5R2). The gain is 20 db. An output DC bias of approximately 2.5V for 0 to 5V input telemetry SCO's is injected by A5R4 from the -12V power supply. For the output DC bias, A5AR1 operates as an inverting operational amplifier with A5R3 as the feedback resistor. Output voltage swing is restricted by a zener diode (A4VR1) to prevent overload of the telemetry SCO input. Protection from output short circuits is provided by resistor A4R6.

*All of the reference designators on the simplified schematics are the same as those of the complete schematic (drawing C80039), figure IV-8.

A DC/DC converter provides transformer isolation between the signal and power circuits, while providing regulated and filtered output voltages for the amplifiers. The converter still regulates for input voltages as low as 21.5V to ensure that AC riding on the DC input power will not get into the amplifier circuits (i.e. to reduce conducted susceptibility).

Detailed drawings of the circuit and mechanical construction are provided in figures IV-8 through IV-11. A materials list is included as Table IV-II. The resulting performance of the signal conditioner is given below:

Gain:	continuously variable between 40 and 60 db
Noise Floor:	-100 dbV re input with 1000 ohm source and current supplied to transducer
Frequency Response:	3 db down at 20 Hz and 4000 Hz
Input Power:	under 20 ma at 27 to 31V dc short-circuit protected
Output Impedance:	less than 100 ohms
Output Bias:	approximately 2.5 volts dc
Output Limiting:	better than -1.0 to + 6.5V dc
Insulation Resistance:	greater than 900×10^6 ohms from power to signal circuits and from either to case at 90V dc (NOTE: Transducer case must <u>not</u> be grounded during measurements.)
Physical Size:	1-1/2" x 5/8" x 2-1/2"

The packaged signal conditioner is shown in figure IV-12. It is housed in an aluminum extrusion with through mounting holes. Internally, the unit is made up of four cordwood electronic modules. The mocules are encapsulated as one assembly with RTV 615 silicone plastic. Electrostatic shielding of copper foil, insulated with polyester sheeting, surrounds the assembly inside the outer aluminum case. External connections are made with subminiature rectangular-block connectors from Winchester Electronics.

In conclusion, the design philosophy of minimizing components to reduce size has been successfully completed without sacrificing performance. For a transducer with -102 dbV/μbar sensitivity, the output of the signal conditioner can be set to be 1 volt rms for 116 to 136 db SPL. The equivalent electrical noise floor of the system should be about 85 db SPL in the 4 kHz bandwidth. It has been found experimentally that the system performance is not degraded by environment exposure as discussed in section V-B.

TABLE IV-I

MICHROPHONE CHARACTERISTICS SURVEY

MANUFACTURER	MODEL	TYPE	SIZE (DIA.x LENGTH)	ACCUSTIC SENSITIVITY (dBv/μbar)	EXCITATION (MILLIWATTS)	VIBRATION SENSITIVITY (SPL/g)	FOM. (dB)
AVCO	CT-4S	CRYSTAL W/FET	1/4" x 1"	-102*	20*	115*	-217
AVCO	CTI-20S	CRYSTAL W/FET	1/2" x 1"	-102*	20*	119*	-221
BBN	370	CRYSTAL W/FET	1/4" x 7/8"	-102*	10*	115*	-217
BYTREX	HFD	SEMI-COND. STRAIN	1/8" x 1/8"	-146*	300*	98*	-244
BYTREX	HFA	SEMI-COND. STRAIN	1/2" x 1/2"	-146	300	122	-268
CEC	4-312A	STRAIN GAUGE	5/8" x 3/4"	-157	75	146	-303
ELECTRA SCIENTIFIC	MA299507	CRYSTAL	3/4" x 7/8"	-105*	0	100*	-205
ENDEVCO	2510	CRYSTAL	7/8" x 1 1/4"	-112*	0	105*	-217
ENDEVCO	2503	CRYSTAL	1/4" x 1/4	-121*	0	127*	-248
GIANNINI	4715	SEMI-COND. STRAIN	1" x 3/4"	-144	100	118	-262
KISTLER	201	QUARTZ W/FET	3/8" x 1"	-128*	100*	134*	-262
MICRO-SYSTEMS	P03BA4	SEMI-COND. STRAIN	1/4" x 1/4"	-146	300	124	-270
SCIENTIFIC ADV.	SA-SD	STRAIN GAUGE	1/4" x 1/4	-154	30	128	-282
STATHAM	PA-222TC	STRAIN GAUGE	1/4" x 5/8"	-160	40	134	-294

*Measured

TABLE IV-II

MATERIAL LIST

MATERIAL LIST	BOLT BERANEK & NEWMAN INC.	REV DATE	ML	REV LTR
TRANSITION DETECTOR – MODEL 370A	AUTHENTICATION	CONTRACT NO	CODE IDENT	SHT____ OF ____ SHTS

ITEM OR FIND NO	QTY REQ	ASSY USED ON	UNIT OF MEAS	CODE IDENT NO	PART OR IDENTIFYING NO	NOMENCLATURE OR PART DESCRIPTION	VENDOR	ALT SOURCE
1	1		EA		CYK02BV104K	CAP. .1UF,± 10% 50V	CORNING	
2	2		EA		8003-000-W5R471K	CAP. 470 PF ± 10% 100V	ERIE	
3	2		EA		8003-000-COG 220K	CAP. 22 PF ± 100V	ERIE	
4	2		EA		150D685X9006A2	CAP. 6.8 UF ± 10% 6V	SPRAGUE	
5	2		EA		CYK01BT103K	CAP. .01UF ± 10% 50V	CORNING	
6	1		EA		CYK01BT472K	CAP. .0047UF ± 10% 50V	CORNING	
7	1		EA		8003-000-COG 101K	CAP. 100 PF ± 10% 100V	ERIE	
8	1		EA		1N5297	DIODE	MOTOROLA	
9	1		EA		1/4 M5.6AZ-5	DIODE ZENER		
10	2		EA		MC1709CG	INTEGRATED CIRCUIT	MOTOROLA	
11	2		EA		RC07GF152J	RES. 1500 OHMS,± 5% 1/4W		
12	1		EA		RN55C1503F	RES. 150K OHMS ± 1% 1/10W		
13	1		EA		RN55C6192F	RES.61.9K OHMS ± 1% 1/10W		
14	1		EA		3282H-1-204	RES. 200K OHMS (POT)	BOURNS	
15	1		EA		RN55C6981F	RES. 6.98K OHMS ±1% 1/10W		
16	1		EA		RN55C1301F	RES. 1.3K OHMS 1/10W 1%		
17	1		EA		RN55C2212F	RES. 22.1K OHMS ±1% 1/10W		
18	3		EA		RN55C2213F	RES. 22.1K OHMS ±1% 1/10W		
19	1		EA		RN55C1501F	RES. 1.5K OHMS ± 1% 1/10W		
20	1		EA		RN55C1002F	RES.10.0K OHMS ± 1% 1/10W		

TABLE IV-II (Cont'd)

MATERIAL LIST	BOLT BERANEK & NEWMAN INC	REV DATE	ML	REV LTR
TRANSITION DETECTOR – MODEL 370A		AUTHENTICATION	CONTRACT NO	CODE IDENT	SHT____ OF ____SHTS

ITEM OR FIND NO	QTY REQ	ASSY USED ON	UNIT OF MEAS	CODE IDENT NO	PART OR IDENTIFYING NO	NOMENCLATURE OR PART DESCRIPTION	VENDOR	ALT SOURCE
21	2		EA		RC07GF102J	RES.1K OHMS ± 5% 1/4W		
22	1		EA		RN55C6982F	RES. 69.8K OHMS ± 1% 1/10W		
23	1		EA		RN55C1472F	RES. 14.7K OHMS ±1% 1/10W		
24	4		EA		6121	EYELET	UNITED SHOE	
25	1		EA		C60048 µV-12	DC/DC CONVERTER DC/DC CONVERTER	BBN MIL-ASSOC.	
26	1		EA		370 CT-4S	TRANSDUCER TRANSDUCER	BBN AVCO	
27	35grms				RTV-615	POTTING COMPOUND	G.E. CO.	
28	4"x4"		SHT		FL-GB02001/0	PLASTIC SHEET LAMINATED		
29	3 FT		ROLL		#8053	WIRE ELECT. #26SGL BELDSOL	BELDEN	
30	4"x8"		SHT			.001 MYLAR		
31	4"x4"		SHT			.0005 COPPER FOIL		
32	4"x4"		ROLL		80SLP1 LOT 116 1 x 8	TAPE PRESSURE SEN.	SCOTCH	
33	1 FT		FT		#8640-250	WIRE, BELDFOIL	BELDEN	
34	20grms				20/20	EPOXY ADHESIVE BLACK	ALLACO PROD INC.	
35	1		EA		SMRE7PJ	CONN. MALE	WINCHESTER	
36	1		EA		SMRE7SJ	CONN. FEMALE	WINCHESTER	
37	1		EA		8003-000-COGO-221K	220 PF 10% 100V	ERIE	
38	1-1/2"		TUBE		.1560Dx.130ID	BRASS TUBE		

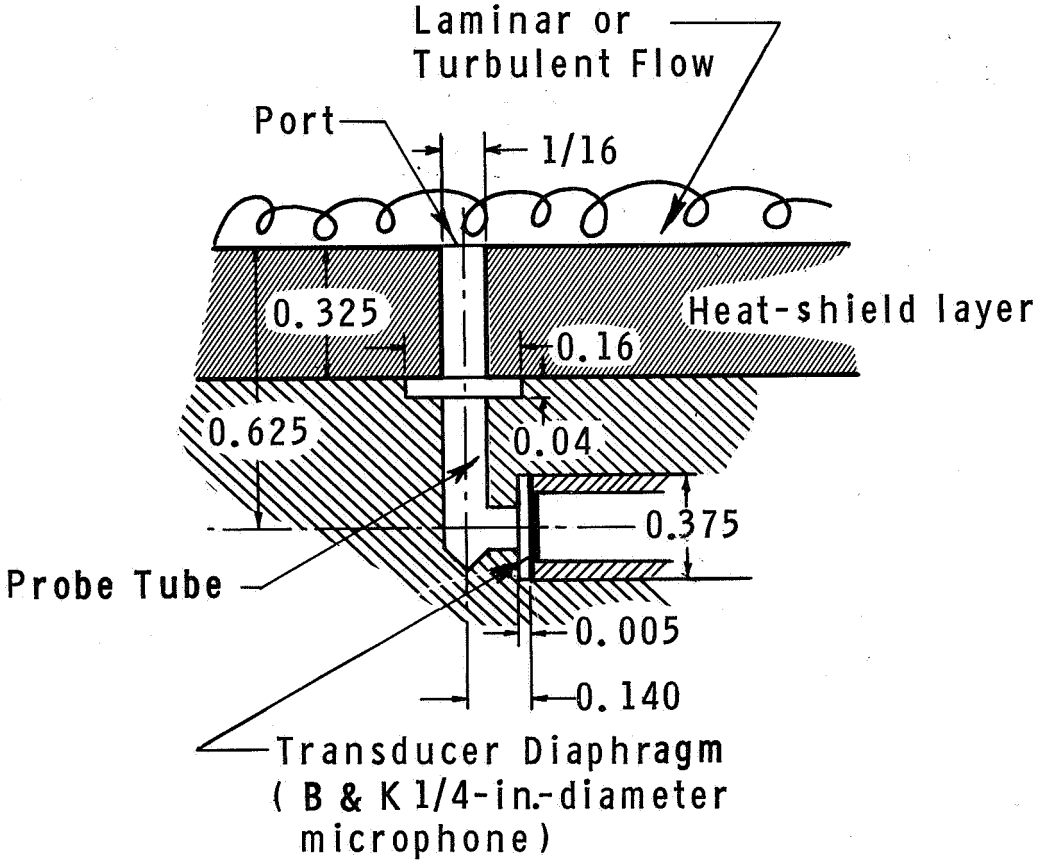

Figure IV-1 ACOUSTIC COUPLER CONFIGURATION

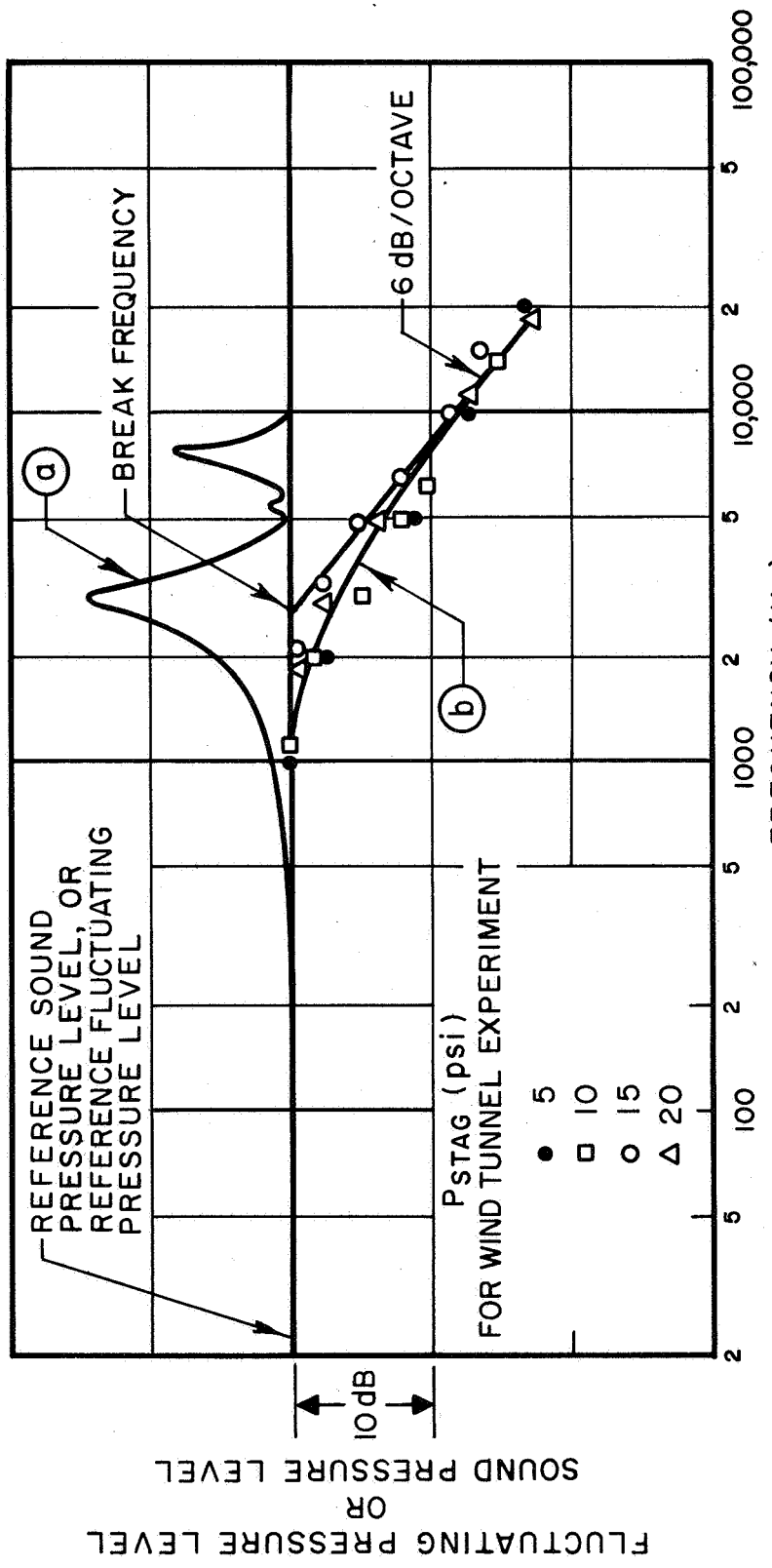

Figure IV-2 FREQUENCY RESPONSE OF TRANSITION DETECTOR PORT

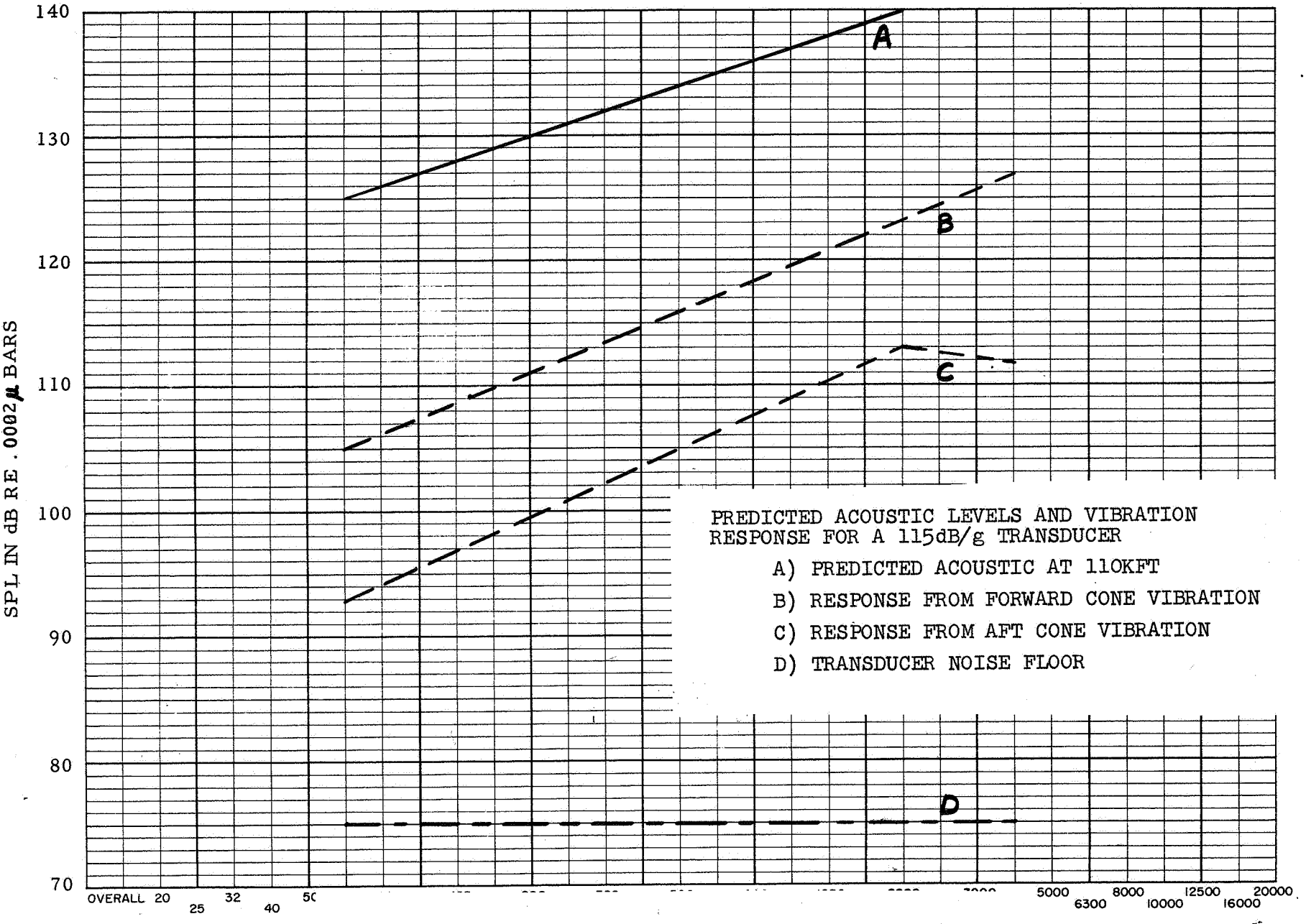

Figure IV-3 TRANSITION DETECTOR PERFORMANCE MARGIN

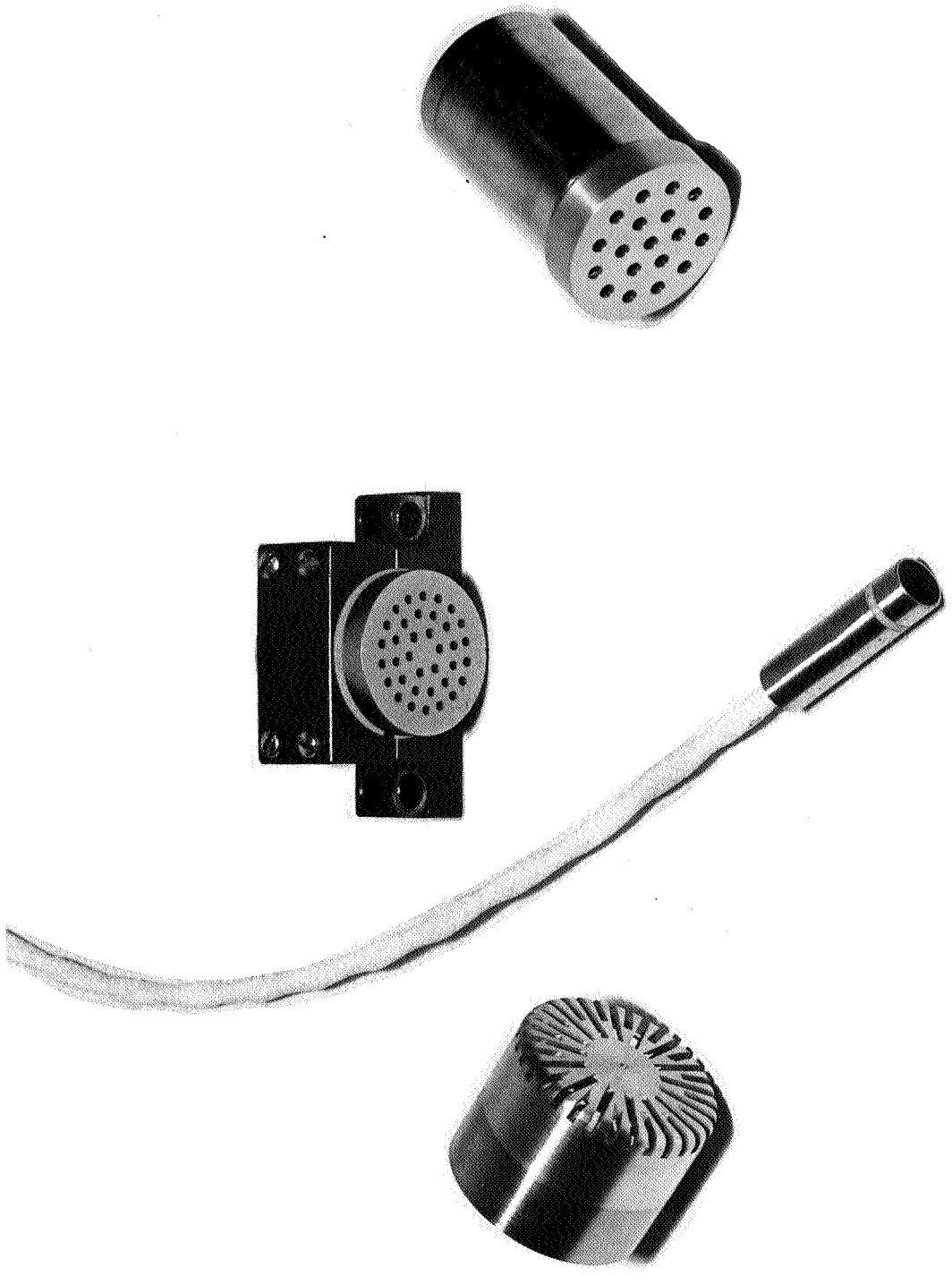

Figure IV-4 TYPICAL MICROPHONES

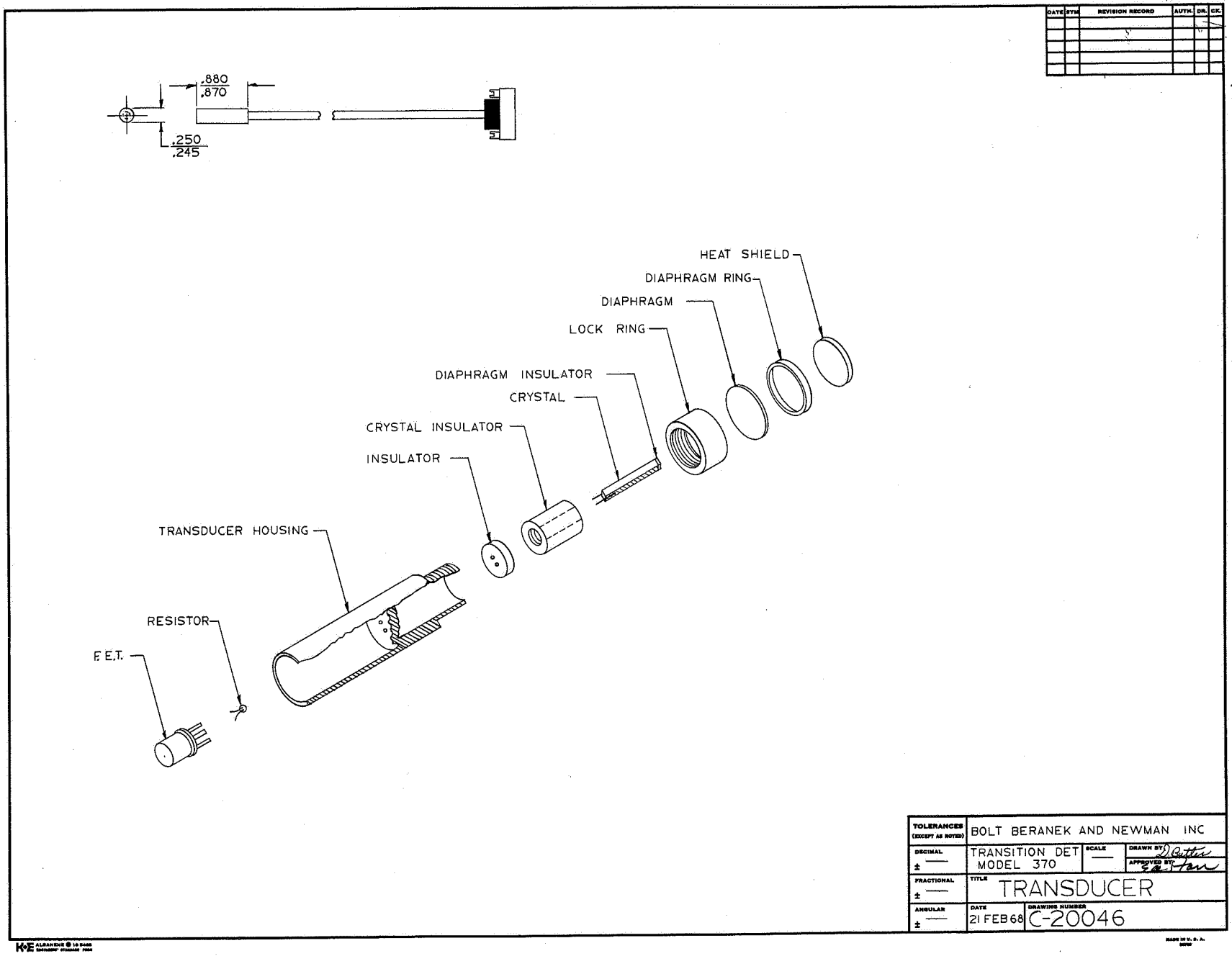

Figure IV-5 EXPLODED VIEW OF BBN MODEL 370

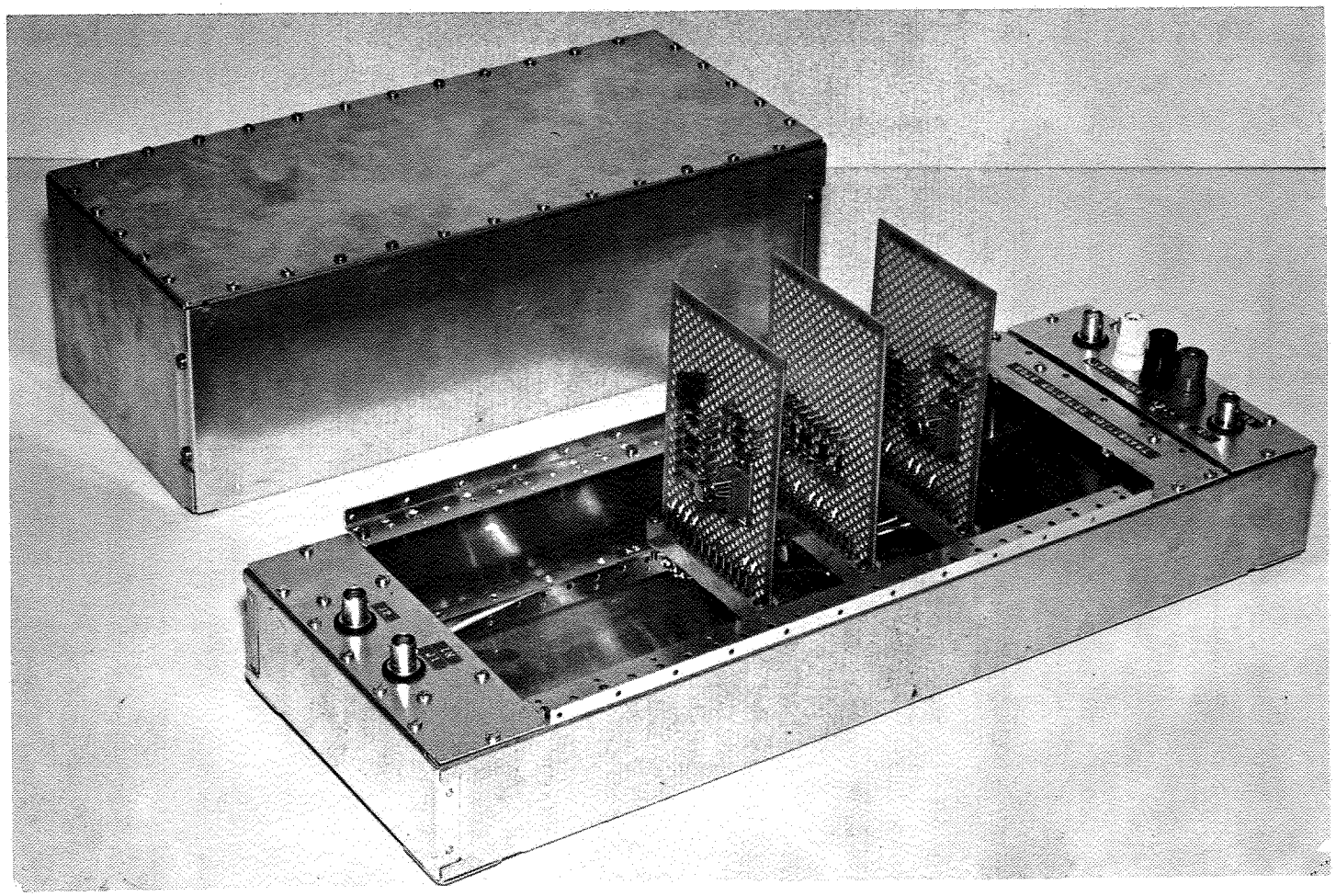

Figure IV-6 ENGINEERING PROTOTYPE

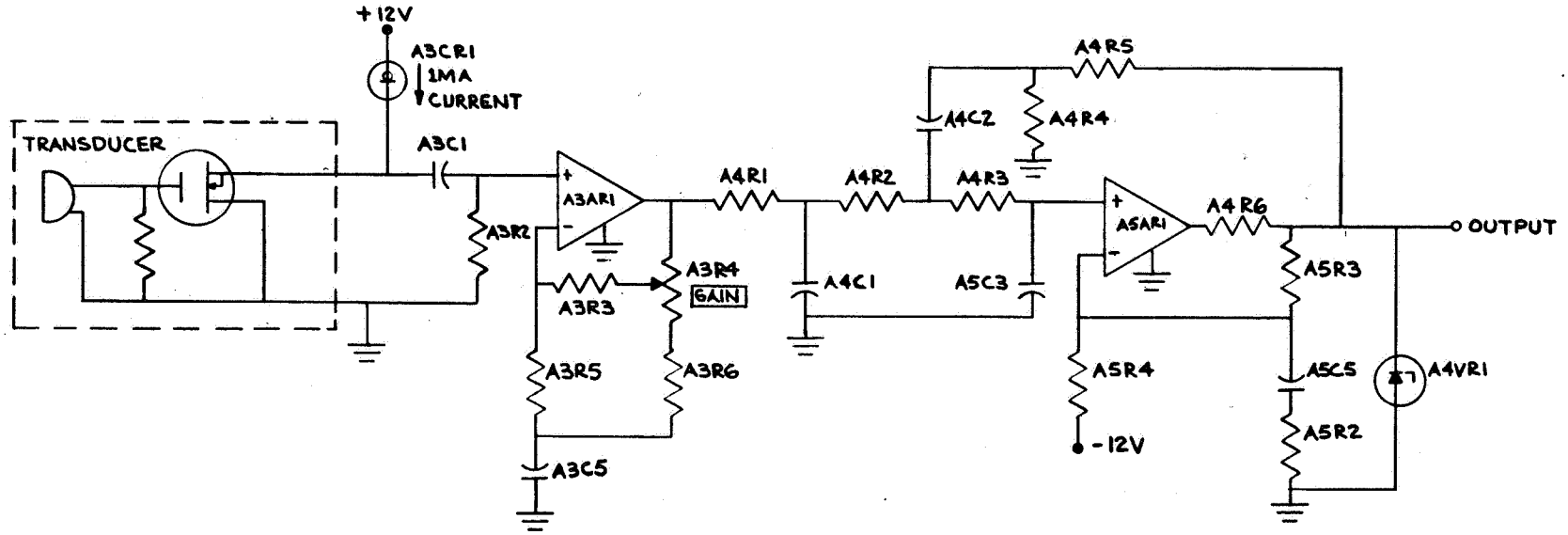

Figure IV-7 SIMPLIFIED SCHEMATIC

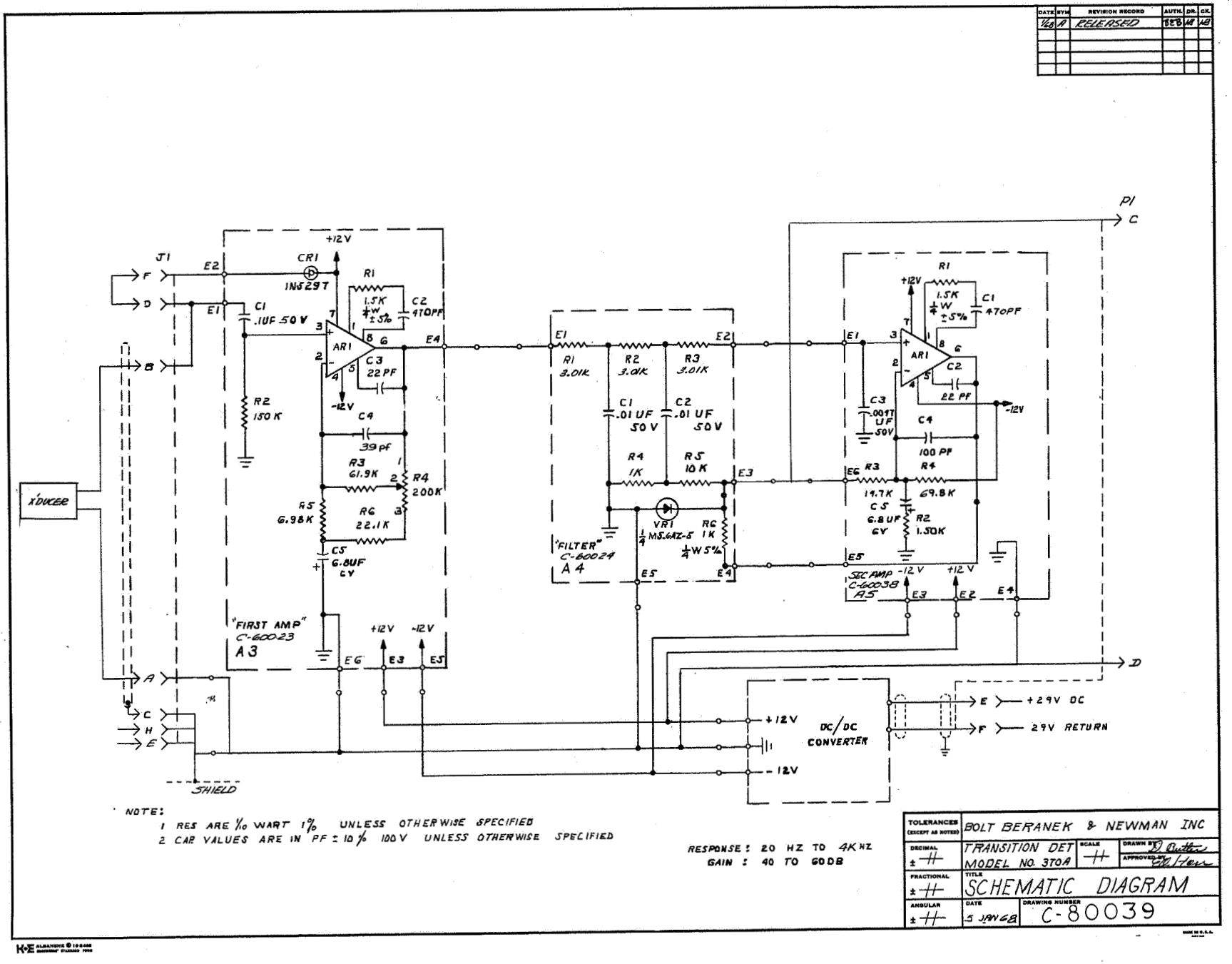

Figure IV-8 DETAILED SCHEMATIC

REVISIONS				
LTR	SYM	DESCRIPTION REQUIRED	APPR.	DATE
	A	RELEASED		14FEB68

A1 - MOTHER BOARD
A2 - DC/DC CONVERTER
A3 - FIRST AMPLIFIER
A4 - FILTER LOW PASS
A5 - SECOND AMPLIFIER

CONNECTOR WIRING		
FROM:	COLOR:	TO:
A1 E21	BLACK	J1-A
J1-A	JUMPER	J1-C
J1-C	JUMPER	J1-E
J1-E	JUMPER	J1-H
—	—	P1-A
A1 E24	BLUE	P1-C
*	RED	P1-E
—	—	P1-H
—	—	P1-B
A1 E25	BLACK	P1-D
*	WHITE	P1-F
J1-D	JUMPER	J1-B
A3 E1	GREEN	J1-D
A3 E2	TAN	J1-F
A1 E19	BLACK	WRAP AROUND SHIELD
*	BLACK (SHIELD)	J1-H
—	—	—

* LEADS ARE FROM SHIELDED CABLE B-30285.

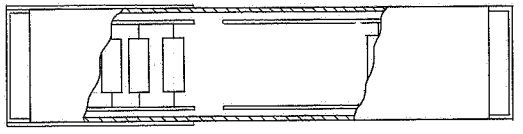

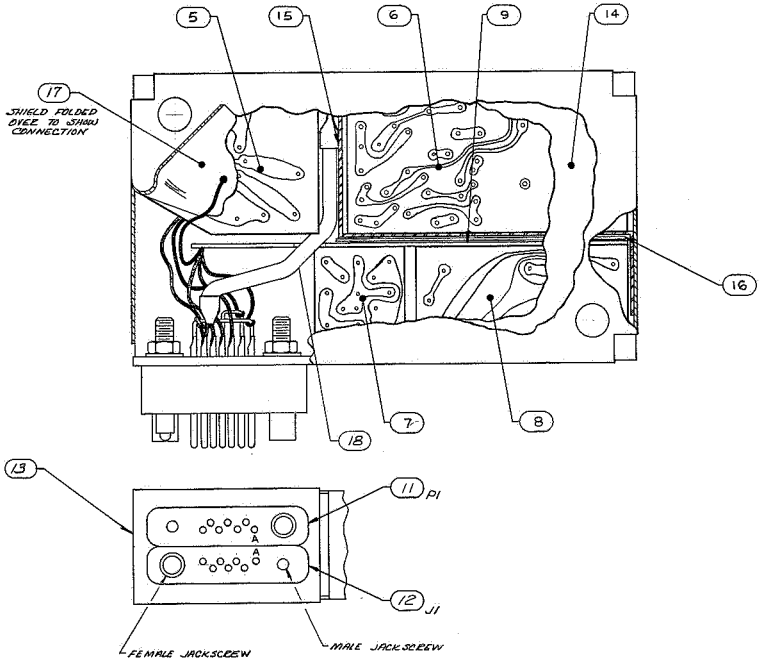

NOTE:
1. ASSEMBLE ALL MODULES TO MOTHER BOARD (A1) PER WIRE RUN LIST ON DWG NO. B-60035 USING ASSY JIG, DWG NO. C-30253
2. ASSEMBLY TO BE POTTED WITH RTV-615, (G.E.CO.) USING POTTING FIXTURE, DWG NO. C-30256 OVEN CURE FOR 2.5 HOURS AT 80°C.
3. WRAP SHIELD, DWG NO. C-30270 AROUND POTTED ASSEMBLY.
4. BOND DC/DC CONVERTER SHIELD TO MAIN SHIELD DWG NO. A-30270
5. REMOVE YELLOW AND WHITE LEADS FROM CONVERTER MODULE A2 AND REPLACE WITH SHIELDED CABLE, B-30285, CONNECT RED LEAD TO E1 AND WHITE LEAD TO E2 OF CONVERTER.

QUANTITY		PART/DWG NO.	DESCRIPTION	ITEM
				19
1	1	B-30285	SHIELDED CABLE	18
1	1	C-30270-1	SHIELD	17
1	1	A-30328	PROTECTIVE MYLAR	16
1	1	A-30327	CONVERTER SHIELD	15
2	2	A-30325	PROTECTIVE SHEET	14
1	1	B-30232	CONNECTOR PLATE	13
1	1	SMRE 75J	CONN FEMALE WINCHESTER	12
1	1	SMRE 7PJ	CONN MALE WINCHESTER	11
1		C-60037	FILTER LOW PASS A4	10
1	1	B-60035	MOTHER BOARD A1	9
1	1	C-60038	SECOND AMPLIFIER A5	8
	1	C-60024	FILTER LOW PASS A4	7
1	1	C-60048	DC/DC CONERTER A2	6
	1	C-60052	FIRST AMPLIFIER A3	5
1		C-60034	FIRST AMPLIFIER A3	4
X	X	C-80045	SCHEMATIC DC/DC CONV	3
X		C-80041	SCHEMATIC-SYSTEM	2
X	X	C-80039	SCHEMATIC-SYSTEM	1

MATERIAL LIST

MODEL 370B / MODEL 370A

BOLT BERANEK & NEWMAN INC.

TOLERANCES EXCEPT AS NOTED: DECIMAL ±.005; FRACTIONAL ±——; ANGULAR ±——

SCALE 4/1

TITLE TRANSITION DETECTOR (CONFIG 2) POTTED ASSEMBLY

DATE 14FEB68

DRAWING NUMBER D-20038

"DO NOT SCALE DRAWING"

Figure IV-9 ASSEMBLY DRAWING

DATE	SYM	REVISION RECORD	AUTH.	DR.	CK.
12/67	A	RELEASED	BTB	MF	MR
1/69	B	INCORP E.C.N 3	BTB	MF	MH
1/69	C	INCORP ECN 9	BTB	DD	MH
9/69	D	INCORP ECN 17	BTB	MF	MH

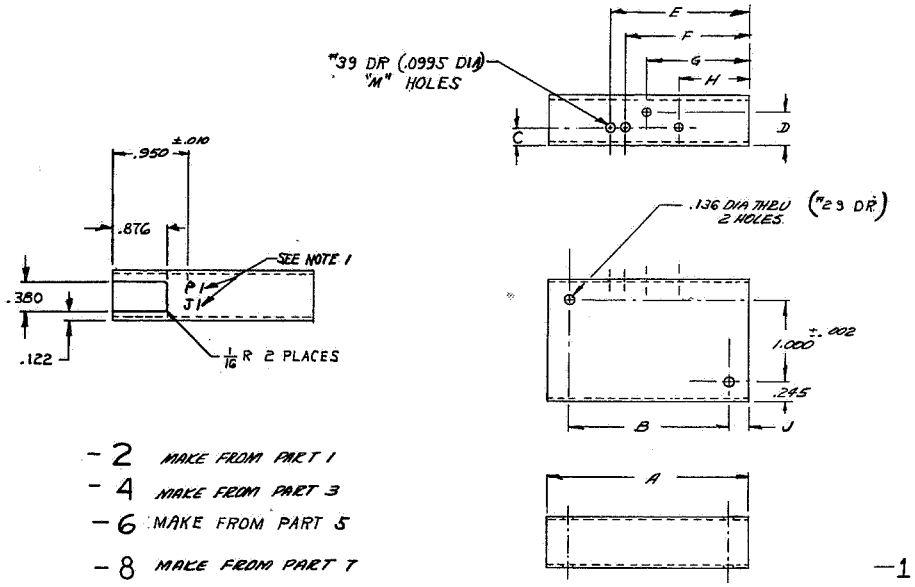

-2 MAKE FROM PART 1
-4 MAKE FROM PART 3
-6 MAKE FROM PART 5
-8 MAKE FROM PART 7

-1 -7
-3
-5

TABLE I

PART	A	B ±.002	C	D	E	F	G	H	J	K	L	M	APPROX WEIGHT	
-1	2.450	2.000	.200	—	1.690	—	—	—	.230			1	.0044 lbs	TRANS. DET. MOD. 370
-3	3.650	3.100	.315	—	3.095	2.925	—	1.620	.230			3	.0062 lbs	PRESS. SYS. MOD 360 C,D
-5	3.550	3.100	.315	.315	2.790	2.610	2.430	1.620	.230			4	.0062 lbs	PRESS. SYS. MOD 360 B,E
-7	3.800	3.100	.315	.420	2.770	2.590	2.300	1.610	.480			4	.0062 lbs	PRESS. SYS. MOD 360 A

NOTE:

1. ENGRAVE P1, J1 1/8 HIGH LETTERING APPROX AS SHOWN FILL WITH WHITE LACQUER STICK AFTER FINISH.
2. ASSEMBLE AND FINISH HOUSING PER DWG C-30283 TYPICAL FOR ALL HOUSINGS.

QUANTITY									MATERIAL LIST		
								C-30283	HOUSING ASSY & FINISH	2
4 IN	4 IN	3 11/16 IN	3 5/16 IN	3 5/16 IN	3 5/16 IN	2 3/16 IN	2 3/16 IN	C-30230	EXTRUSION	1
-8	-7	-6	-5	-4	-3	-2	-1	DWG PART NO.	DESCRIPTION	ITEM

MINIATURE PRESSURE SYS MODEL 360A (STRAIN GAGE) (EXTENDED CASE)
MINIATURE PRESSURE SYS MODEL -360B,E (CRYSTAL)
MINIATURE PRESSURE SYS MODEL - 360 C,D (STRAIN GAGE)
TRANSITION DETECTOR MODEL - 370

TOLERANCES (EXCEPT AS NOTED)	BOLT BERANEK AND NEWMAN INC.		
DECIMAL ± .005		SCALE FULL	DRAWN BY N Smith
FRACTIONAL ± 1/64	TITLE HOUSING		APPROVED BY
ANGULAR ± 1/2°	DATE 7 OCT 67	DRAWING NUMBER C-30231	

K+E ALBANENE © 10 BASE

Figure IV-10 PACKAGING DRAWING

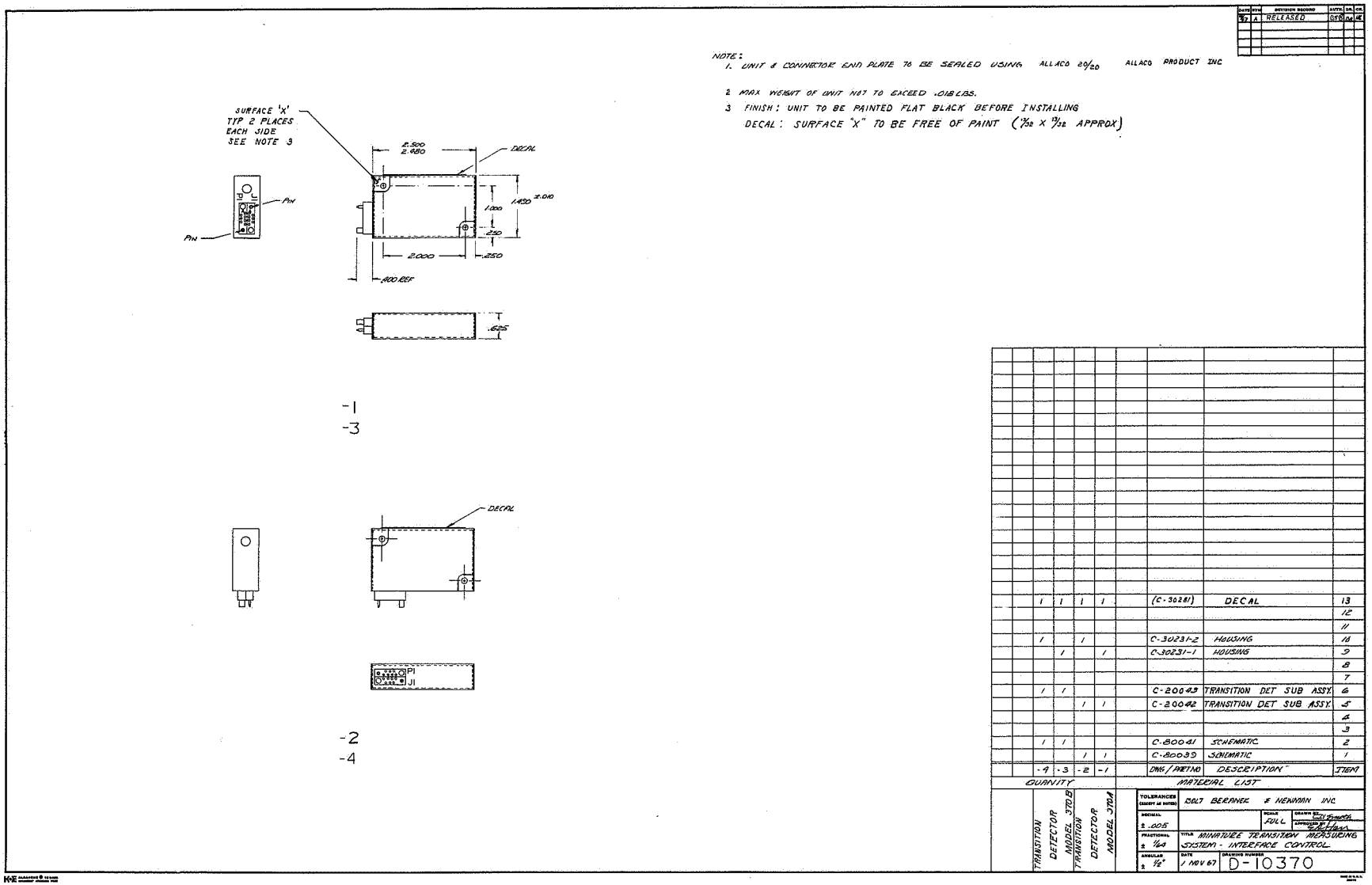

Figure IV-11 INTERFACE DRAWING

Figure IV-12 ELECTRONIC PACKAGE PHOTO

V. TEST PROGRAM

A. Acoustic Coupler Evaluation

The proper design and function of the acoustic coupler (porting arrangement) that provides the direct communication between the boundary layer and microphone is of utmost importance. The relatively extensive test program specifically designed to evaluate the acoustic and mechanical aspects of the port reflect its critical role. The test program was implemented by the integrated use of facilities at BBN, Avco and MIT.

1. Wind Tunnel

A wind tunnel study of flow transition was accomplished in the MIT Naval Supersonic Wind Tunnel at Mach 3 to assess the influence of blocked ports on the generation of turbulence and characterize the spectrum of laminar, transitional and turbulent flow. A flat plate one inch thick with a leading edge angle of 15 degrees and sharpness of 0.002 inch radius was installed in the wind tunnel (figure V-1). The planform of the plate and instrumentation is detailed in figure V-2. The combination of hot-wire probes and flush mounted microphone was chosen to conclusively define the various flow regimes and study the onset of transitional flow. Diagnostic sensors consisted of a model 4636 vibration pickup mounted at the center pylon and static pressure taps along the trailing edge of the plate.

The vibration pickup confirmed that the test plate vibration was at least 30 db below the useful signal levels and the pressure taps allowed the determination of Mach-number distribution across the plate. It should also be noted that the microphones located 3 inches from the tunnel wall appeared to be influenced by the wall and consequently the data are not presented in this report. A complete discussion of these data and other subsidiary experiments is presented in reference 13.

The turbulence over the plate was controlled by changing the tunnel stagnation pressure (variable from 1 to 30 psia) and hence the transition point from the plate leading edge. Starting at the leading edge, a laminar boundary layer builds up that gradually increases in thickness. At a certain distance downstream from the leading edge, the boundary layer becomes unstable and intermittent outbursts of turbulence occur. The number of the turbulent outbursts per time unit increases in the downstream direction and, finally, the flow becomes turbulent. The intermediate phase between

laminar and turbulent flow is called the transition range. The first spacial onset of transitional flow and the extent of the transition range depend primarily on a Reynolds number composed of the distance from the leading edge, a typical flow speed (usually freestream speed), and the kinematic viscosity of the gas. The transition Reynolds number varies with the Mach number. The transition Reynolds number as a function of freestream Mach number, as reported by various experimenters[15], for both smooth and roughened tips of bodies of revolution, is shown in figure V-3. Figure V-4 gives results for similar experiments under conditions of no pressure gradient[16].

From these two figures, one should expect flow transition starting at a Reynolds number of $0.8\text{-}1.2\times10^6$ and to see turbulent flow at a Reynolds number of $2.0\text{-}2.8\times10^6$ for a Mach number of 3. Using the boundaries for the expected transition range (namely, $Re=0.8\times10^6 - 2.8\times10^6$) the range of flow transition on a test plate was determined for the conditions in the MIT Wind Tunnel. The per-foot Reynolds number of the MIT Wind Tunnel at M=3 and a stagnation temperature of 100°F is

$$Re_{\text{per foot}} \approx 0.115 \times 10^6 P_{\text{stag}},$$

where P_{stag} is the tunnel stagnation pressure in psi. Figure V-5 shows the transition range plotted in terms of the distance from the leading edge as a function of tunnel stagnation pressure.

The simulated ports used to assess the possible premature triggering of transition by the hole itself are depicted in figure V-6. The diameter of the holes was selected to be compatible with typical porting arrangements. It was also considered necessary that the boundary layer displacement thickness as compared with the hole diameter be comparable or greater than the anticipated flight relationship. Table V-1 illustrates that the displacement thickness, 8 inches downstream of the plate leading edge, is considerably thinner than the flight condition for either the typical NASA vehicle or several typical Endo-Decoy vehicles. This obviously causes the test to be very conservative.

A qualitative measure of the boundary layer thickness is provided by figure V-7 which is a typical example of one of the Schlieren photographs taken during the tests. The photo, taken at a stagnation pressure of 12 psia, shows the tunnel-floor boundary layer (dark area) and the tunnel ceiling boundary layer (light area), both with a thickness on the order of 1 inch.

TABLE V-I

DISPLACEMENT THICKNESS COMPARISON

	Tunnel Stagnation Pressure (psi)		
	5	15	25
Turbulent Displacement Thickness δ^* (in.)	0.09	0.07	0.06

Typical Endo-Decoys	Aft Cone		
Transition Altitude (kft)	80	70	90
Displacement Thickness δ^* (in.)	0.325	0.5	0.48

	Station (distance from tip in ft.)	
Typical NASA Vehicle	2.85	1.0
Flight Altitude (kft)	135	110
Displacement Thickness δ^* (in.)	0.702	0.365

These shaded areas do not necessarily represent the actual extent of the boundary layer. In other words, it is not possible to determine the exact boundary-layer thickness, or displacement thickness, from such a flow visualization. The boundary layer on the test plate (dark area) is discernible as it develops and increases in thickness in the downstream direction. Both the forward measuring location (8 in. downstream from the leading edges) and the predicted onset of transitional flow are marked in the figure. The transitional range at 12 psi should extend from 7 in. to 24 in. downstream from the leading edge. It is, however, very hard to visualize the expected sudden increase in boundary-layer thickness at the predicted distance from the leading edge; although, there is an apparent increase in the thickness of the dark area above the test plate at 8-10 inches. We should keep in mind that: (1) transition does not necessarily occur at one distinct line across the test plate, rather, it occurs quite irregularly; and (2) our view is across the entire 18-in. -wide test plate and, thus, through the boundary layer extending the same width, so that we obtain an integrated view of the flow. If we assume that the dark area above the test plate gives us a measure of the boundary-layer thickness, then we can estimate that the boundary-layer thickness towards the trailing edge (region of turbulent flow) of the plate is about 1/4 inch. If we further assume that the displacement thickness is about 1/3 of the boundary-layer thickness, then the turbulent-displacement thickness, which was calculated to be approximately 0. 08 in. , is of the right order of magnitude.

The test setup and flow conditions as previously discussed were utilized for two major experiments: 1) the characterization of laminar and transitional flow and 2) the assessment of the effect of the port on inducing turbulence in the flow. The possible contamination of data from the aft microphone (wall interference)* required an additional experimental configuration to characterize the turbulent flow. A test plate that formed part of the tunnel bottom wall in the test section was exposed to turbulent Mach-3 flow. The installation (figure V-8) utilized a half-nozzle block with artificial roughness to establish supersonic turbulent flow across the test plate. Five B and K 1/2-in. -diameter microphones were flush-mounted to the surface of the test plate in a row perpendicular to the flow and approximately five feet from the leading edge (see figs. V-8 & V-9). The Schlieren-optical photograph of the flow along the test plate at P_{stag}= 10 psi (figure V-10) shows the turbulent boundary layer as a dark region on top of the test plate. The boundary layer is much thicker than on the transition test plate (figures V-7 and V-10 are of equal scale). The displacement thickness was calculated to be approximately 0. 22 inch.

*Additional diagnostic measurements of tunnel background noise and pressure distribution across the tunnel are provided in reference 18.

The initial experiment of flow characterization utilized the test plate illustrated in figure V-1 prior to the simulated ports being drilled in it. The turbulent flow study was conducted with the test arrangement shown in figure V-8. Data from the hot wire probes and flush mounted microphones were both analyzed to characterize the laminar and transitional flow. A hot wire probe is capable of sensing small scale velocity fluctuations due to its small dimensions. In addition, a hot wire responds primarily to fluid-flow fluctuations and is rather insensitive to acoustic disturbances whereas a microphone picks up both acoustic noise and pressure fluctuations resulting from flow across its diaphragm. Consequently, the hot wire studies were invaluable for the definition of flow regimes and the determination of the onset of transitional flow. The hot wire data were especially helpful in interpreting data obtained simultaneously by flush-mounted microphones. The investigation of the flow field by means of microphones, of course, was necessary since the transition detector incorporates such an acoustic device. Furthermore, we were interested in the characteristic signals for the different flow regimes, as obtained through a microphone.

Figure V-11 presents hot wire signals analyzed in 1/3-octave bands for various tunnel stagnation pressures. Here, the hot wire probe responded to undisturbed flow. Since it was not possible to calibrate the hot wire probes in supersonic flow, the data is presented in relative levels. The most striking feature of these data is the cluster of spectra for stagnation pressures from 2-10 psi followed by the sudden level increases up to 20 psi. Evidently, the range below 10 psi constitutes the laminar-flow regime (or, more accurately, the flow regime with an extremely low degree of turbulence since in the oncoming flow there will always be some unavoidable turbulence). Consistent with the predictions from figure V-5, transitional flow sets in above 10 psi and the spectra at 15-20 psi do represent the onset of turbulent flow. This interpretation is confirmed by the display on the oscilloscope screen, where velocity fluctuations appear as a function of time. The overall hot wire signal is presented in figure V-12 as a function of time for various stagnation pressures. One unit on the time scale corresponds to 1 msec. Figure V-12a represents single-sweep signals, whereas figure V-12b shows an integrated display of several sweeps over approximately 1 sec. Note that the gain was decreased by a factor of 10 (for voltage) for 15 and 20 psi as compared to the data at 2, 5, and 10 psi.

At 10 psi (single sweep) we find only one turbulent spike during the period of display, whereas, at 15 psi, and more so at 20 psi, the number of turbulent spikes has increased considerably so that we may consider the flow at 20 psi to be almost fully turbulent. The corresponding result is obtained with the prolonged display of the signals in figure V-12b.

The flush mounted microphone data for the identical flow field were analyzed in one-third octave bands for the various tunnel stagnation pressures. Data from the three microphones, shown in figure V-2, are depicted in figures V-13, V-14 and V-15. The apparent increase in level in the 20 kHz band is due to the change in mechanical damping of the B and K 1/2-in. -diameter condenser microphones for decreased, ambient static pressure (see figure V-16). In the test section, there is a decrease in static pressure to only about 3% of the tunnel stagnation pressure at a Mach number of 2. 9.

The data have been normalized with a common tunnel stagnation pressure (e. g. 10 psia) and the spectra plotted as

$$\text{FPL} - \left(20 \log \frac{P_{stag}}{P_{stag_{ref}}} \right) \quad \text{versus frequency.}$$

This relatively simple normalization was considered adequate since the Mach number and displacement thickness were essentially constant throughout the test series for a given measurement location. Consequently, it was not necessary to normalize the fluctuating pressures with the dynamic pressure or to non-dimensionalize the frequency by means of the Strouhal number in order for a particular flow regime to collapse as shown in Figure V-17. Three different clusters of normalized spectra may be identified as follows:

1) The spectra for 2 and 3 psi show a flat peak somewhere between 500 and 1000 Hz, representing the highest (normalized) levels in this plot. Strong low-frequency acoustic disturbances, associated with tunnel operation, dominate the spectra at these low stagnation pressures. (Later measurements, in a different context, for turbulent flow confirmed this finding).

2) The spectra for 5 and 10 psi collapse in this normalized plot, and, according to the findings of the hot-wire study, we may safely assume that they represent the laminar flow-regime. For true laminar flow across a pressure transducer, there should be (in theory) no signal at all. It is, however, very likely that the microphone, at these stagnation pressures, senses (a) the tunnel generated oncoming flow turbulence and (b) the acoustic radiation from the side-wall and ceiling-wall turbulence. The boundary layer, along the four tunnel walls, is certainly turbulent at the test section and may act as an efficient acoustic radiator.

3) The spectra for pressures exceeding 10 psi show a significant increase in their levels indicating the onset of transition. The cluster of spectra for 20 and 25 psi probably represents the highest levels achieved during flow-transition. This pattern conforms with that found in the hot-wire studies.

The data from the turbulent experiment (test setup illustrated in figure V-8 and V-9) are presented as one-third octave fluctuating pressure spectra depicted by figure V-18. The spectra are enveloped for the 10 and 20 psia levels obtained from all five microphones. To compare the data obtained during turbulent flow with the data obtained during the flow-transition test, we must keep in mind that the displacement thicknesses were different in these two tests. Hence, the peak frequency of a turbulent-boundary-layer spectrum depends on the freestream flow speed U and the displacement thickness, such that

$$f_{peak} = S(U/\delta^*)$$

where the Strouhal number S is constant. The flow speeds in the two tests were equal, whereas the displacement thicknesses differed by a factor of about $0.22/0.08 \approx 2.75$. Although the peaks of the spectra in both tests were beyond our measurement range, we can compare the spectra by merely shifting them apart by a factor of 2.75 on the frequency scale.

A comparison of transitional and turbulent flow based in part on the above rationale is provided in figure V-19. The figure is a composite showing the normalized spectra for 20 and 25 psia from figure V-17 that represent the highest level transitional spectra achievable for the test arrangement. These data cannot be compared directly to the normalized turbulent spectra from figure V-18 since the boundary layer displace thickness is considerably different between the two sets of data. Consequently, we must shift the spectra as described above by a factor of 2.75 in terms of frequency to compare the levels on the basis of an equal displacement thickness (0.08 inches). The decrease in displacement thickness shifts the spectra toward higher frequencies and lowers the level for a given frequency band. Figure V-19 indicates that the levels for turbulent flow in equivalent bands are approximately 10 db lower than transitional levels when compared on the basis of equal boundary layer displacement thickness.

In conclusion, the characterization of the laminar, transitional and turbulent boundary layer in supersonic flow indicates a rapid increase in fluctuating pressure level as transition approaches with peak levels occurring during transitional flow. The level decreases by approximately 10 db

after turbulent flow is established. This apparent level increase during transitional flow may be caused by the sudden increase in boundary layer thickness accompanying transition with attendant shock induced oscillation accounting for the increased fluctuating pressures in the measurement range (i. e. <10 KHz). The onset of transition is characterized by turbulent bursts that occur more frequently as the transitional phase progresses. The spectrum shape of the pressure fluctuations during the transitional phase is apparently very similar to that of turbulent flow with essentially a flat spectral density of very broadband energy.

The previous discussion established the characteristics of laminar, transitional, and turbulent flow as measured both by flush-mounted microphones and hot-wire probes. The second important question as described earlier was to find if a hole of appropriate size in the test plate disturbs the laminar flow in such a way that transition is prematurely induced.

Comparison of the normalized spectra obtained from the center microphone (figure V-20) sensing flow that has passed an upstream hole with the data obtained prior to the hole being drilled (figure V-17) indicates no difference in these data. Premature triggering of flow transition by the upstream hole would have caused the level increase shown to be typical for transition onset at a lower tunnel stagnation pressure. This result is corroborated by the hot-wire probe that measured the characteristics of the flow after passing over the upstream hole (see figure V-6). Comparison of the data in figures V-11 and V-21 indicate that the level increase typical of transition onset occurs at the predicted stagnation pressure of 10 psia independent of the upstream hole. The incremental difference between the 15 and 20 psia spectra in the figures compared above are different by slightly less than 5 db. This disagreement may be the result of a slightly different height of the two hot-wire probes used to accomplish the measurements.

Consequently, it was concluded that upstream holes of practical size do not prematurely trigger flow transition. There was, however, still a possibility that this experiment was not conclusive since any disturbance generated at the hole might decay prior to reaching the sensing element. To preclude this possibility, an experiment utilizing a configuration very similar to the transition detector was accomplished to directly sense the flow at the port. If the port disturbed the flow, the simulated transition detector would respond differently from a flush-mounted microphone with no upstream flow disturbance. Since the typical response of a microphone to transitional flow had been characterized the experiment could be accomplished with confidence.

The response of the experimental transition detector to the flow field on the test plate is presented in figures V-22 (raw data) and V-23 (normalized data). The normalized data (neglecting the 3 psia spectrum that has been degraded by tunnel acoustic disturbances) displays the characteristic laminar flow regime composed of the 7 and 10 psia spectra. The 12 psia spectrum is generally slightly higher suggesting the onset of transition and the 15 psia spectrum clearly indicates the transitional regime. The 20 and 25 psia spectra are clearly in a range of highly turbulent flow. The peak in the raw data spectra at 8 KHz is apparently caused by a mechanical resonance within the experimental detector configuration since it occurs at a specific frequency (although with different levels) independent of the stagnation pressure and the particular flow regime.

The experiments conducted with simulated ports and an experimental transition detector configuration indicate that the presence of the hole does not generate premature turbulence. This conclusion must be restricted to the frequency range over which the measurements were taken ($\sim$10 KHz) and should not be used indiscriminately for flight conditions (primarily boundary layer displace thickness) significantly different from those discussed in this report.

2. Arc Facility

A study of the acoustic coupler and crystal microphone (BBN Model 370) was conducted in the Avco 10 MW Arc facility. The test was accomplished primarily to verify that adequate protection is afforded the transducer by the relatively simple acoustic coupler and that the nylon-phenolic heat shield material does not ablate in a manner that blocks the port. A secondary consideration of the test was determination of temperature in the straight portion of the port and the comparison of spectra from the transtion detector transducer with similar data obtained by a standard laboratory microphone.

The test specimen is detailed in figure V-24 which shows the two thermocouples used to obtain gas temperature in the straight portion of the ports and a third thermocouple to obtain the heat shield backface temperature over the general area of the microphones. A fourth thermocouple was included as an integral part of the BBN Model 370 crystal microphone to detect the gas temperature immediately forward of the transducer heat shield. The thermocouples all incorporated miniature sensing elements to avoid thermal lag and preclude blockage of the port by the protruding thermocouples in the straight tube section. The two microphones shown in their side by side mounting arrangement conclude the test instrumentation except for still and cine (64 frames per second) photography. The test specimen was mounted at a ten degree angle as referenced to the arc exit as shown in figure V-25.

The reference flight conditions for the transition-ablation vehicle mission have been previously reported in reference 6. The primary parameters to be simulated in the arc were a final ablated depth of 0.08 inches and a total integrated heating of approximately 10,500 BTU/ft^2. The actual test conditions were:

a) $\dot{q}$ = 885 BTU/FT^2 - Sec
b) Hs/RTo = 208
c) plenium pressure = 6.725 atmosphere
d) air flow through the arc = 0.304 lb/sec
e) run time = 12.15 seconds
f) Qc = 10,750 BTU/FT^2

In order to achieve the required integrated heating, it was necessary to increase the heating rate from the desired reference flight condition value. This dictated a shorter test run time from that previously specified. The higher heating rate produced a corresponding higher shear level which caused more surface recession than expected. This resulted in a more severe test than planned which suggests that the results of the experiment are conservative by a significant margin.

This impression of conservatism is reinforced by a test anomaly revealed by the high speed cameras. The film shows what appears to be a shock wave traveling from its initial point of occurrence at the interface of the sample and the arc to essentially the downstream end of the test specimen. The shock is apparently generated by a discontinuity resulting from ablation of the sample (initially very close to the arc exit) which progressively moves downstream. A significant amount of ablation erosion takes place downstream of the shock which visually appears as though the shock was forcing the material downstream. The progression of material removal associated with the shock front is illustrated by segemnts of the cine film (figures V-26a through V-26d) extracted at intervals from the total coverage. The shock passes over the ports at approximately 8.4 seconds into the run and apparently forces hot gases into the holes as described later in the discussion of the temperature measurements. The abrupt change in overpressure was apparently sufficient to rupture the diaphragm of the B & K condenser microphone used as the reference sensor for obtaining fluctuating pressure spectra.

The mechanical evaluation of the heat shield and acoustic coupler in terms of ablation and port blockage will be discussed first to provide both an indication of the severity of the experiment and the appropriate portion of the post-test analysis. A qualitative indication of the extent of char and material removal is provided by figures V-27 and V-28 which show respectively the pre and post-test condition of the specimen. The ablated sample shows some char remaining on the surface, however, the majority of the severely degraded material has been sheared off (average shear was approximately 38 lb/ft^2). The ports show some evidence of aggravation and it is apparent that more surface recession has occurred in the center of the nylon-phenolic than at the forward or aft ends. The measured surface recession at the edges and center of the heat shield is provided in figure V-29. The data illustrate the severity of the test since the measured recession is approximately a factor of three greater than the recession required to simulate the transition-ablation vehicle reference mission. Further examination of the test specimen after removal of the two microphones indicated that the ports were not blocked, however, a small amount of tacky dark residue was deposited on the B & K microphone face. This deposit is apparently an ablation product of the heat shield that was carried into the port as a vapor either during or immediately after the test.

Valid temperature data were obtained during the test from all four thermocouples. These will be designated numerically to facilitate discussion of the analysis: TC-1 and TC-2 were located across the holes at the heat shield structure interface (0.75 inches from the surface) with ranges of 0-1600°F and 0-200°F respectively in order to accurately monitor a large variation of temperature. TC-3, with a range of 0-200°F, was located above the transition detector between the heat shield and aluminum structure to record the temperature due to heat conduction through the nylon-phenolic material. TC-4 was located just ahead of the crystal microphone heat shield in order to measure the temperature environment close to the sensing element. This thermocouple, with a range of 0-100°F, protruded from the transducer heat shield approximately 50 mils into the center of the cavity immediately forward of the transducer. This location places it approximately 1.12 inches from the upper surface of the nylon-phenolic heat shield. The accuracy of these instruments are 0.5 percent of full scale and the data were recorded at a rate of 20 samples persecond.

The temperature measurements are presented in figures V-30 and V-31. The temperature at the midpoint of both tubes started to rise at arc initiation with TC-2 rising at the faster rate and going off scale (200°F) at approximately 7.4 seconds. It is interesting that TC-2 leads TC-1 throughout the test even though both sensors were located at the same depth in the holes. This difference may be attributed to differences in the thermal environment at the port location due to uneven flow as well as non-symmetric ablation and erosion.

Inspection of data from TC-1 indicates an abrupt temperature rise at 8.4 seconds (approximate time of shock passage) from about 110 to 350°F that is characterized by a double peak and rapid decay to 250°F at the time of arc termination. The data from TC-4, associated with the transition detector transducer, indicates a very slow rise involving only a few degrees Fahrenheit until passage of the shock wave over the ports. The abrupt rise of TC-4 during shock passage was from about 71 to 79°F or a temperature attenuation of a factor of 30 when compared with the mid tube location. This is further illustrated by the cross-plot of TC-1 and TC-4 at selected times as provided by figure V-32. TC-3 installed for diagnostic purposes and located at the backface of the heat shield showed a negligible rise as expected throughout the test.

The conclusions to be drawn from analysis of the temperature data are that a simple acoustic coupler provides significant thermal attenuation of the external environment. In addition, it is apparent that an insulating sensor mounting arrangement to protect against heat conducted through the material is not necessary if a reasonable amount of nylon-phenolic is used for thermal protection of the vehicle.

The secondary objective, comparison of spectra from the transition detector with similar data from a laboratory microphone, was not achieved as a result of malfunction of the Bruel and Kjaev 4135 microphone used as the reference. The fact that the piezoelectric crystal microphone (BBN Model 370), which is one of two selected as most desirable, survived the severe environment that destroyed the reference microphone indicates that the original decision to avoid condenser microphones as a sensor for the transition detector was correct. It also provides confidence that the transducer will function in the reentry environment.

The basic acoustic test concept, failure analysis of the reference microphone and spectra from the BBN Model 370 microphone are provided for general information. The original test concept of spectra comparison from the two microphones required that the acoustic characteristics of the acoustic coupler/microphone combination be identical. This was achieved by exposing the two configurations to a purely acoustic field and a subsequent equalization of their frequency responses. This equalization was obtained by changing the volume of the microphone cavity (volume directly above the microphone diaphragm) until both configurations showed the same basic resonance frequency. After this procedure the basic resonance frequency in both configurations occurred at 1010 Hz ± 2 Hz. It is of interest to note that dependence of the resonance frequency of the configurations to volume changes of the microphone cavity. Table V-II shows various microphone cavity depths (in 10^{-3} inches) and corresponding resonance frequencies for one configuration (the BBN Model 370 microphone). The diameter of the microphone cavity was, of course, constant and equal to 0.255 inch.

TABLE V-II

RESONANCE FREQUENCY DEPENDENCE

Cavity Depth (10^{-3} in.)	Resonance Frequency (Hz)
10	1090
16	1057
22	1023
31	1003

The overall signal output of both microphones was fed to a tape recorder (Kudelski, type NAGRA III-B) vianan amplifier (GR, SLM type 1551-B) and recorded during the arc test. The data were later analyzed in octave bands. Figure V-33 shows octave band spectra of the signal output of the BBN piezoelectric microphone. Two spectra are given, one typical for the first few seconds after the onset of the arc jet, and one for the highest levels observed during the run (approximately at the midpoint of the run). The highest overall levels observed were about 165 db re 2.10^{-4} μ bar. Since reference data were not obtained, the spectra can only be considered in a qualitative sense. Comparison of the overall level with previously obtained data[17] taken at a short distance from the arc during a somewhat similar test indicate that the level (figure V-33) is higher as would be expected since the microphone is directly coupled to the flow. In addition, the data is relatively smooth and consistent throughout the run indicating proper operation of the microphone in a qualitative sense.

The B & K Model 4135 microphone used as the reference was functioning properly just prior to arc operation but ceased to function immediately at arc on. It is possible that the very strong magnetic field (quantative field strength not known) prevented the microphone from functioning and that the overpressure associated with passage of the shock burst the diaphragm. In any event, we do not believe that temperature on the diaphragm contributed to failure of the microphone since the microphone can operate up to 250°C on an intermittent basis with no damage.

B. Measurement System Evaluation

Two hardware end items have been delivered under NAS 1-7439; an engineering prototype and a packaged production system. Both have been evaluated to determine performance characteristics and the packaged unit has been exposed to shock and vibration. The test results from the following hardware evaluation are presented to verify the design and delivered hardware:

a) selected models of the transducers,
b) temperature data on the prototype signal conditioner,
c) quality control tests on the packaged system, and
d) environmental exposure of the complete system.

Vibration data from two samples of the Avco CT-4S transducer are shown in figure V-34. The electrical noise floor of these transducers is shown in figure V-35 in third octave bands, along with the measured absolute sensitivity.

The variation of sensitivity with temperature for the CT-4S transducer is provided in table V-III. A pistonphone was used to provide 124 db SPL at 250 Hz.

TABLE V-III

TEMPERATURE SENSITIVITY

Temperature	Voltage Out
60°C	-52. 1 db V
50°C	-52. 1 db V
40°C	-52. 1 db V
30°C	-52. 05 db V
20°C	-52. 05 db V
10°C	-52. 05 db V

The experiment was not conducted at lower temperatures because the sound source does not operate reliably below freezing.

The operation of the breadboard signal conditioner alone was measured from 5°C to 60°C. The results are shown in figure V-36. All data were within ±4 db, and the frequency response curve was essentially constant.

The packaged signal conditioner and transducer have been evaluated via the quality control procedure contained in reference 1. These tests and results are provided in the completed quality acceptance procedure that has been delivered with the hardware. Included in the tests are exposure to temperature at 140°F and random octave bands of vibration equivalent to . 01 g^2/Hz, followed by a re-test of the electrical characteristics.

Finally, the complete packaged system was exposed to the environments of table V-IV, as required by the NAS 1-7439 statement of work. The system survived all tests and met specifications after the exposure. System performance during the temperature test is shown in figure V-37 where output bias, signal conditioner gain variation, and system sensitivity (including the transducer) are given. The temperature rise of the case when operating in vacuum is shown in figure V-38. The total temperature rise was 4°C in an hour.

In summary, the system has been exposed to severe environments and many hours of testing during which it has performed reliably and maintained characteristics well within the requirements for the system.

TABLE V-IV

ENVIRONMENTAL TEST PARAMETERS

Environment	Specification	Test
Temperature (operating)	$-10^{\circ}C$ to $+60^{\circ}C$	$10^{\circ}C$ steps, 30 minutes at each step
Pressure (operating)	2×10^{-6} torr	1 hour
Vibration Sinusoidal	15Grms, 20-200Hz, 0.8 in DA max, 25Grms, 200-2000Hz	3 orthogonal axes 2 octaves/minute
Sustained Acceleration	100G	2 ways each on 3 orthogonal axes 120 seconds each way
Shock	150G	half cosine pulse, 5-15 ms. 3 shocks each in 2 directions each on 3 orthogonal axes (18 shocks in all)
Vibration Random	$0.31\ G^2/Hz$ 20-2000 Hz (equivalent to 25Grms 20-2000 Hz)	by octave bands, 120 seconds each band each of 3 orthogonal axes. Band — Level 31Hz — + 9dBg 63Hz — 12dBg 125Hz — 15dBg 250Hz — 18dBg 500Hz — 21dBg 1kHz — 24dBg 2kHz — 27dBg

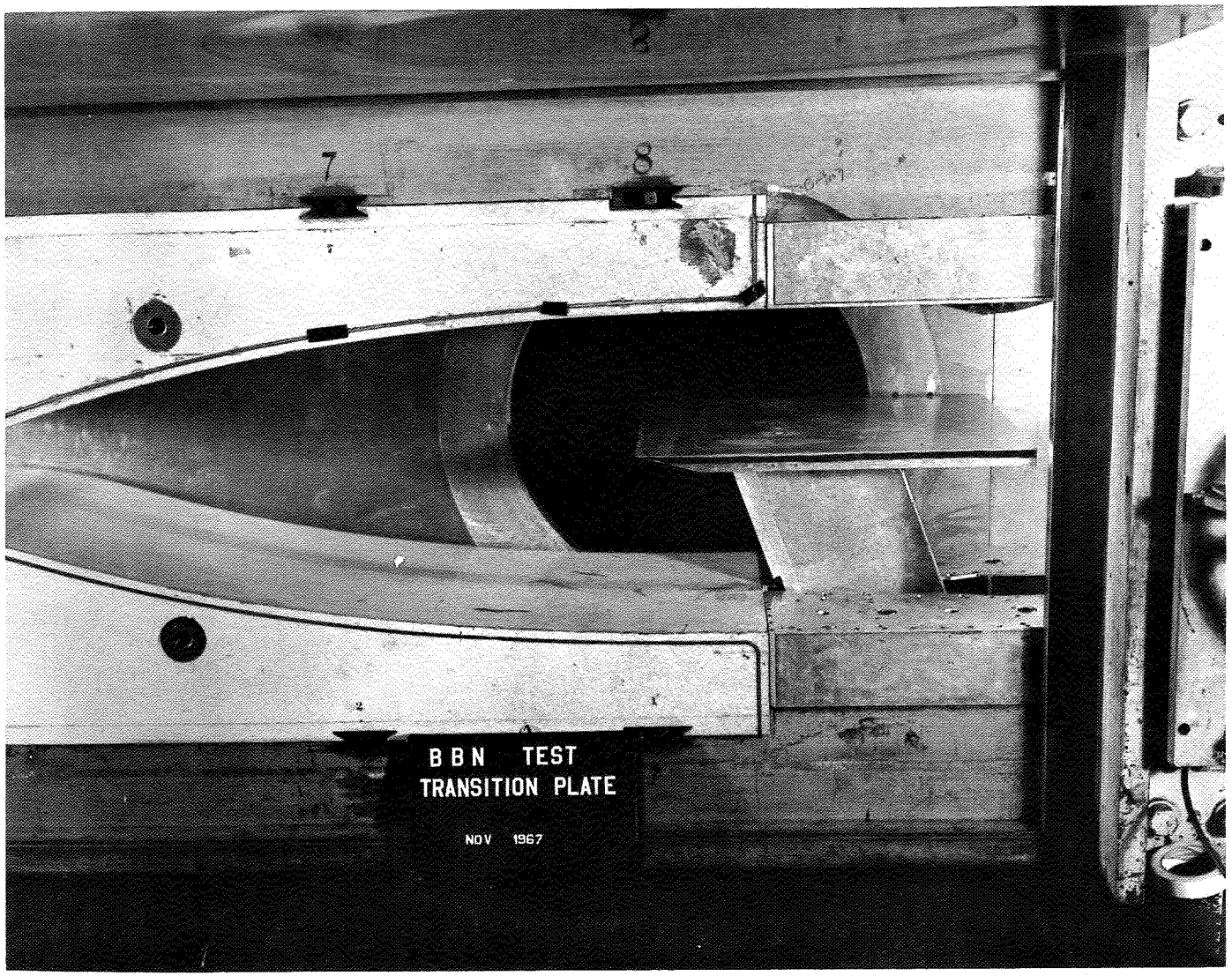

Figure V-1 TRANSITION TEST PLATE INSTALLED IN THE TUNNEL TEST SECTION

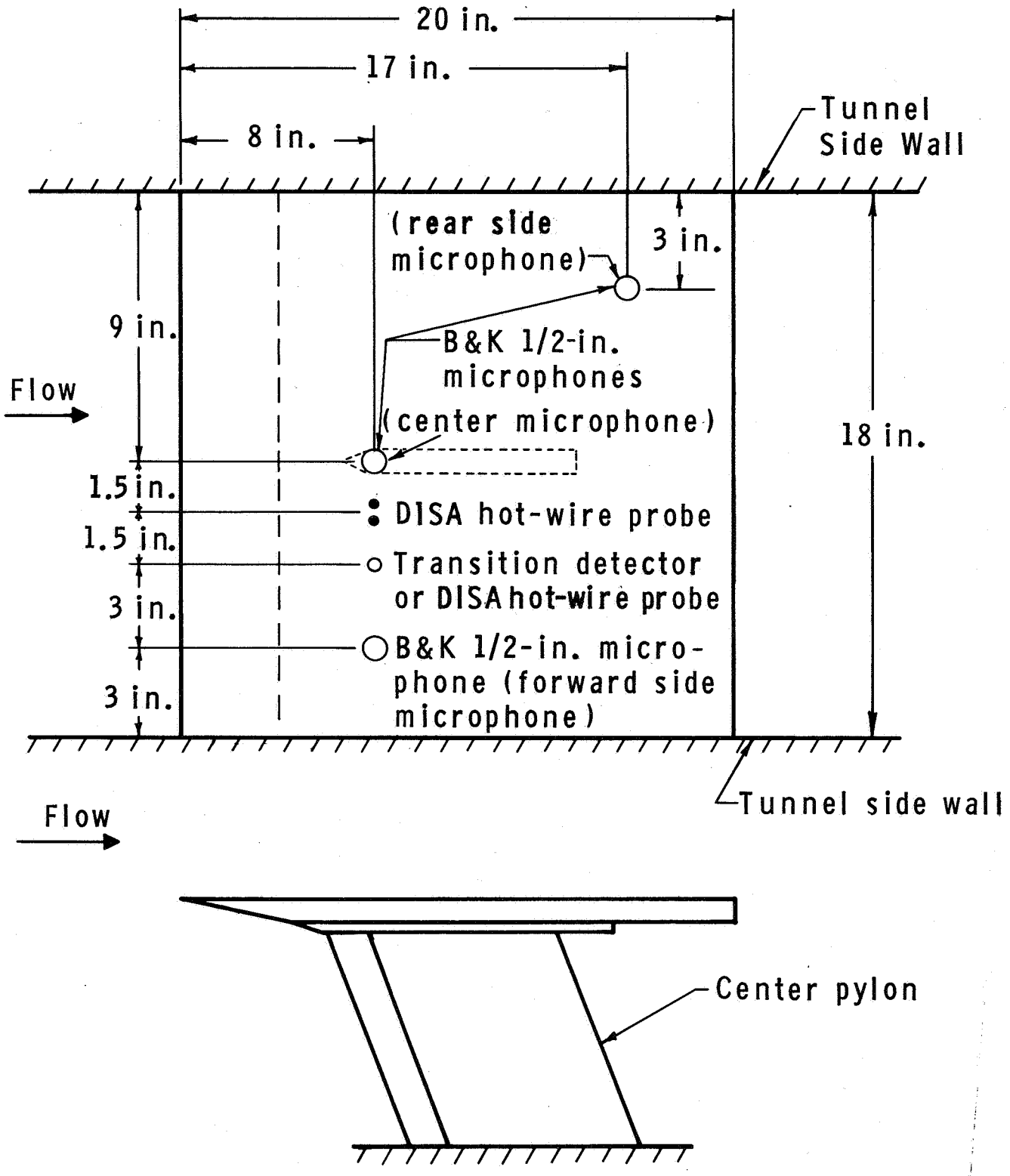

Figure V-2 TRANSITION TEST PLATE PLATFORM

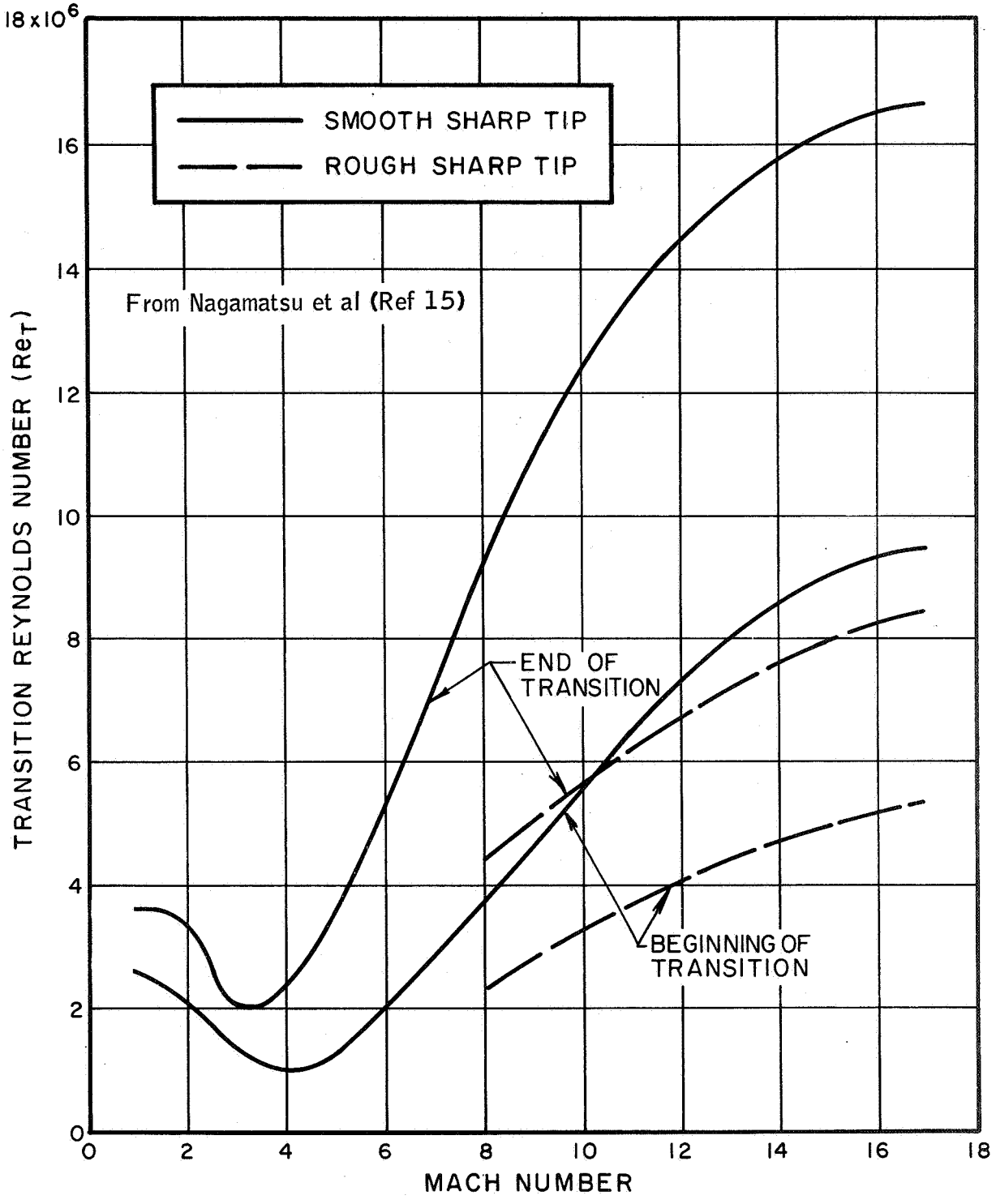

Figure V-3 TRANSITION REYNOLDS NUMBER VERSUS FREESTREAM MACH NUMBER

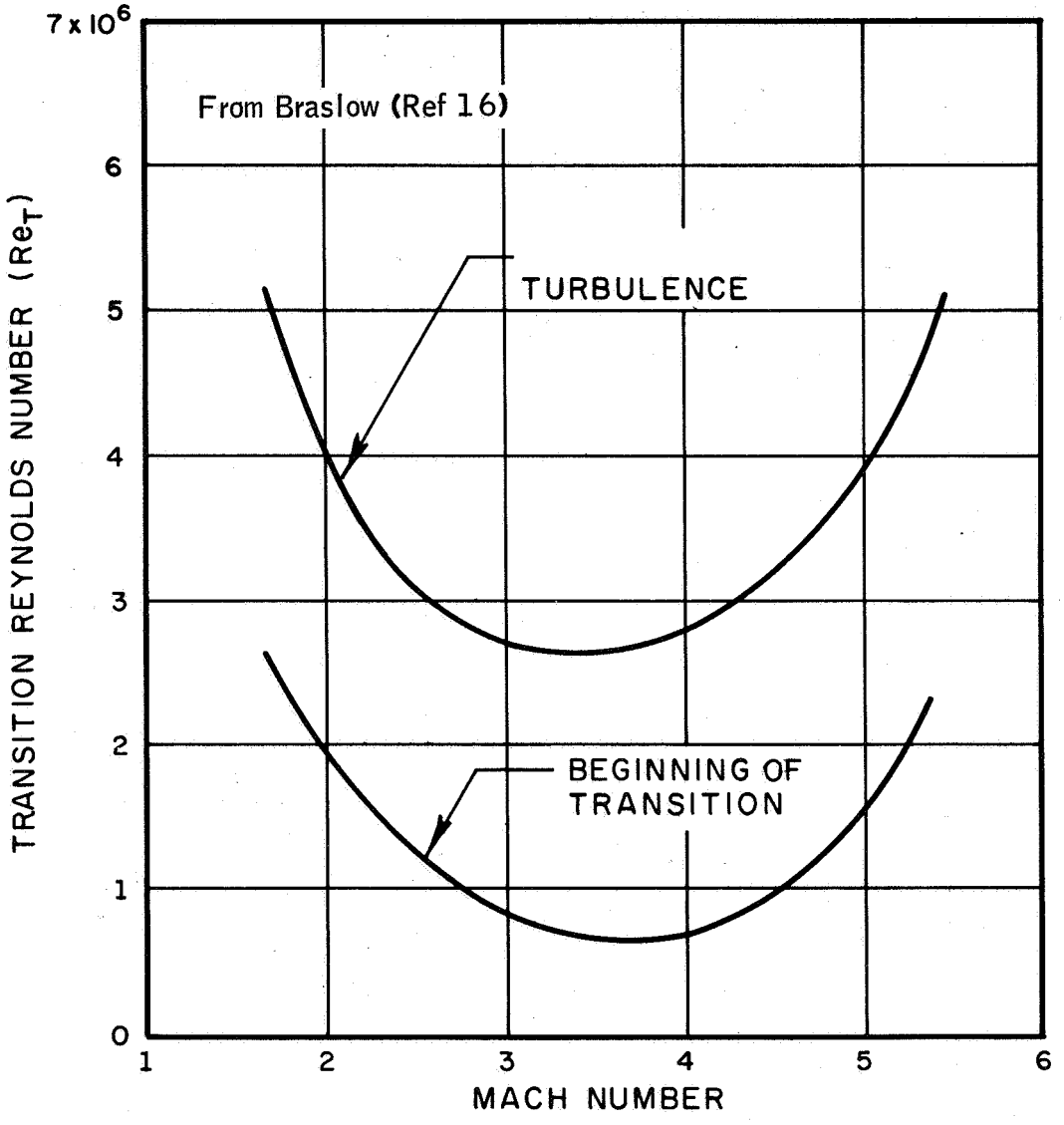

Figure V-4 EFFECT OF MACH NUMBER ON TRANSITION

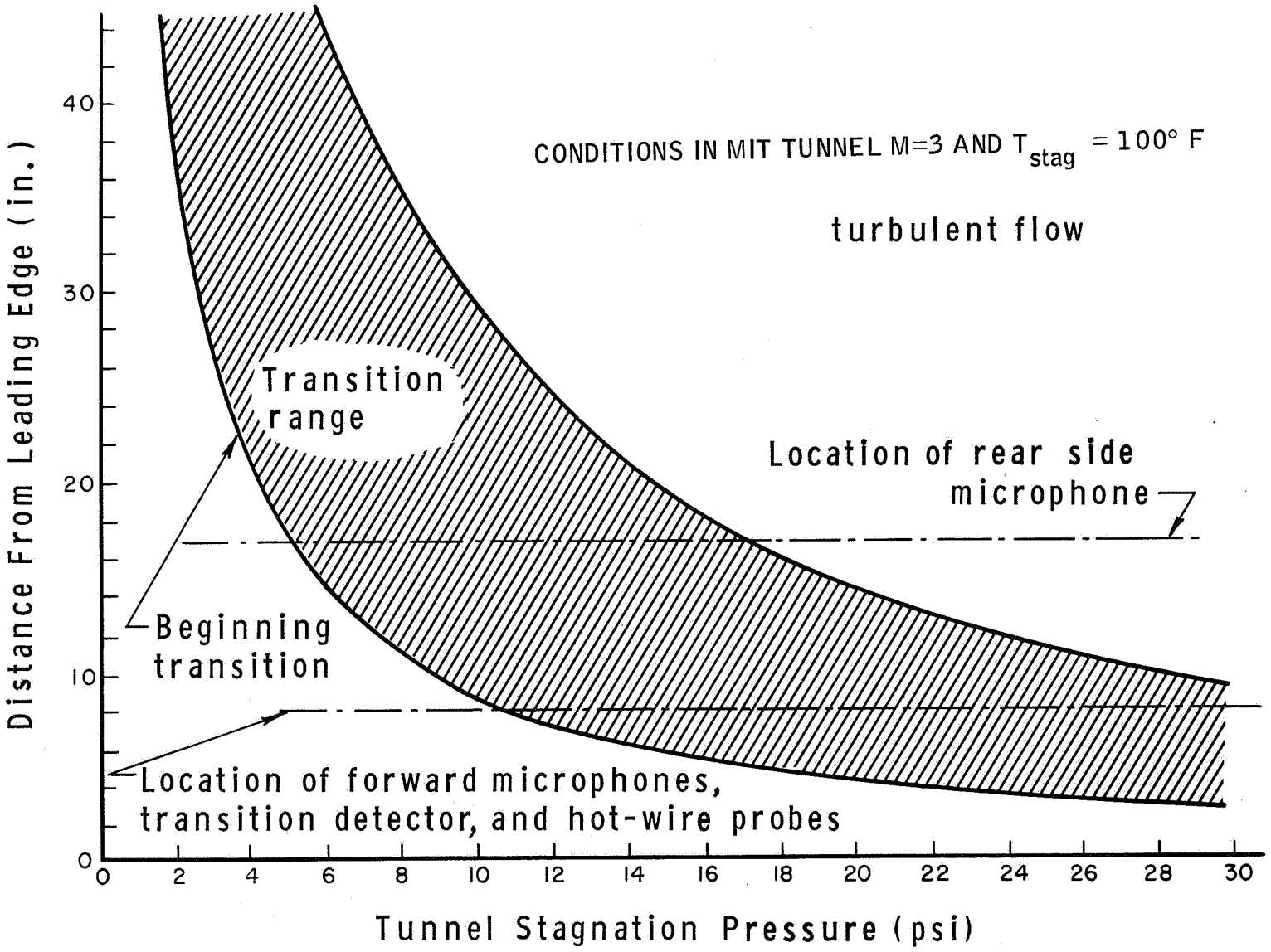

Figure V-5 FLAT PLATE TRANSITION RANGE

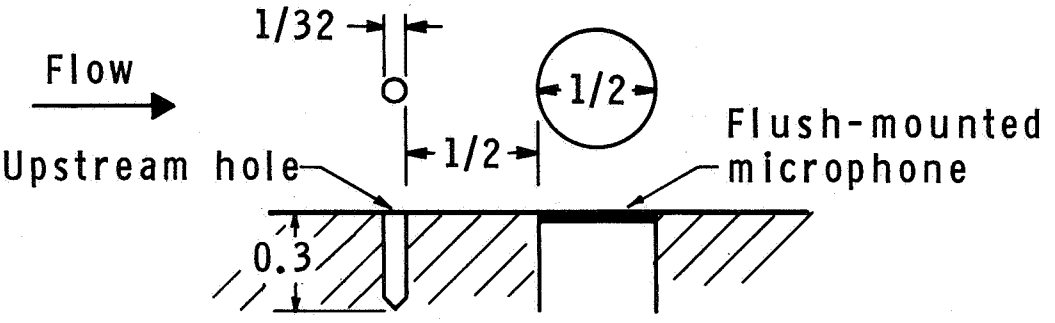

(DIMENSIONS IN INCHES)

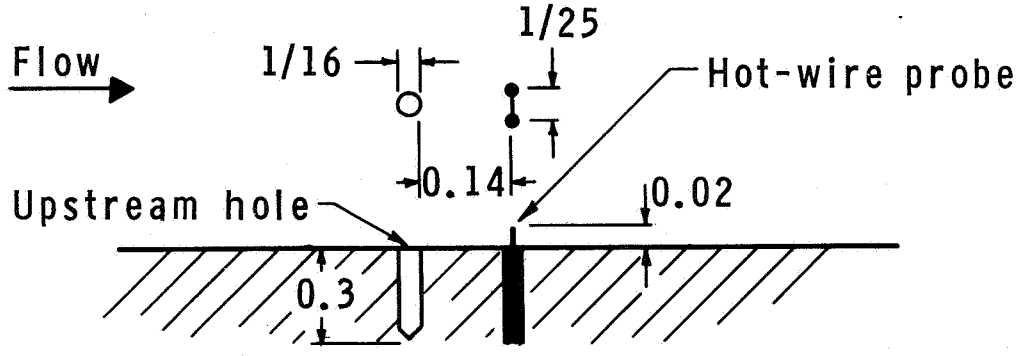

Figure V-6 DETAIL OF HOLE CONFIGURATIONS

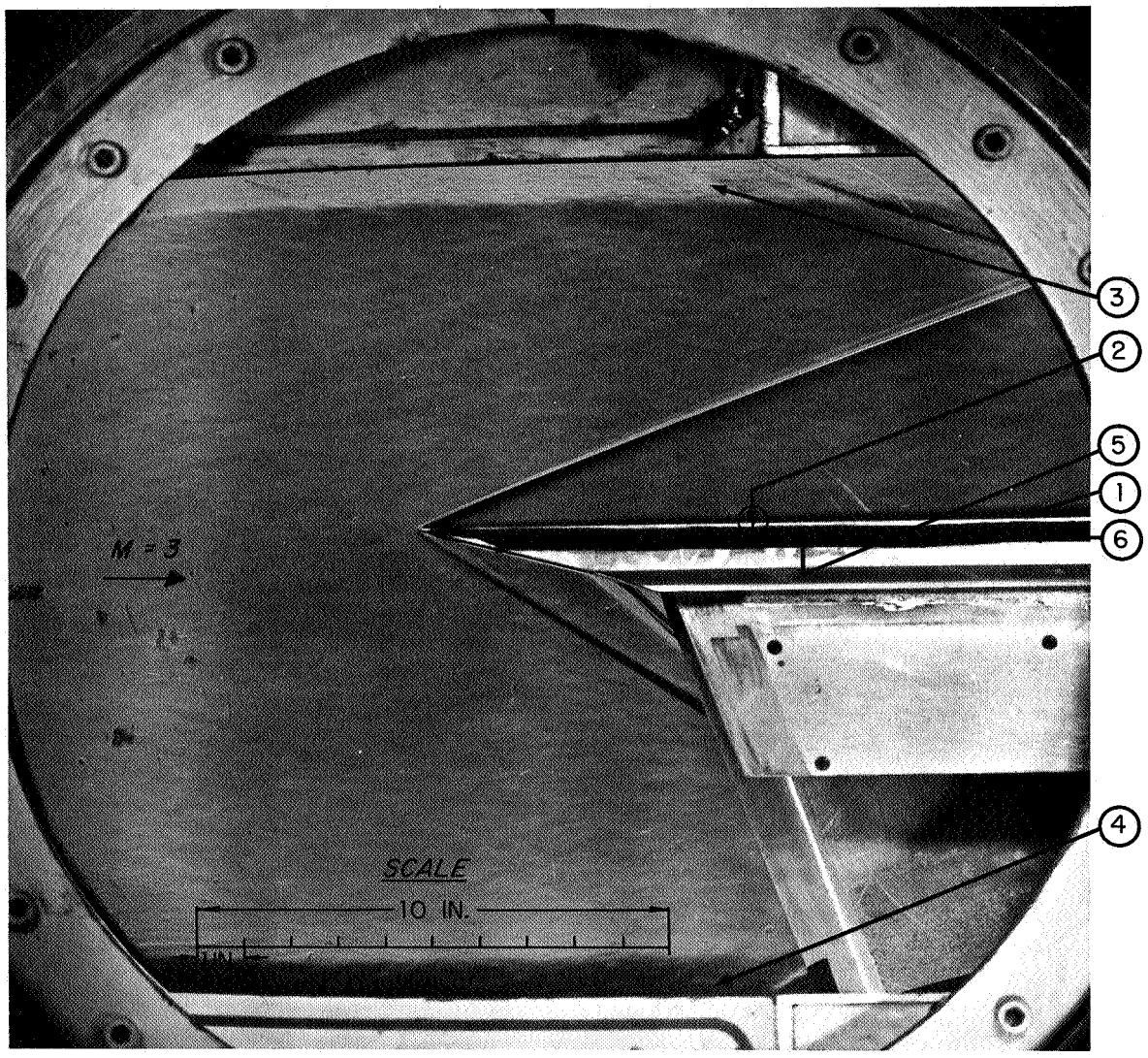

(1) TEST-PLATE BOUNDARY LAYER
(2) PREDICTED TRANSITION ONSET
(3) TUNNEL-CEILING BOUNDARY LAYER
(4) TUNNEL-FLOOR BOUNDARY LAYER
(5) LOCATION OF MICROPHONES, HOT-WIRE PROBES AND TRANSITION DETECTOR
(6) RUBBER SEAL

Figure V-7 SCHLIEREN PHOTOGRAPH OF TRANSITIONAL FLOW

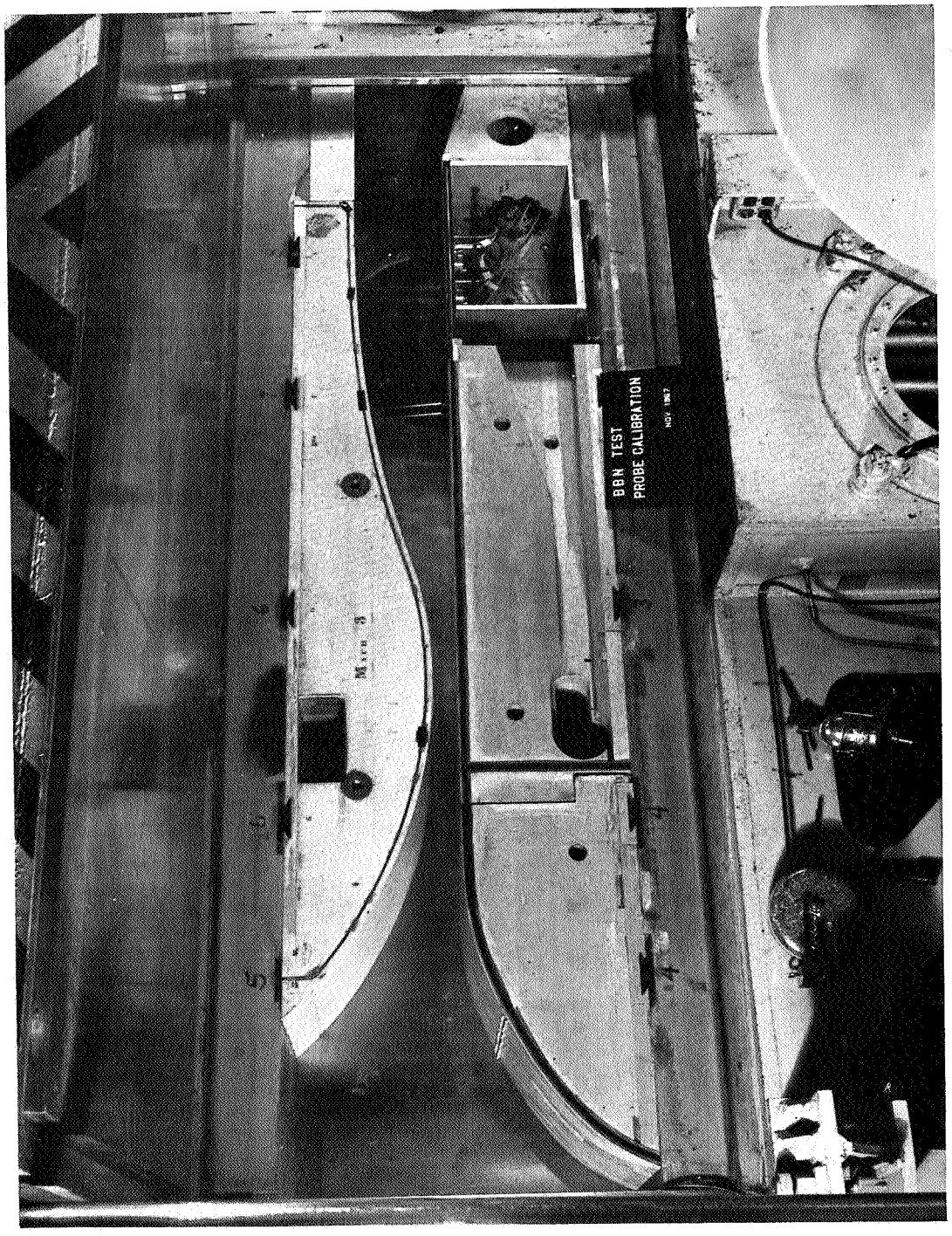

Figure V-8 TURBULENT FLOW TEST SETUP

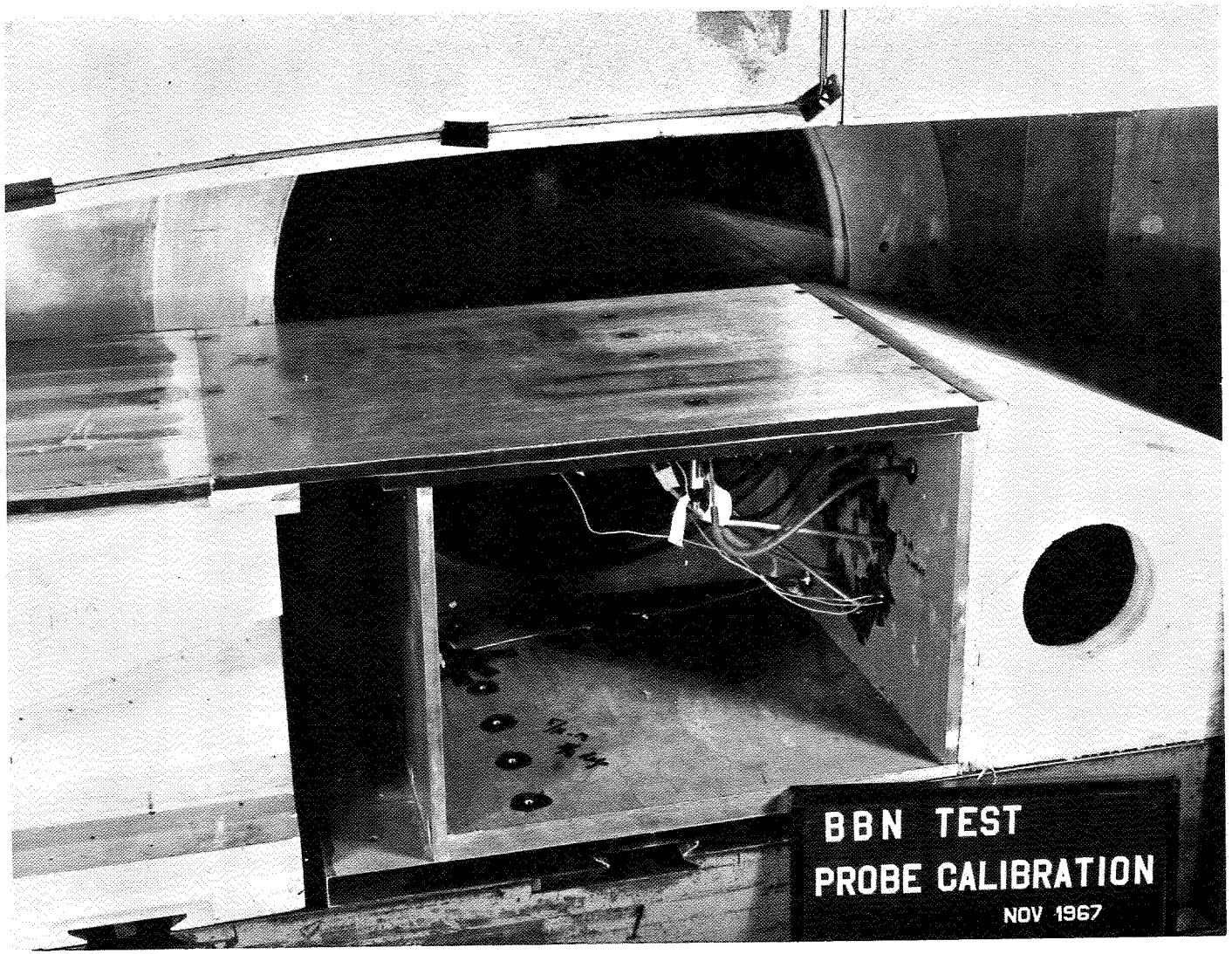

Figure V-9 TEST PLATE WITH FLUSH MOUNTED MICROPHONES

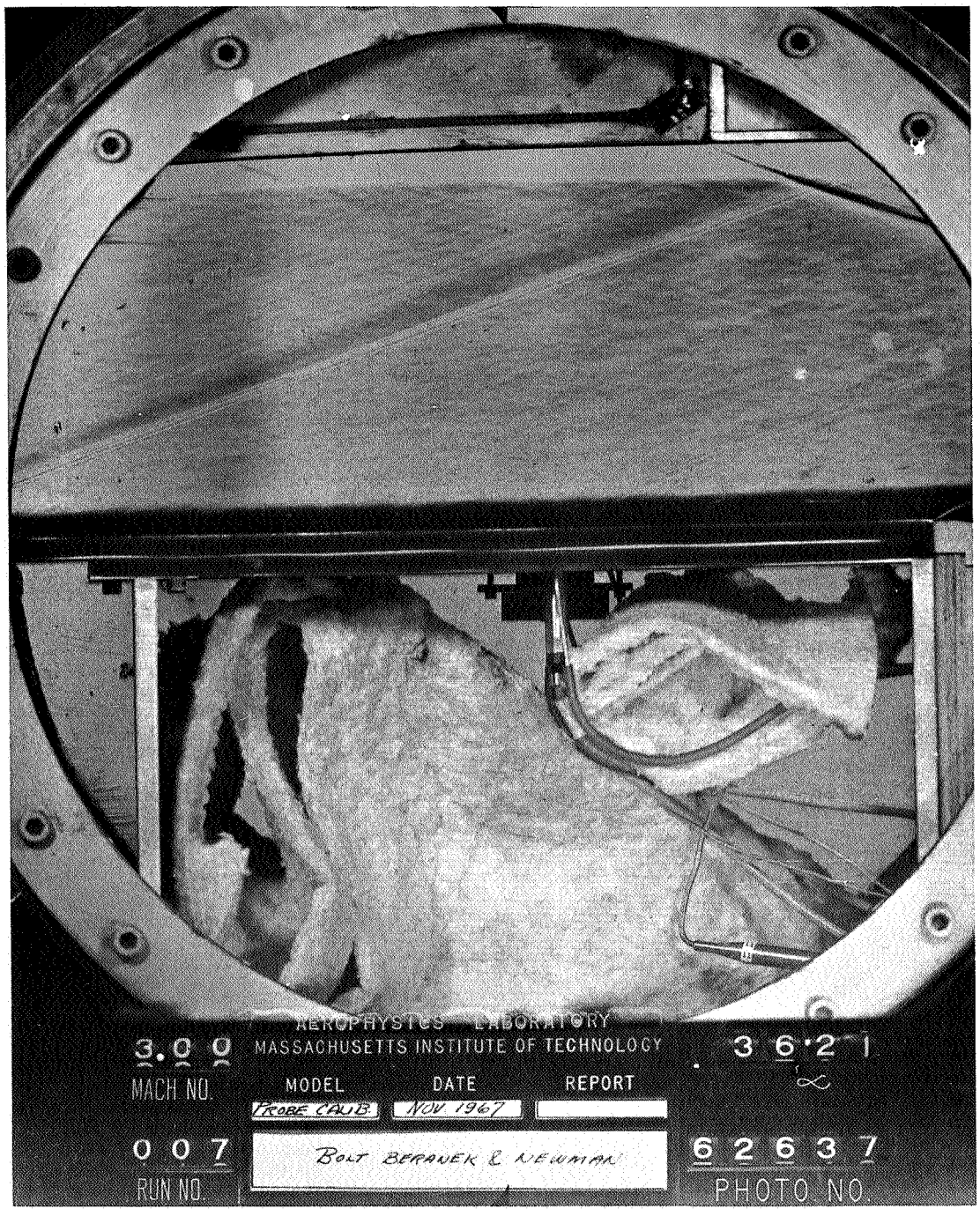

Figure V-10 SCHLIEREN PHOTOGRAPH OF TURBULENT FLOW

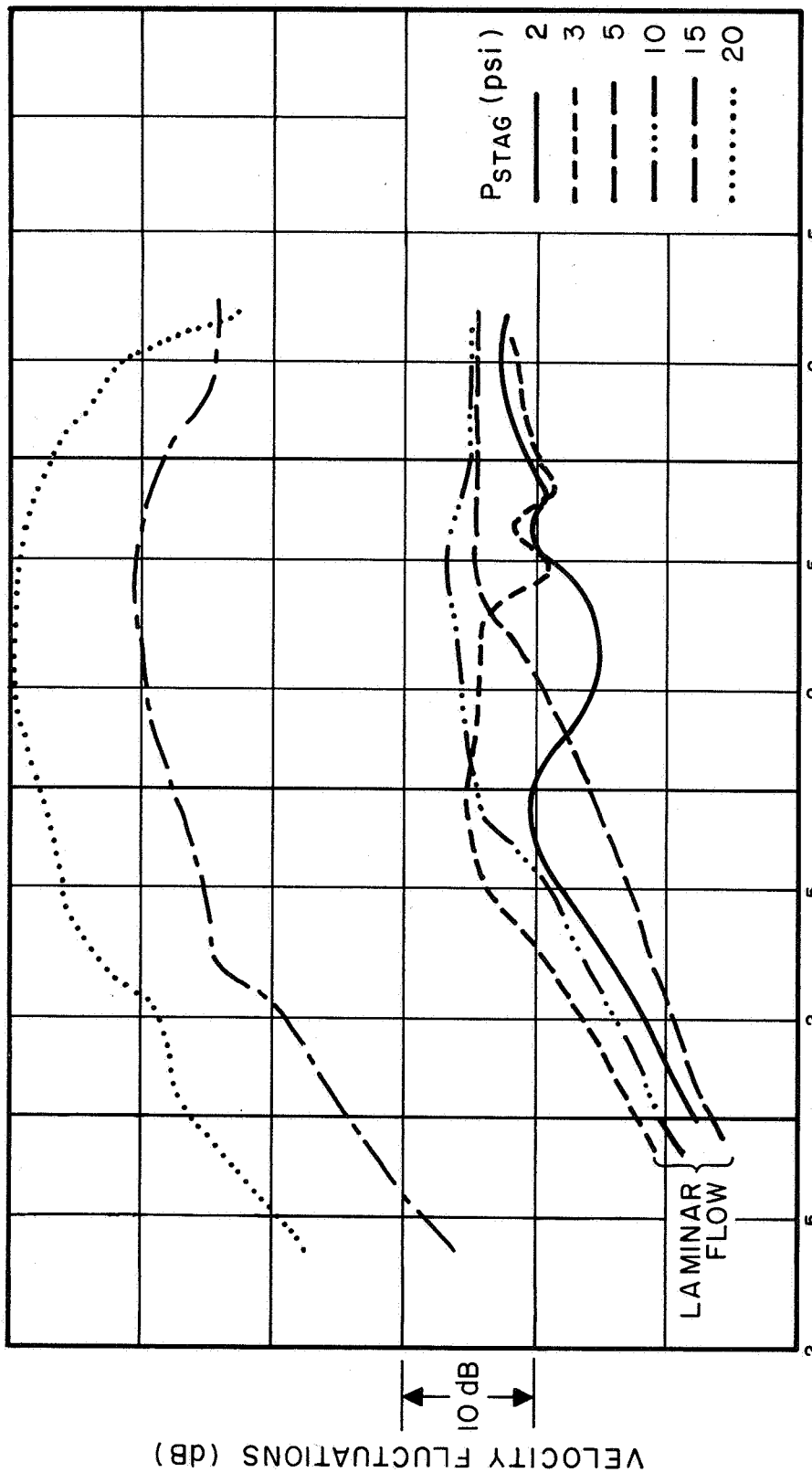

Figure V-11 HOT-WIRE SIGNAL - NO UPSTREAM DISTURBANCE

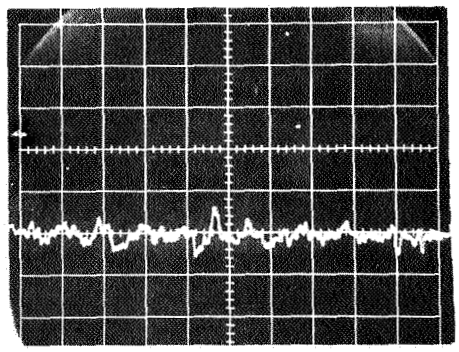

P_{stag}

2 psi

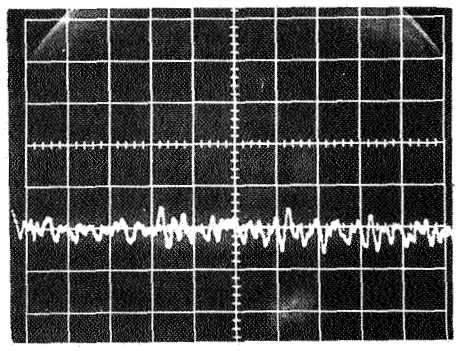

5 psi

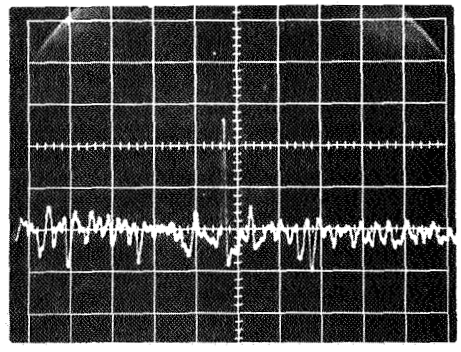

10 psi

Figure V-12a HOT-WIRE SIGNALS - SINGLE-SWEEP SCOPE PHOTOS

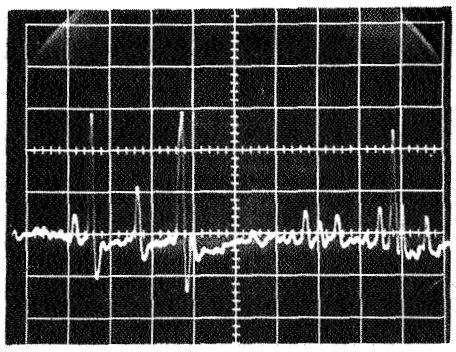

P_{stag}

15 psi

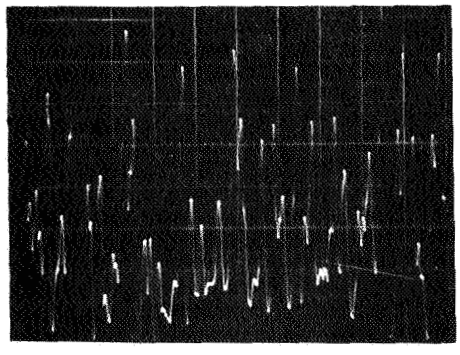

20 psi

Figure 12a (Cont'd)

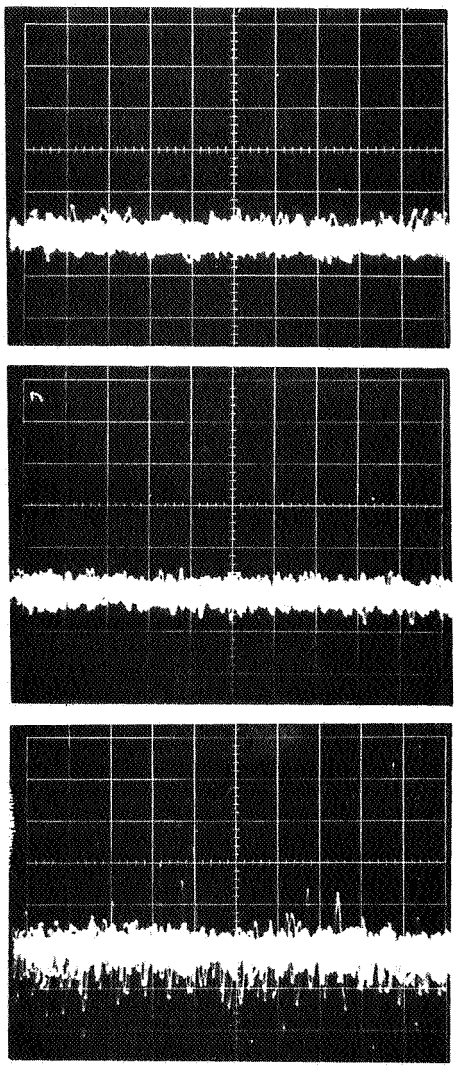

Figure V-12b HOT-WIRE SIGNALS - CONTINUOUS-SWEEP SCOPE PHOTOS

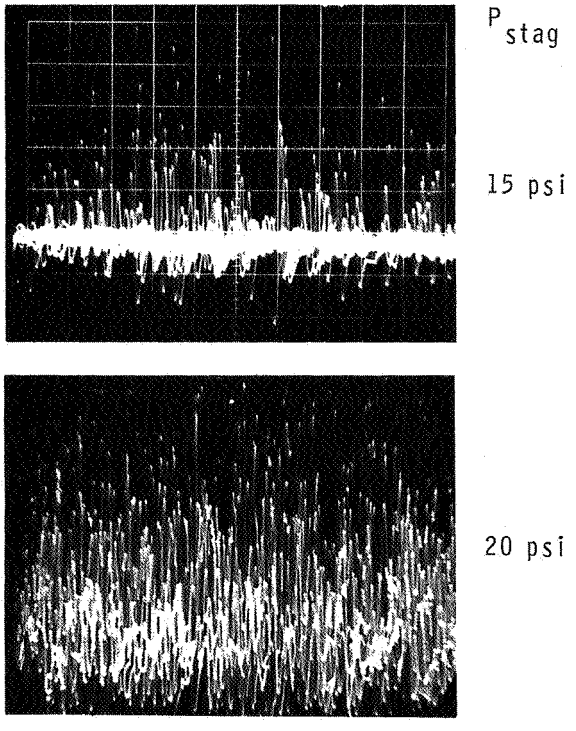

Figure 12b (Cont'd)

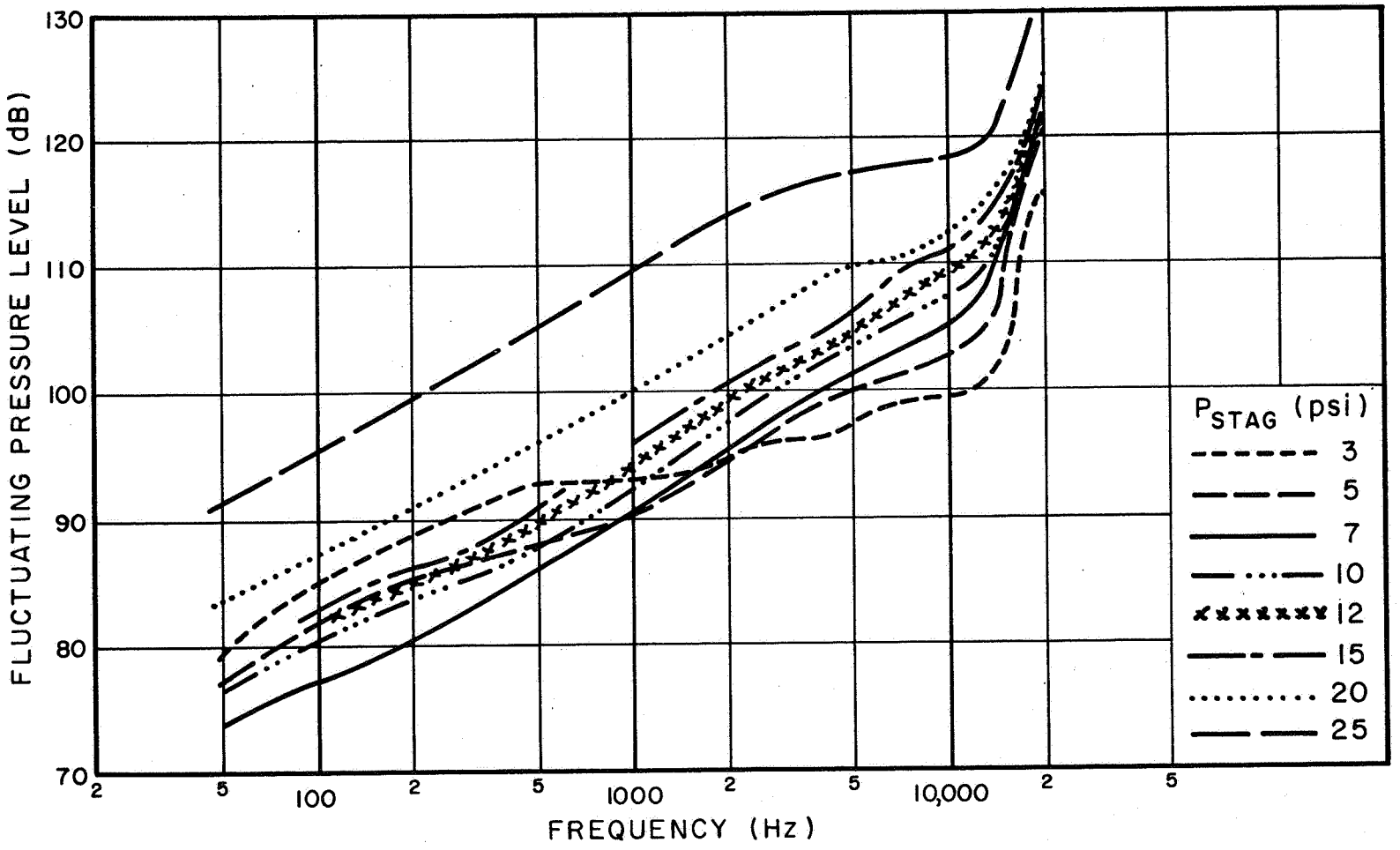

Figure V-13 RESPONSE OF FORWARD SIDE MICROPHONE - NO UPSTREAM DISTURBANCE

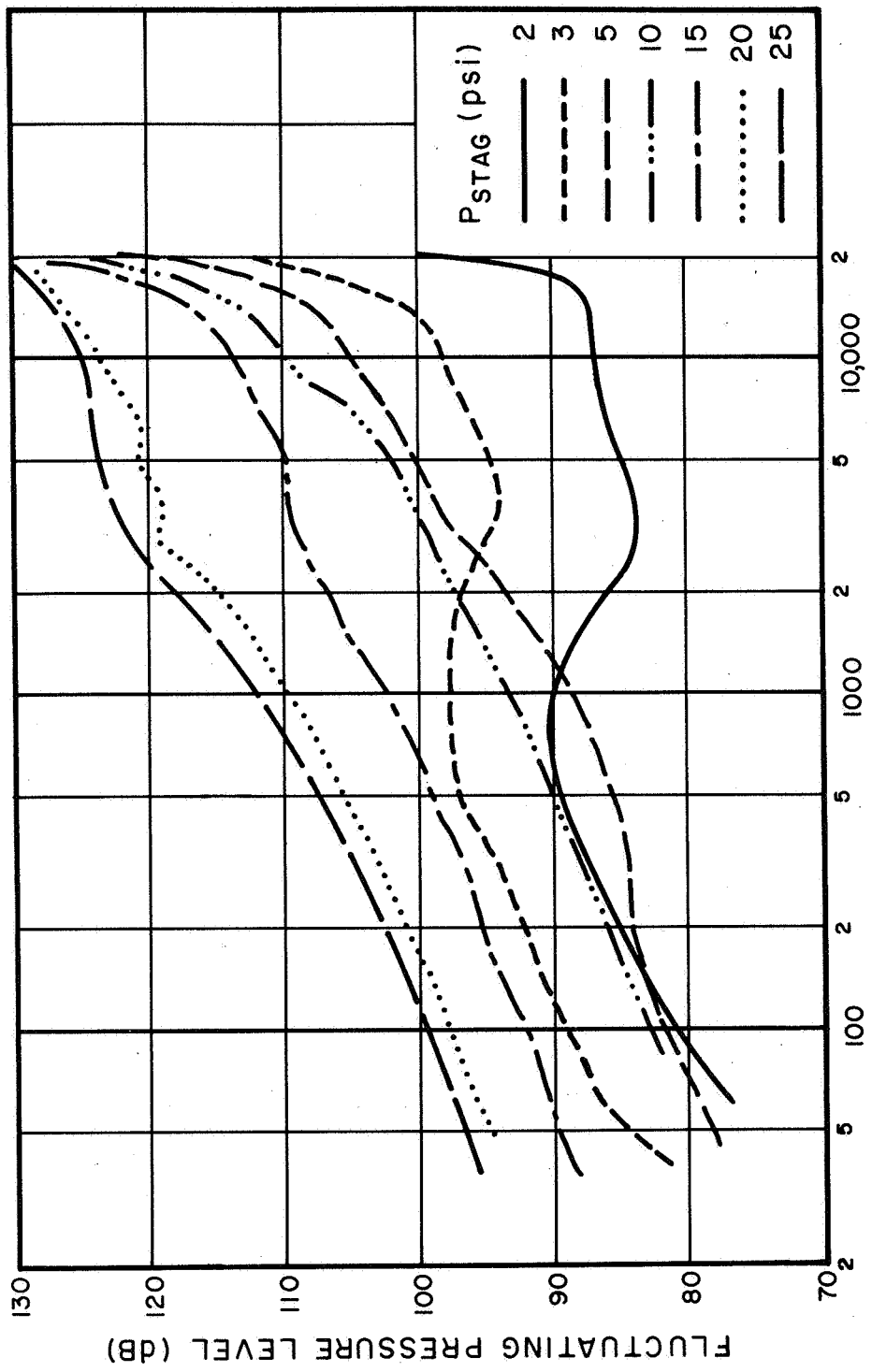

Figure V-14 RESPONSE OF CENTER MICROPHONE - NO UPSTREAM DISTURBANCE

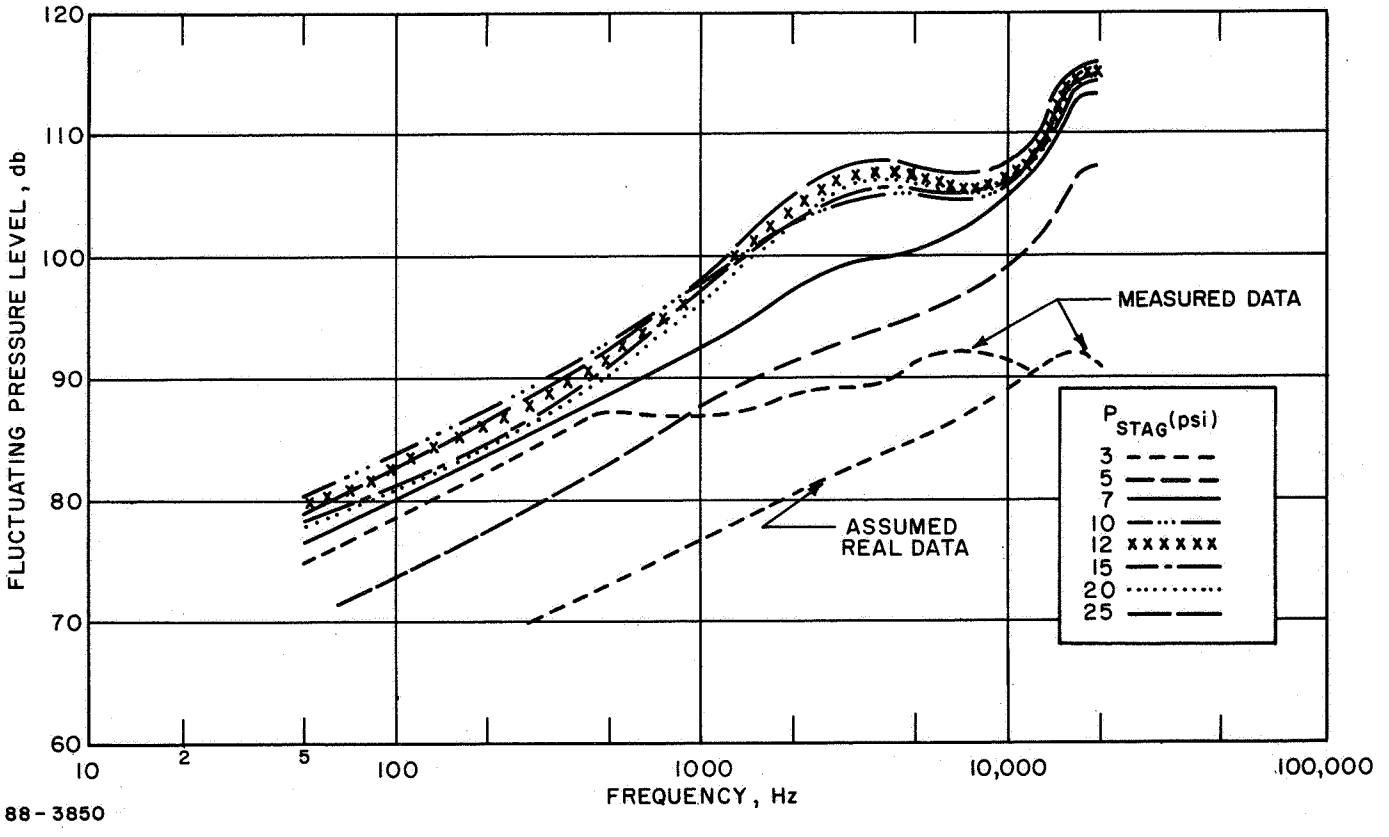

Figure V-15 RESPONSE OF REAR MICROPHONE - NO UPSTREAM DISTURBANCE

Brüel and Kjaer Microphone Static Pressure Characteristics

Half-Inch Condenser Microphone

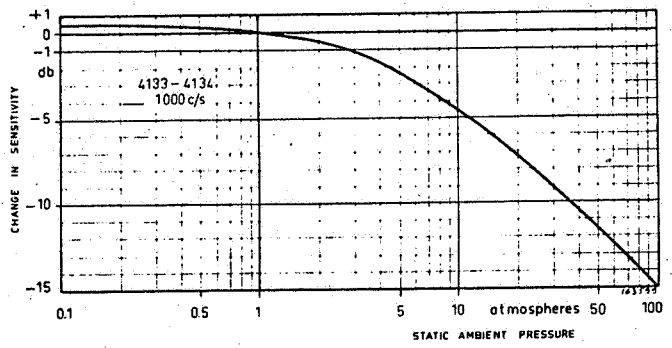

Fig. 25. Variation in microphone sensitivity as function of the ambient pressure.

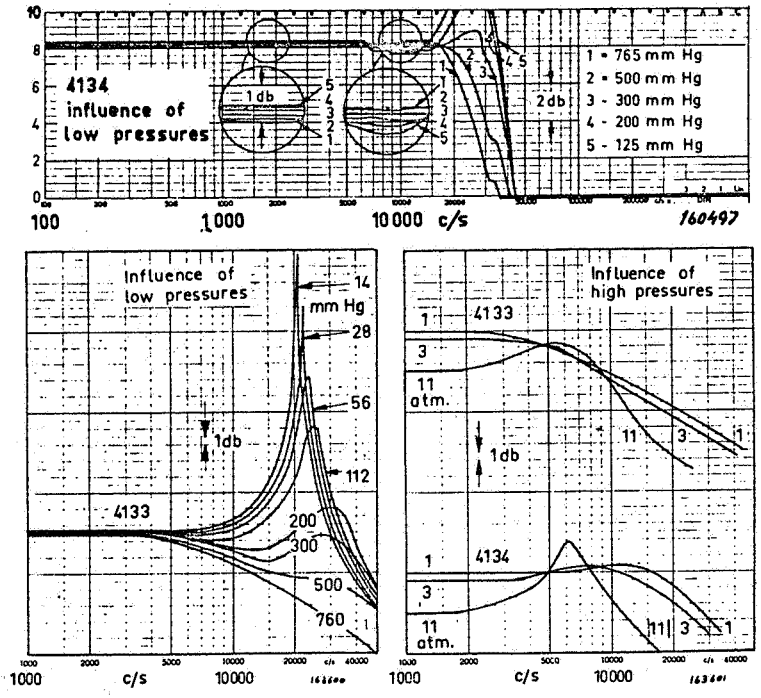

Fig. 26. Charts illustrating the influence of the ambient pressure on the frequency response. Below 200 mm Hg, the response of the 4134 is as shown for the 4133.

Quarter-Inch Condenser Microphone

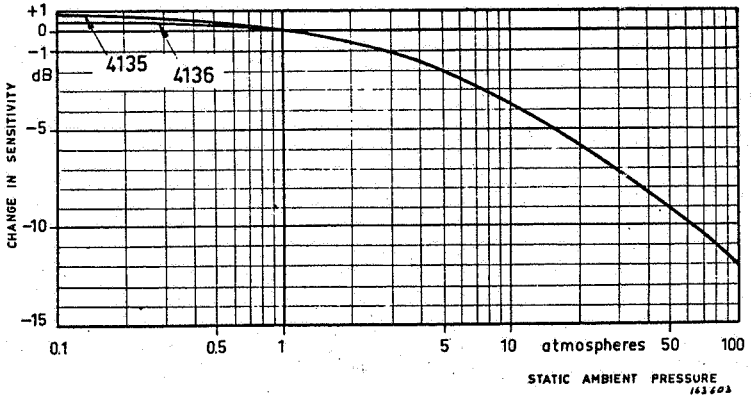

Fig. 1.22. Variation of the quarter-inch microphone sensitivity as a function of the static ambient pressure. Measurements made down to 14 mmHg (0.02 atm., or 26 Km - 86000 ft. altitude) show that the sensitivity in vacuum would be less than 1 dB higher than the sensitivity at 1 atm. (Only valid up to 3000 Hz. See below).

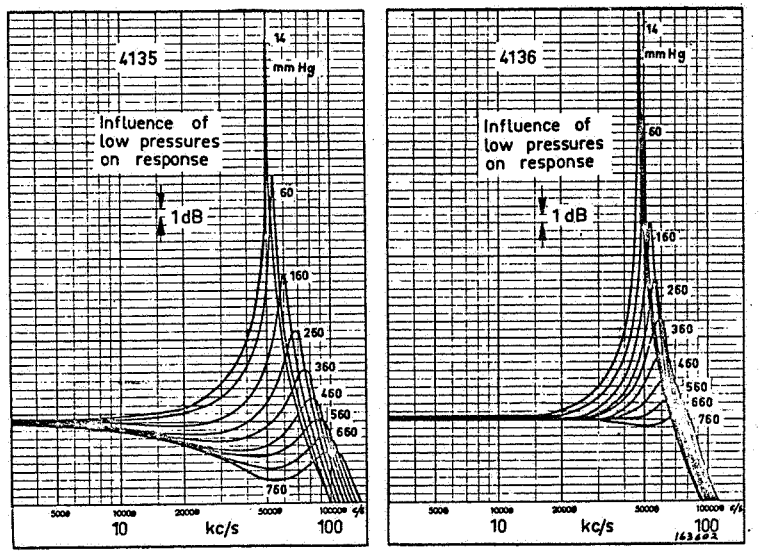

Fig. 1.23. Influence of the static ambient pressure on the frequency response of the quarter-inch microphones.

Figure V-16 BRÜEL AND KJAER MICROPHONE STATIC PRESSURE CHARACTERISTICS

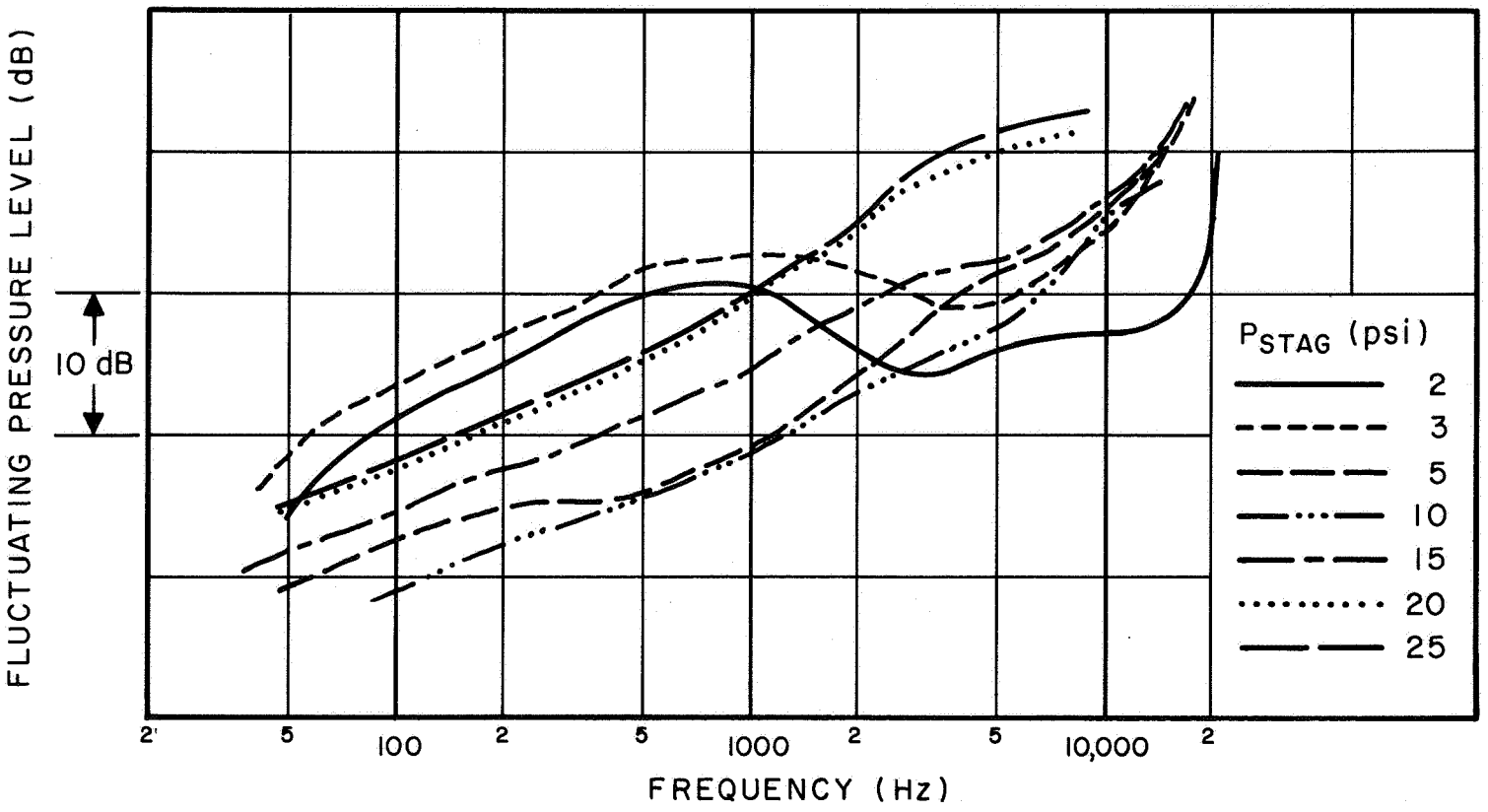

Figure V-17 NORMALIZED RESPONSE OF CENTER MICROPHONE - NO UPSTREAM DISTURBANCE

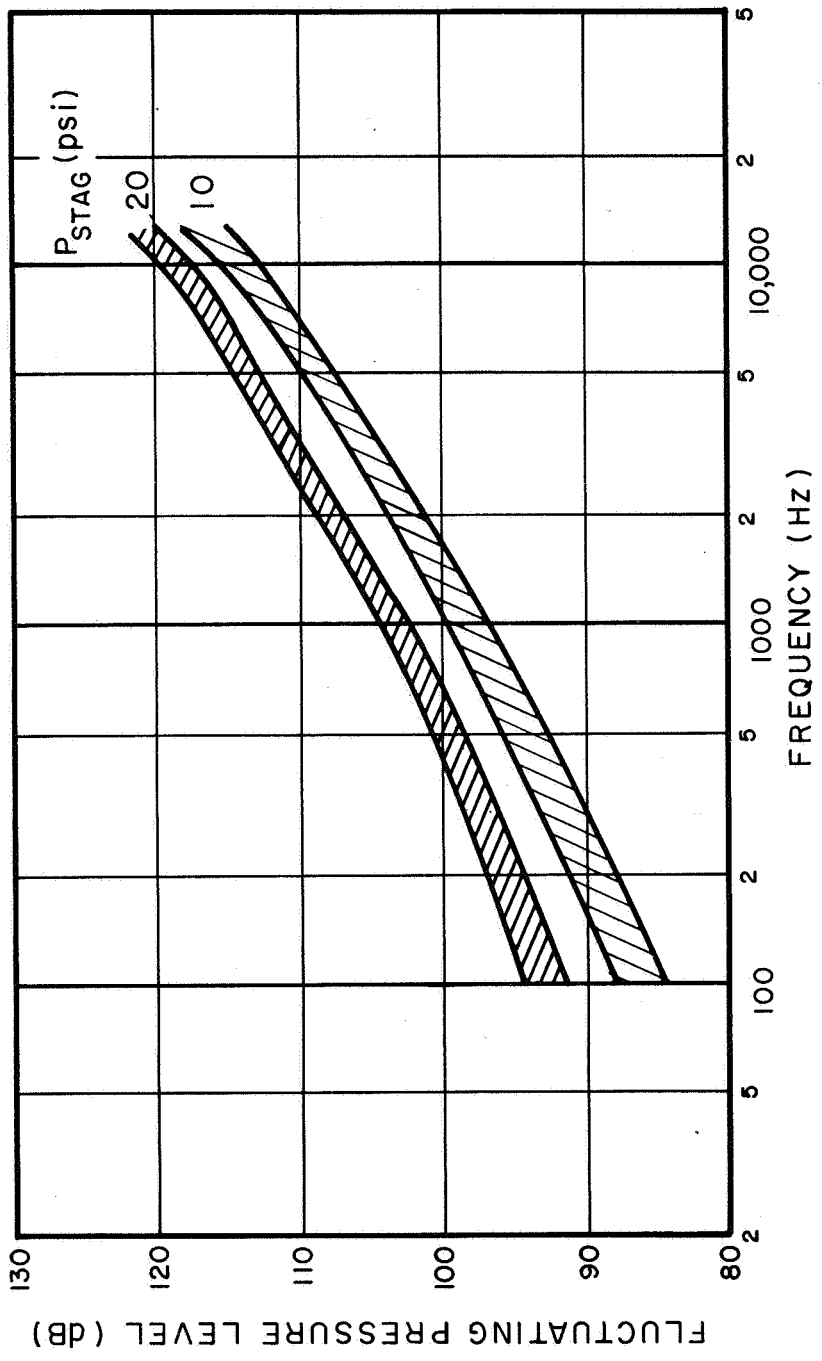

Figure V-18 TURBULENT FLOW FLUCTUATING PRESSURE SPECTRA

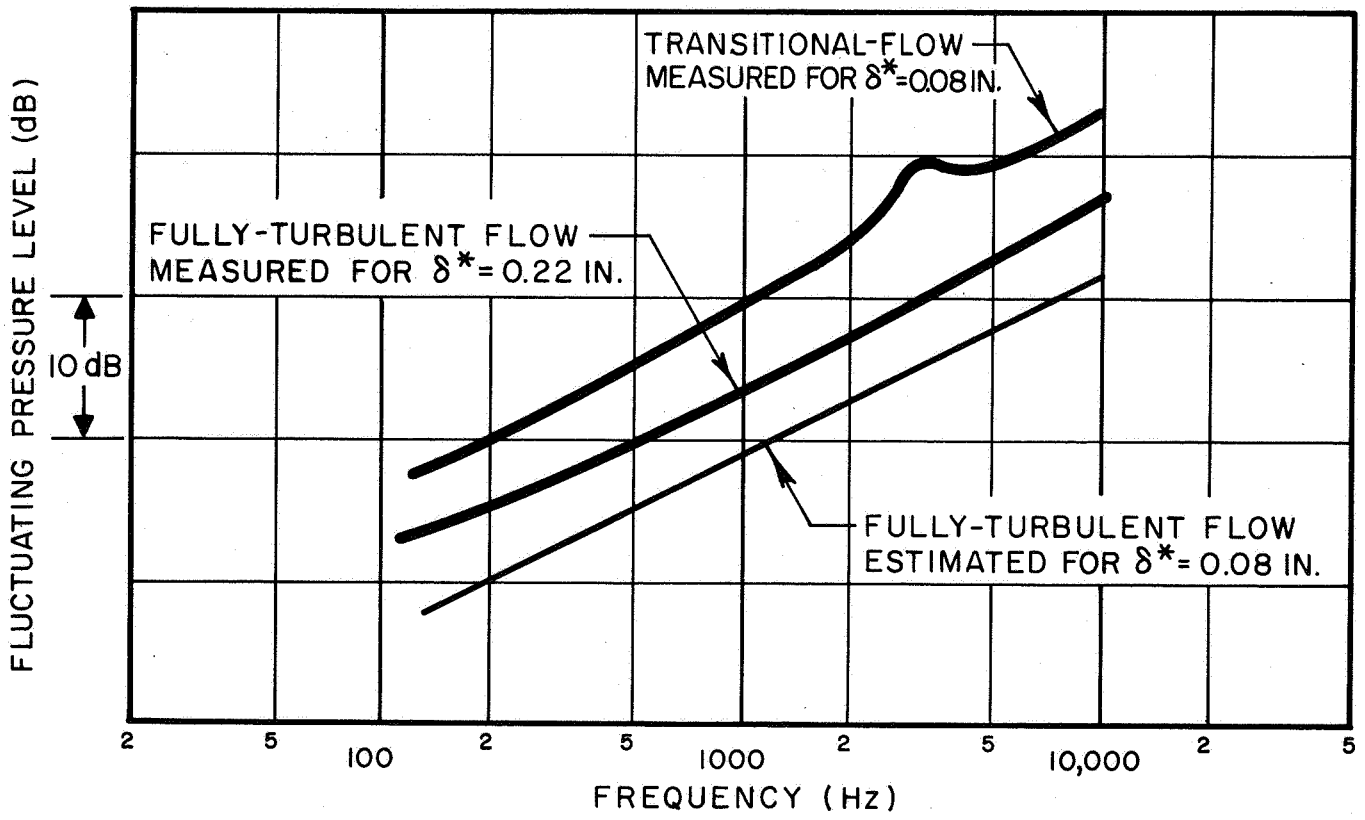

Figure V-19 COMPARISON OF TRANSITIONAL AND TURBULENT FLOW SPECTRA

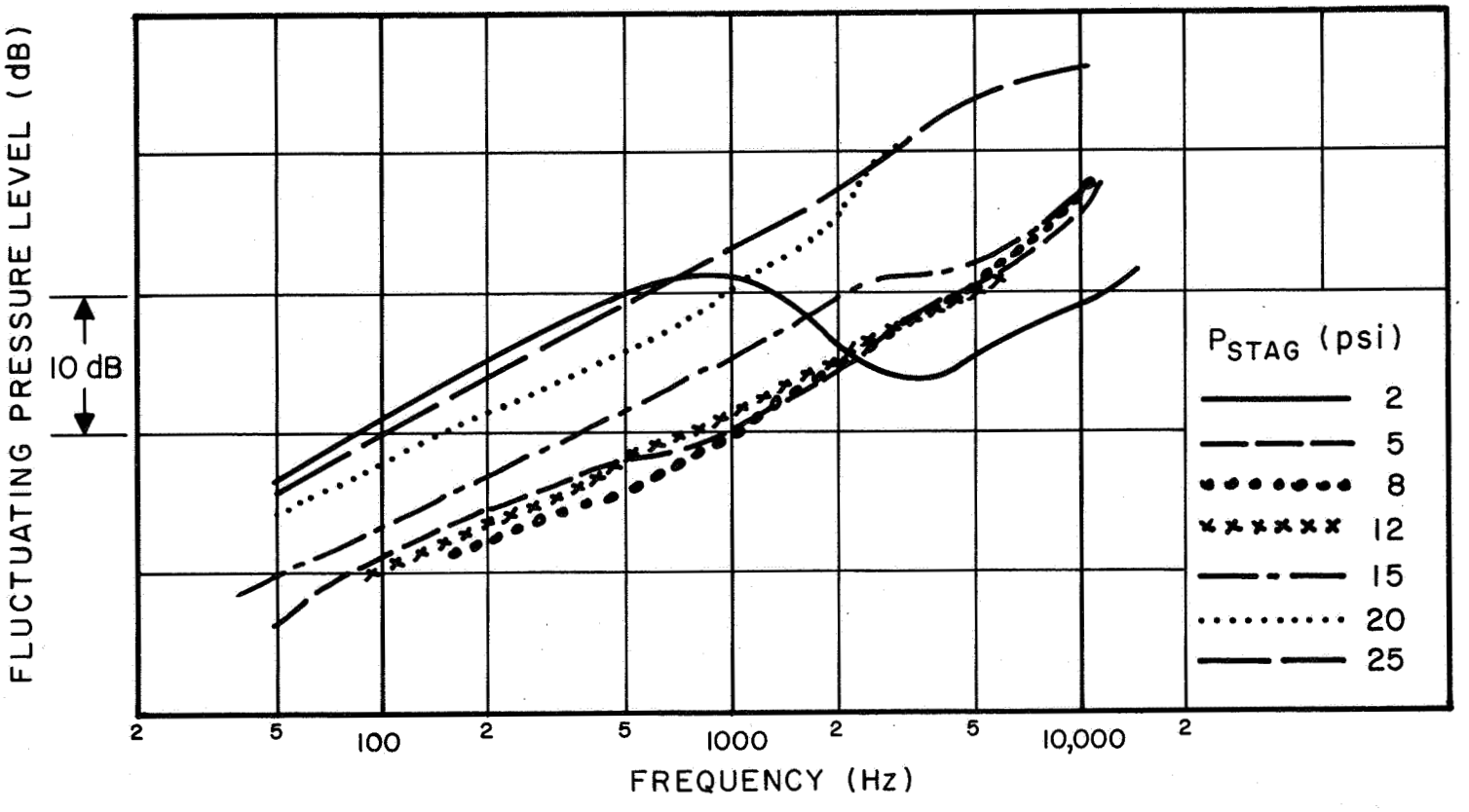

Figure V-20 NORMALIZED RESPONSE OF CENTER MICROPHONE - 1/32 IN. DIA. UPSTREAM HOLE

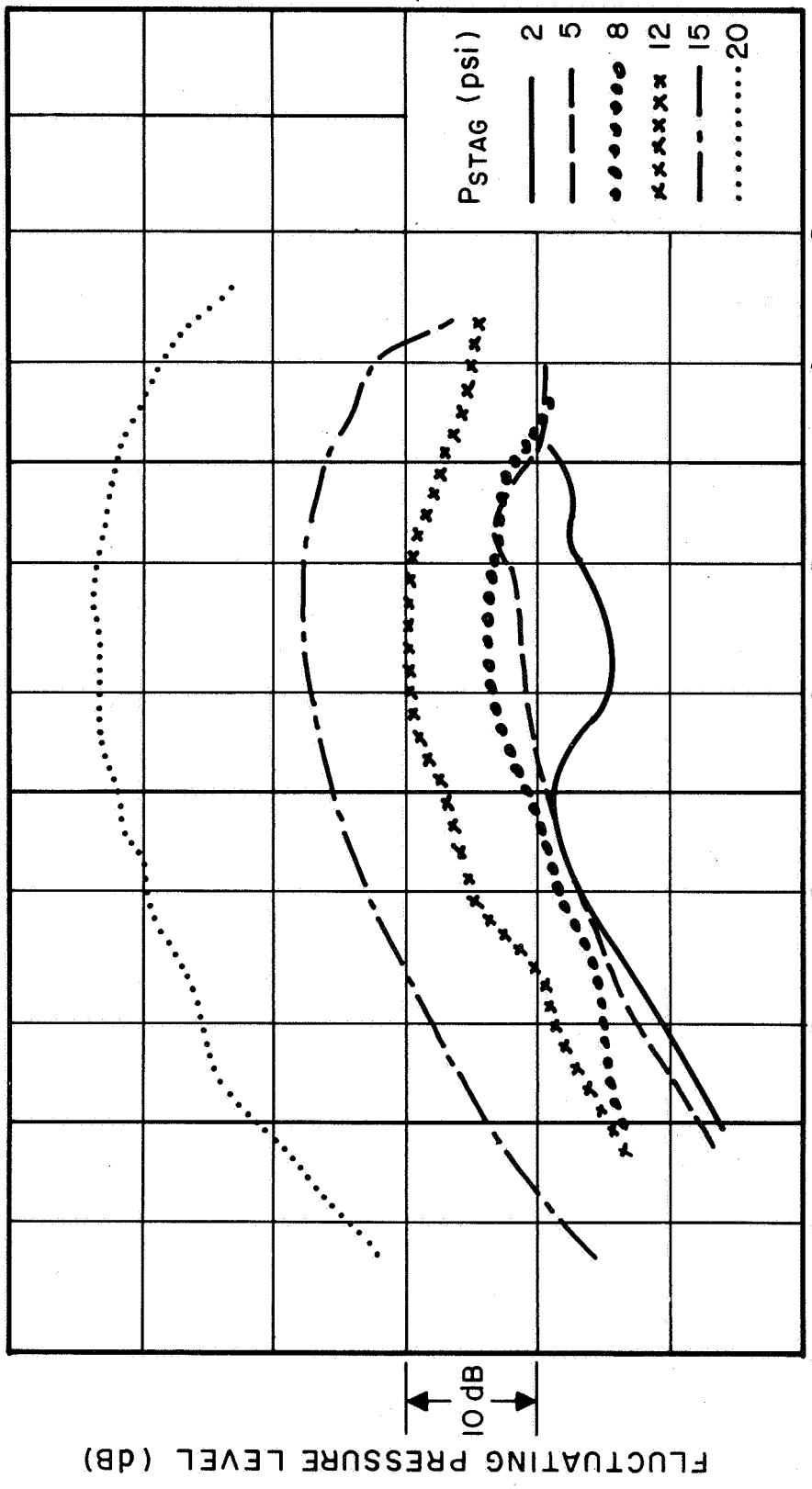

Figure V-21 HOT WIRE SIGNAL - 1/16 IN. DIA. UPSTREAM HOLE

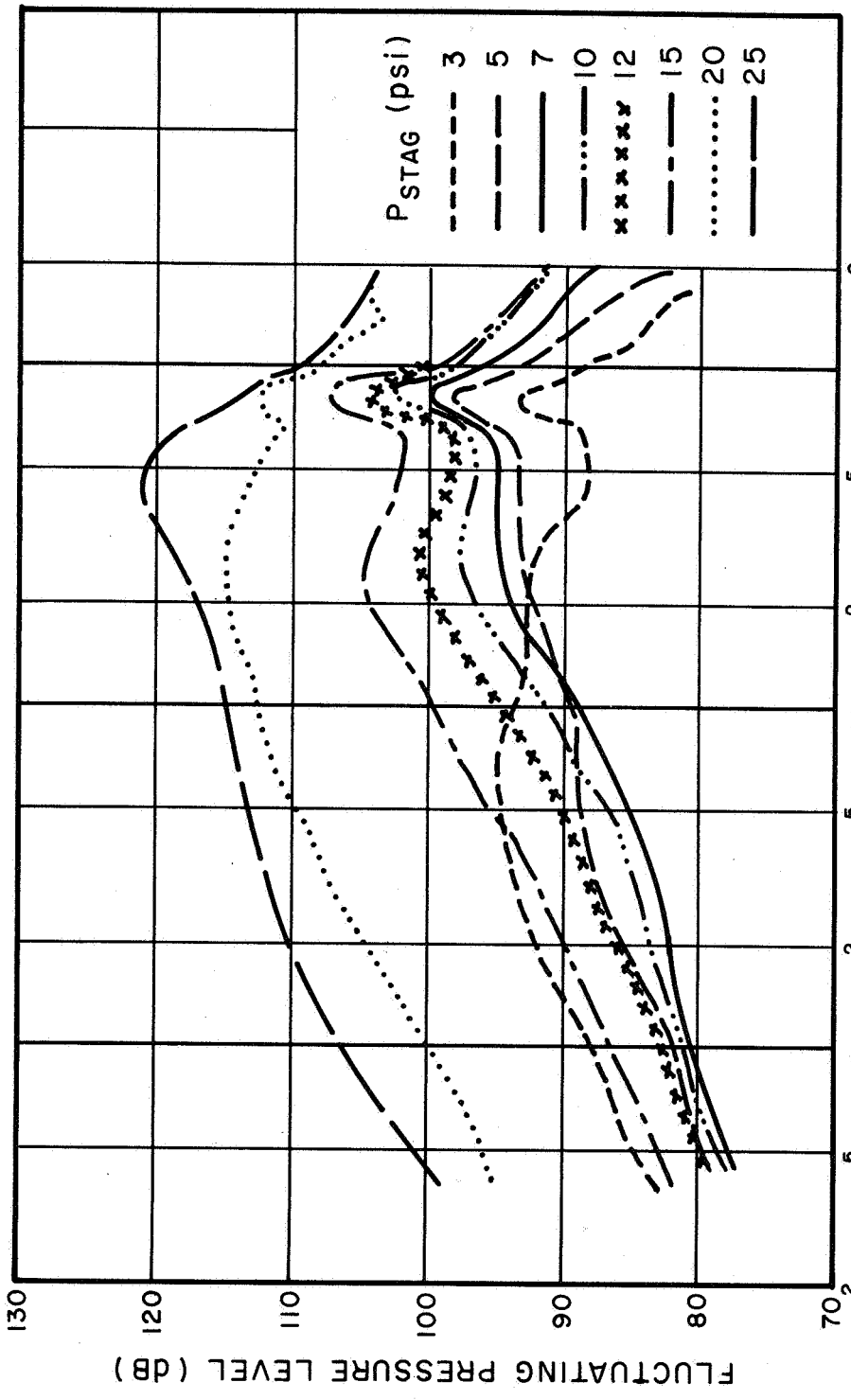

Figure V-22 TRANSITION DETECTOR RESPONSE

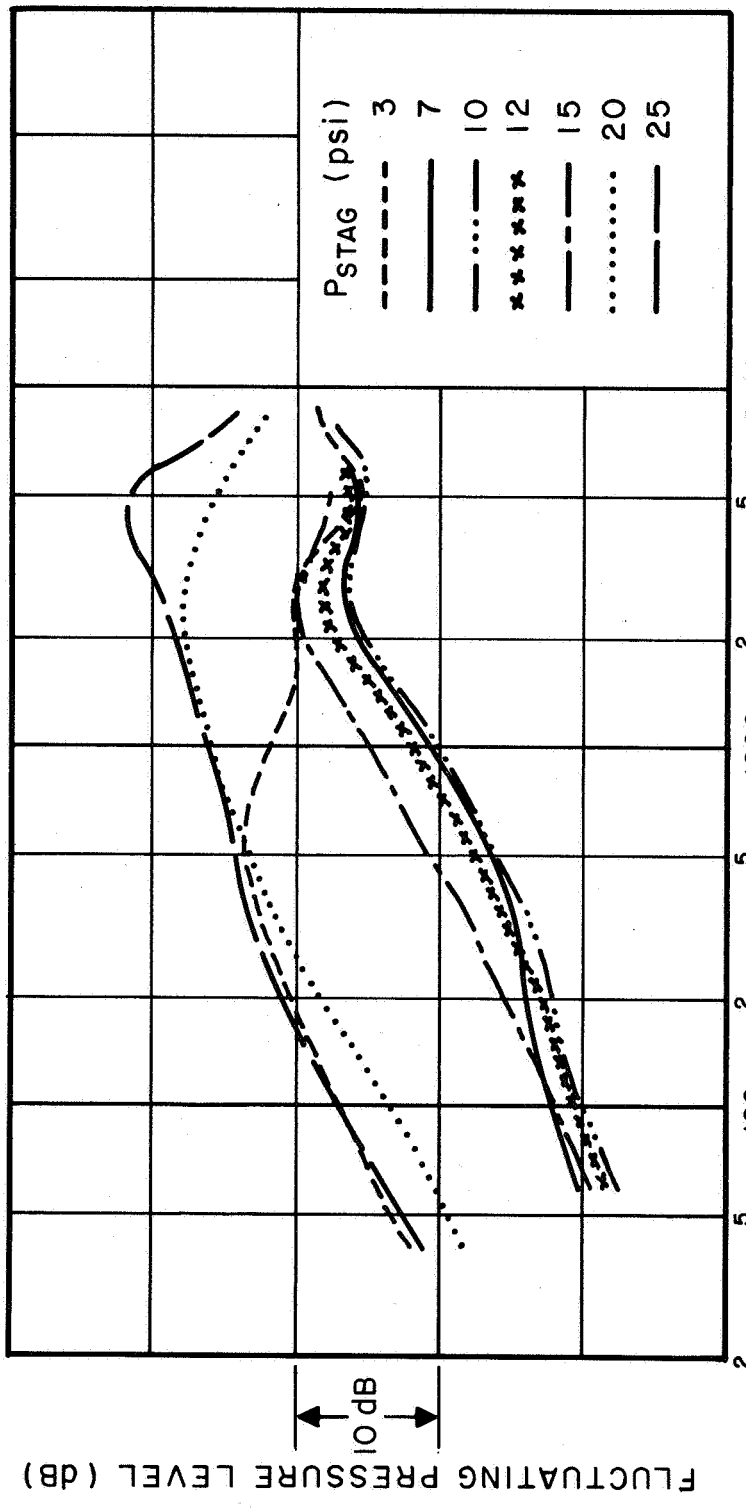

Figure V-23 TRANSITION DETECTOR NORMALIZED RESPONSE

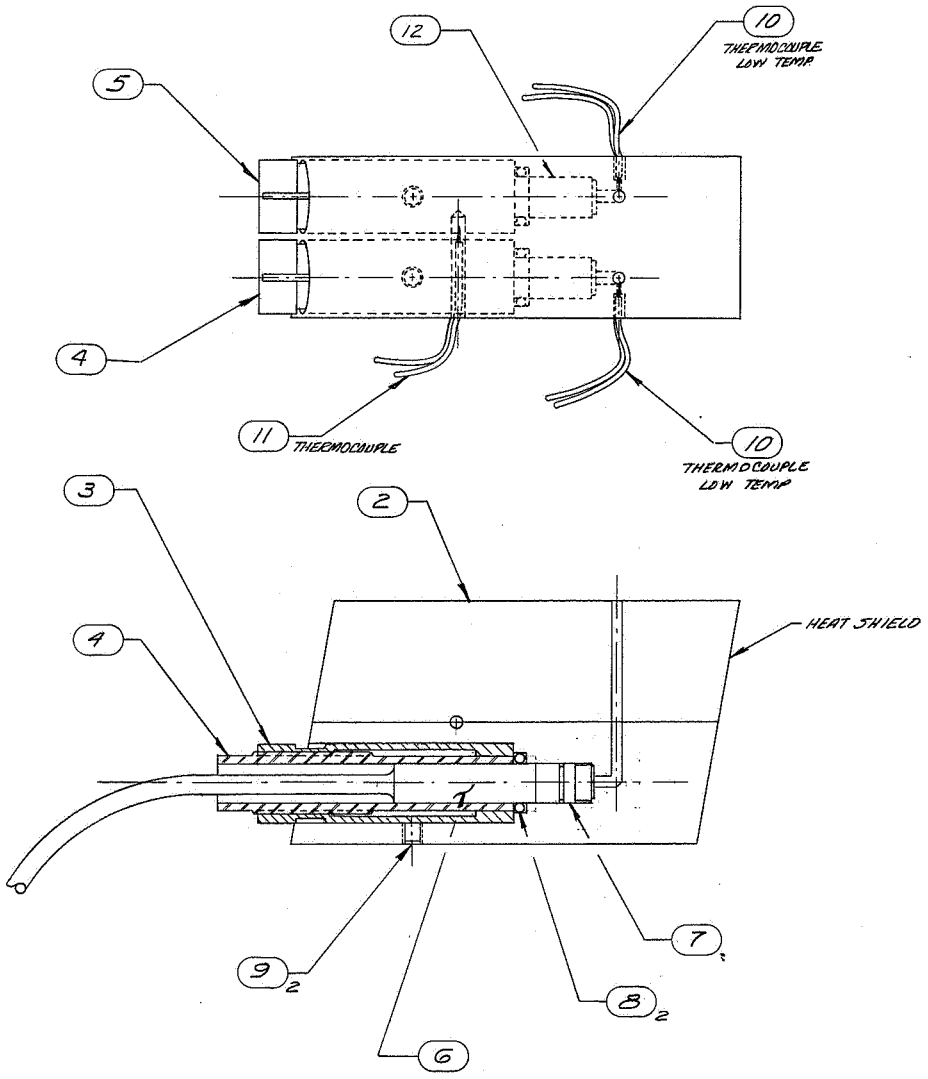

DATE	SYM	REVISION RECORD	AUTH.	DR.	CK.

	1	BBN	TRANSDUCER	12
	1	BBN	THERMOCOUPLE	11
	2	BBN	THERMOCOUPLE LOW TEMP	10
	2	#4-40 X 1/8	SET SCR. SOC. STL	9
	2	2-10	O RING NEOPRENE	8
	1	1/2 INCH	MICROPHONE B&K	7
	1	UA-0123	1/4 B&K FLEXIBLE ADAPTER	6
	1	A-30303	TRANSDUCER HOUSING	5
	1	A-30302	THREADED ADAPTER	4
	1	A-30301	MICROMETER HOUSING	3
	1	C-30300	HOUSING	2
	2	#663-P	MICROMETER HEAD STARRETT	1
	QTY	DWG / PART NO	DESCRIPTION	ITEM

MATERIAL LIST

TOLERANCES (EXCEPT AS NOTED)	BOLT BERANEK AND NEWMAN INC	
DECIMAL ±	SCALE	DRAWN BY N. Smith APPROVED BY
FRACTIONAL ±	TITLE ARC TEST FIXTURE	
ANGULAR ±	DATE 15 JAN 68	DRAWING NUMBER C-20044

Figure V-24 ARC TEST SPECIMEN

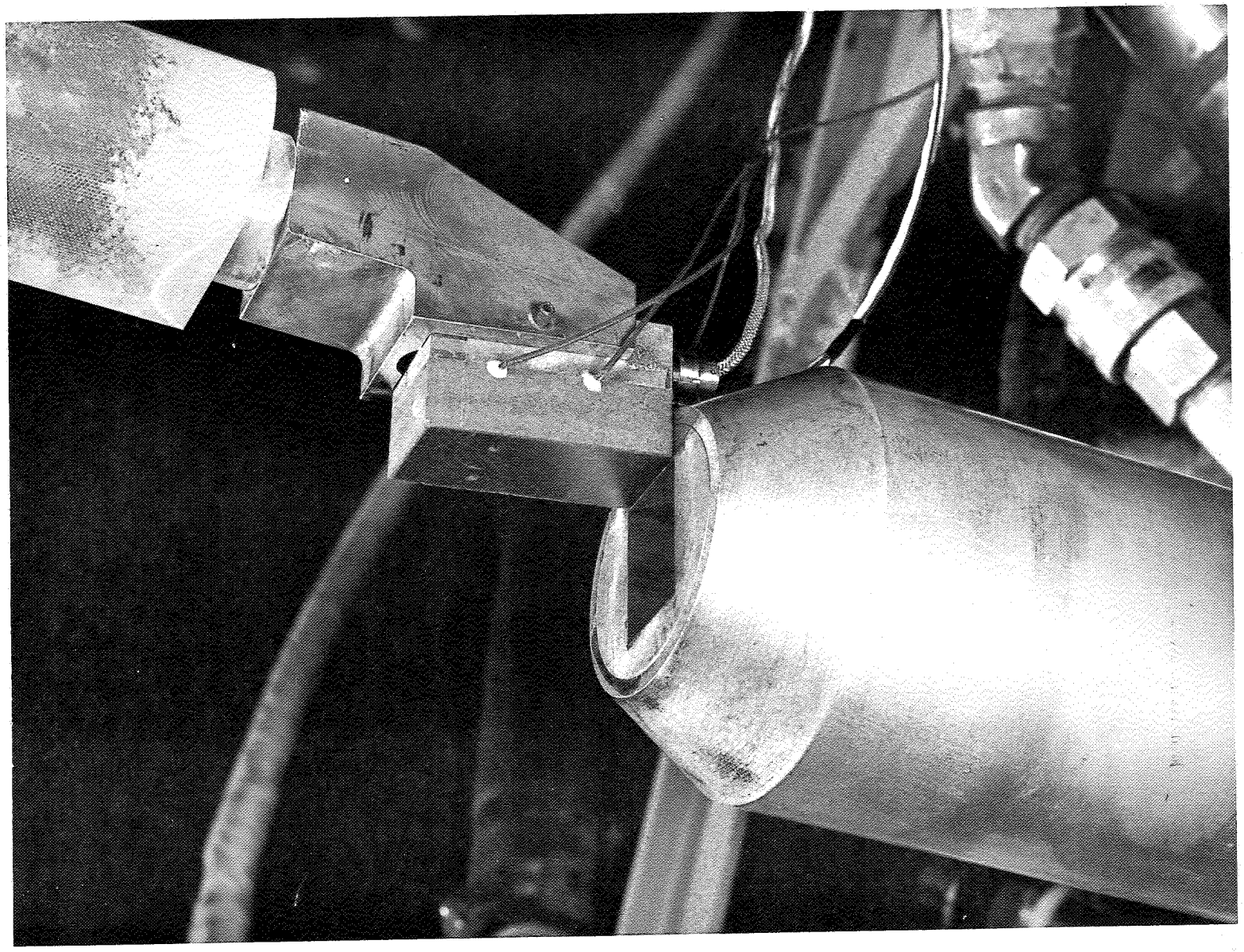

Figure V-25 ARC TEST INSTALLATION

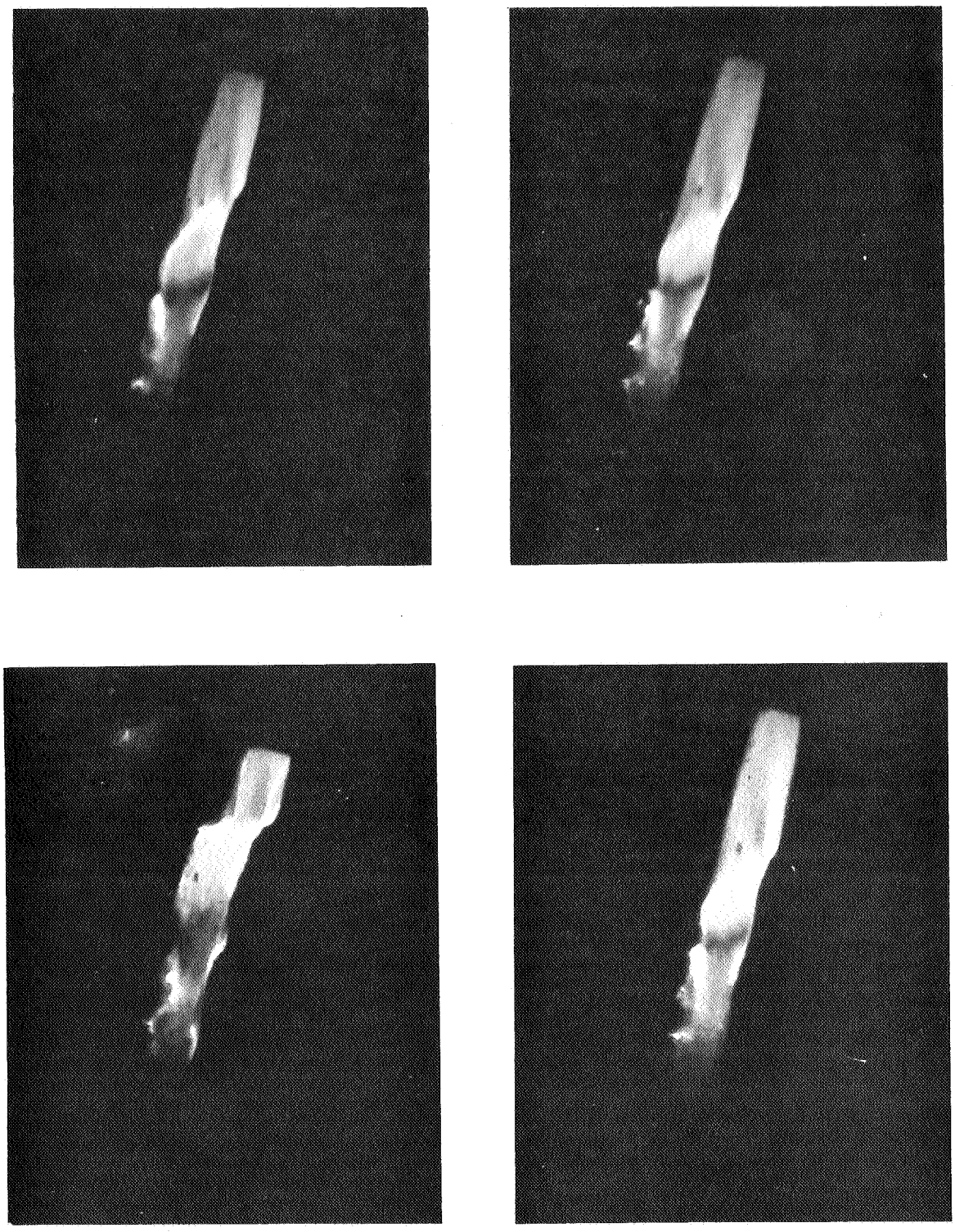

Figure V-26 SEQUENTIAL CINE FILM SEGMENTS

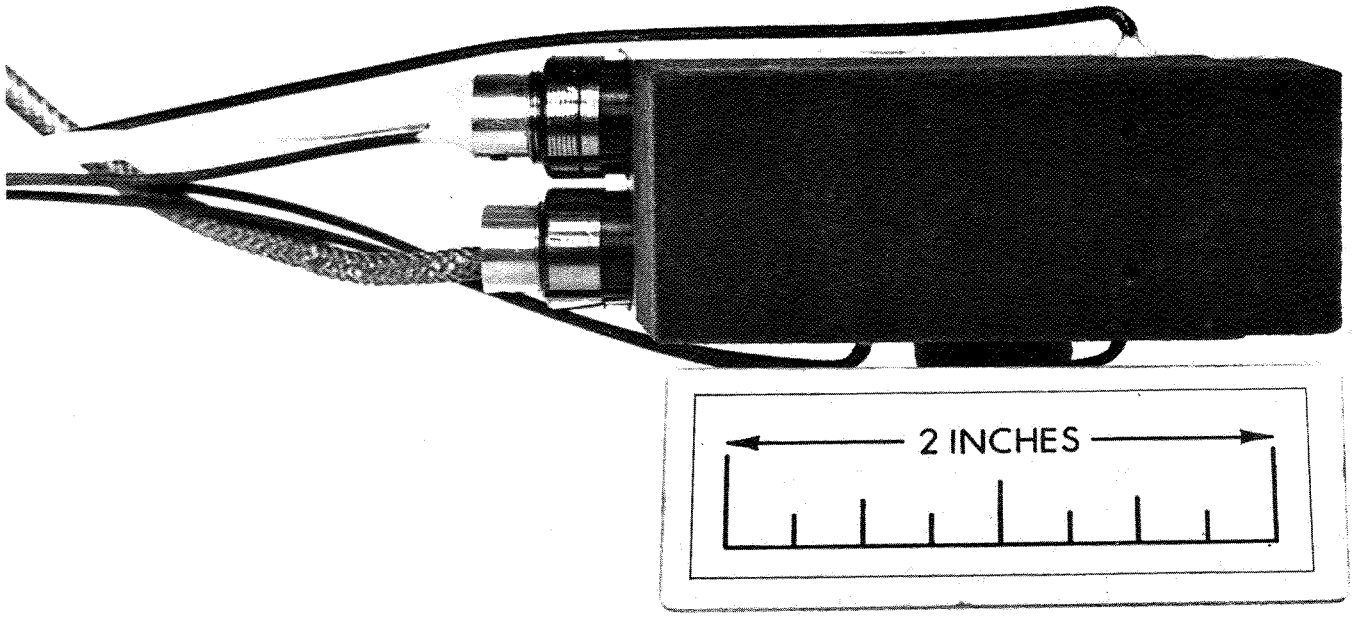

Figure V-27 PRETEST SPECIMEN

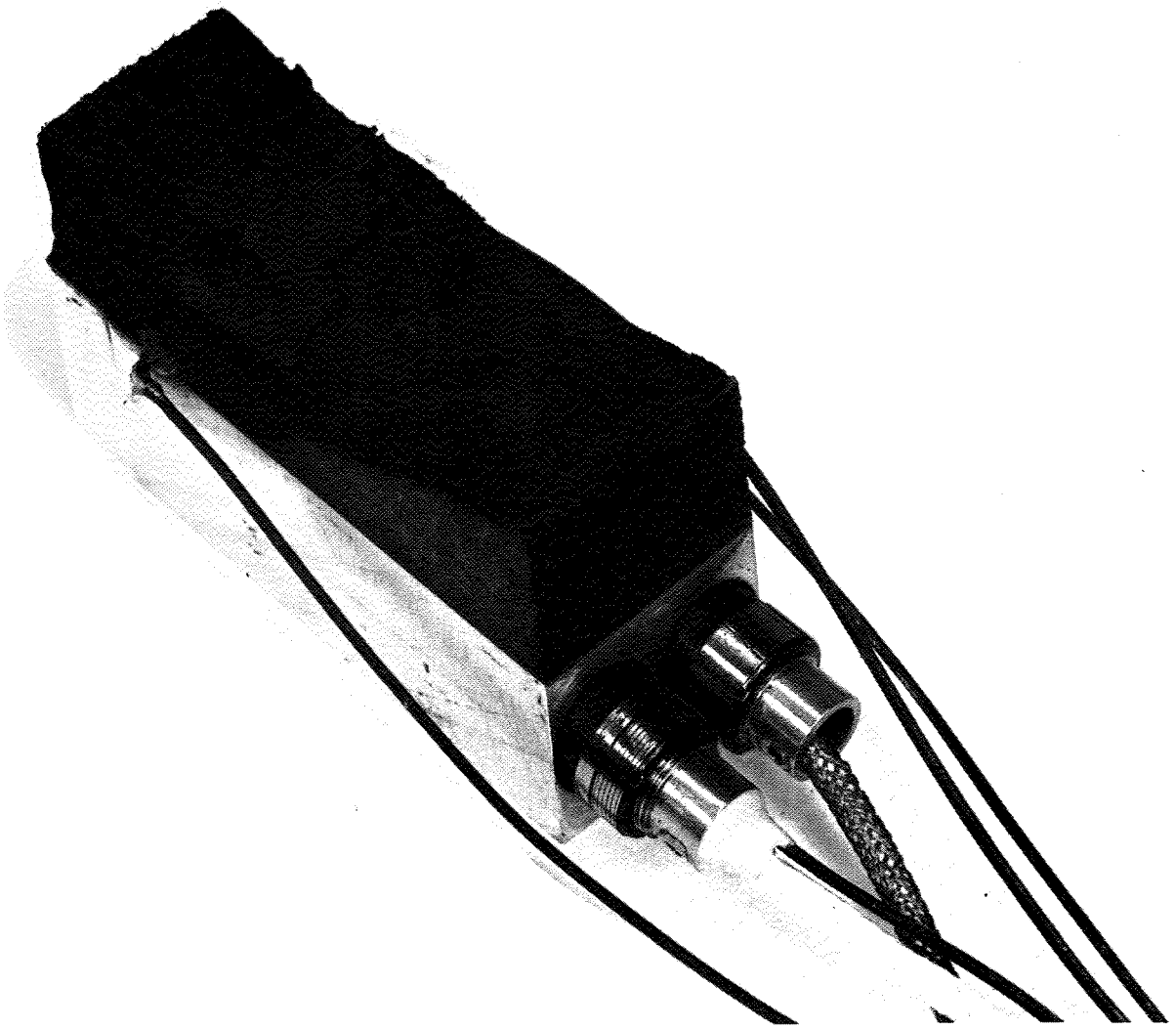

Figure V-28 POST-TEST SPECIMEN

SURFACE RECESSION MEASUREMENTS
(THERMO CHEMICAL PLUS MECHANICAL)

STATION (inches)	SURFACE RECESSION (inches)		
0.0	0.12	0.09	0.07
0.25	0.19	0.17	0.16
0.50	0.26	0.17*	0.21
0.75	0.30	0.19*	0.24
1.0	0.32	0.22*	0.26
1.25	0.28	0.27	0.25*
1.50	0.27	0.22*	0.28*
1.75	0.23*	0.24*	0.31
2.00	0.24*	0.24*	0.28
2.25	0.25	0.25	0.25
2.50	0.22	0.21	0.20

*CHAR INCLUDED

88-3621

Figure V-29 MEASURED SURFACE RECESSION

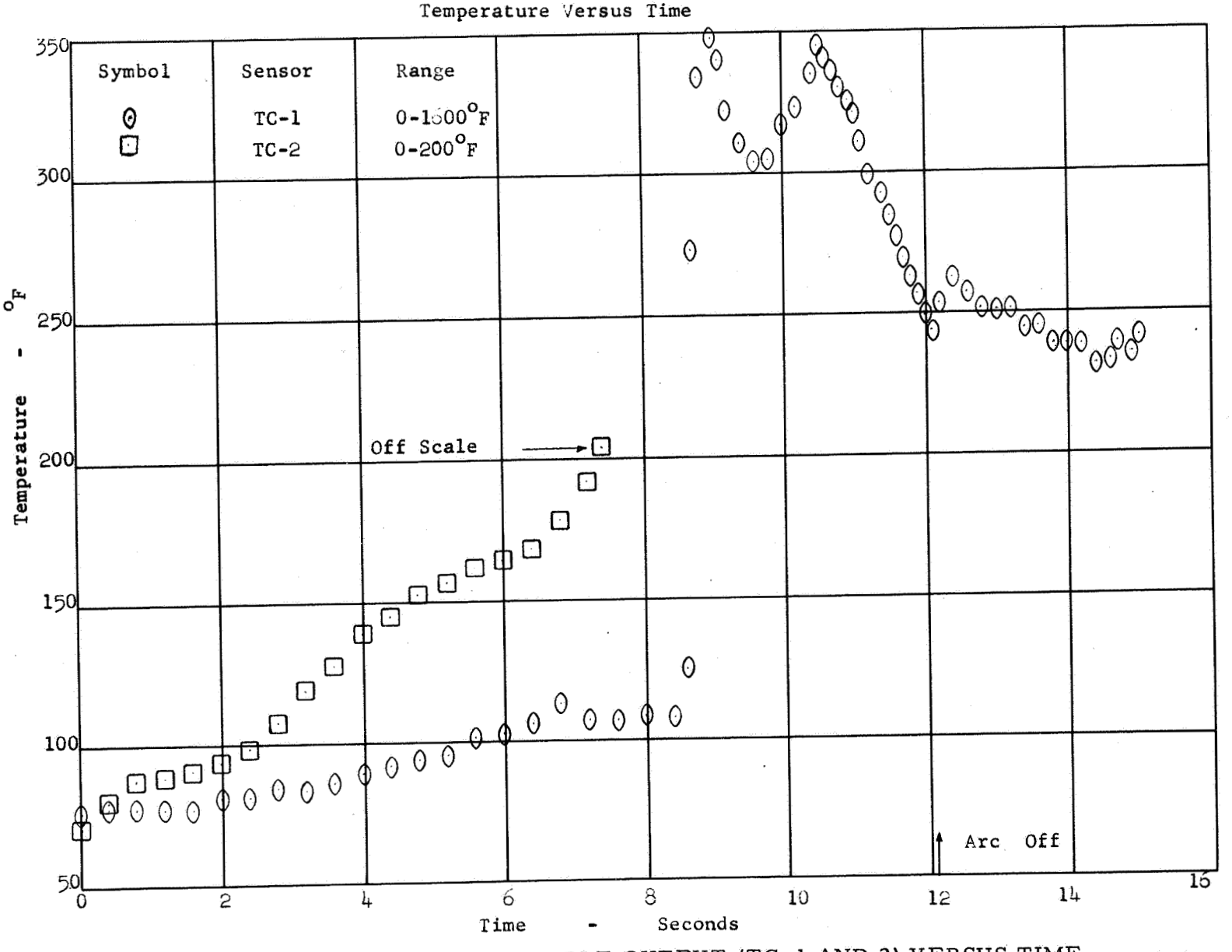

Figure V-30 THERMOCOUPLE OUTPUT (TC-1 AND 2) VERSUS TIME

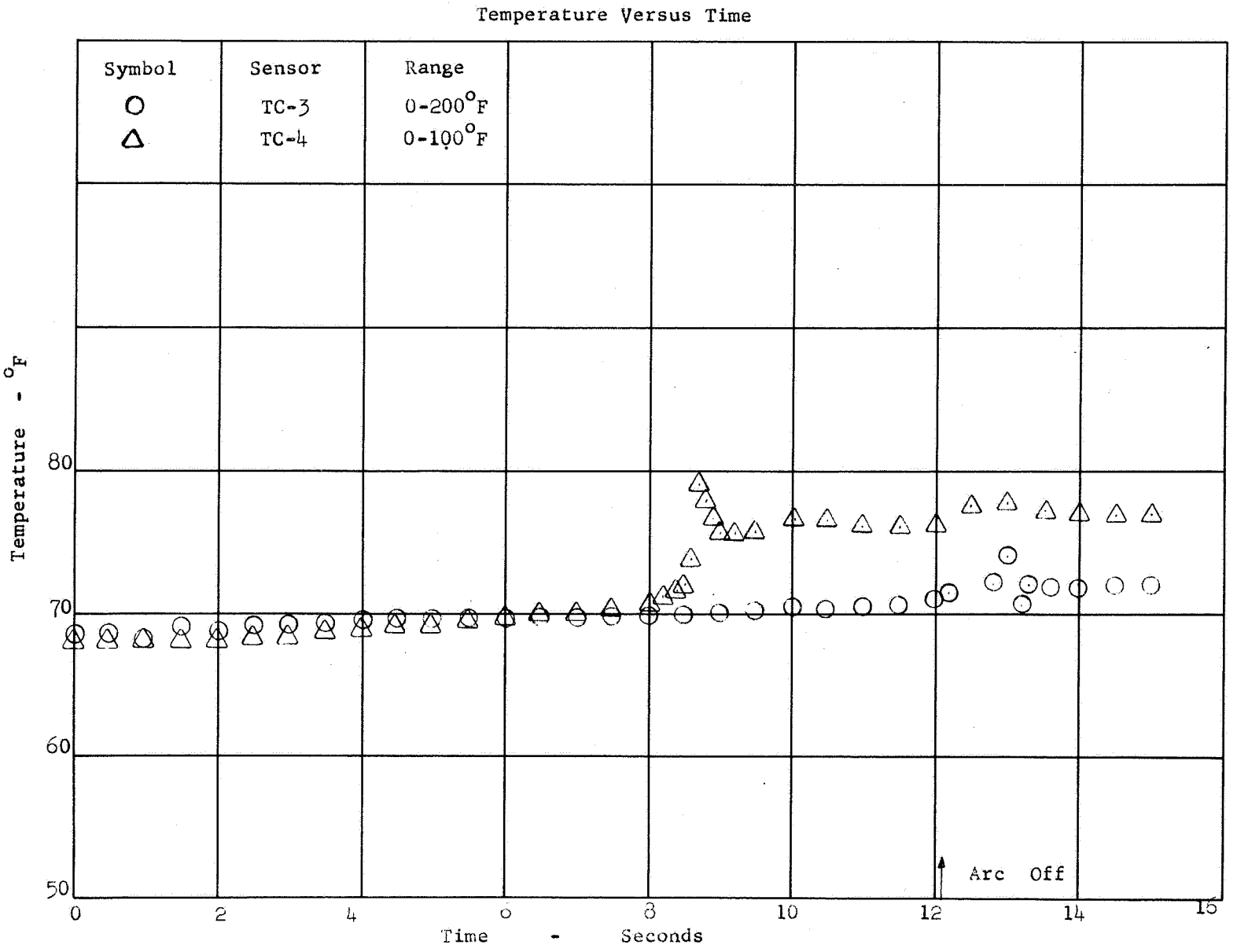

Figure V-31 THERMOCOUPLE OUTPUT (TC-3 AND 4) VERSUS TIME

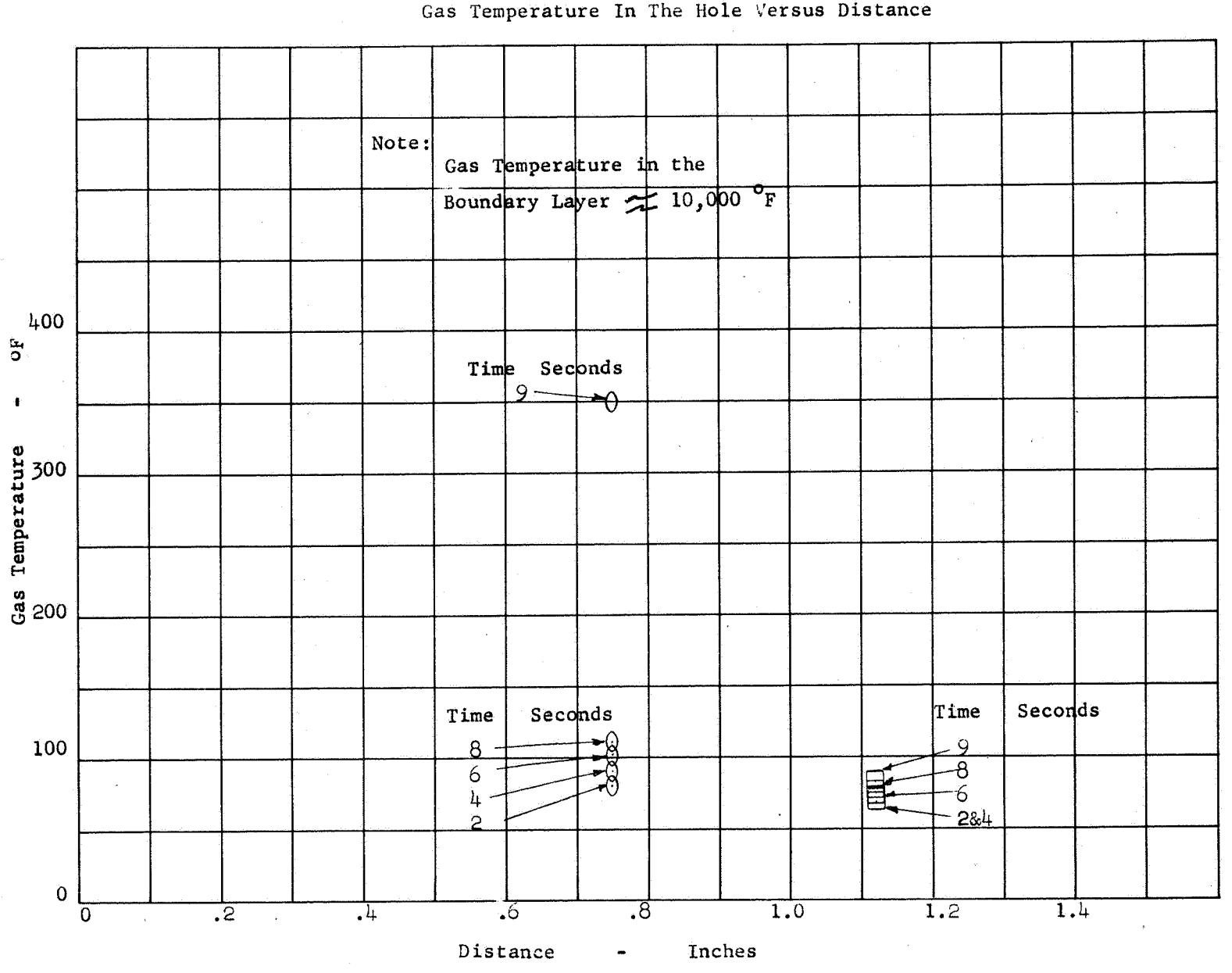

Figure V-32 PORT GAS TEMPERATURE ATTENUATION

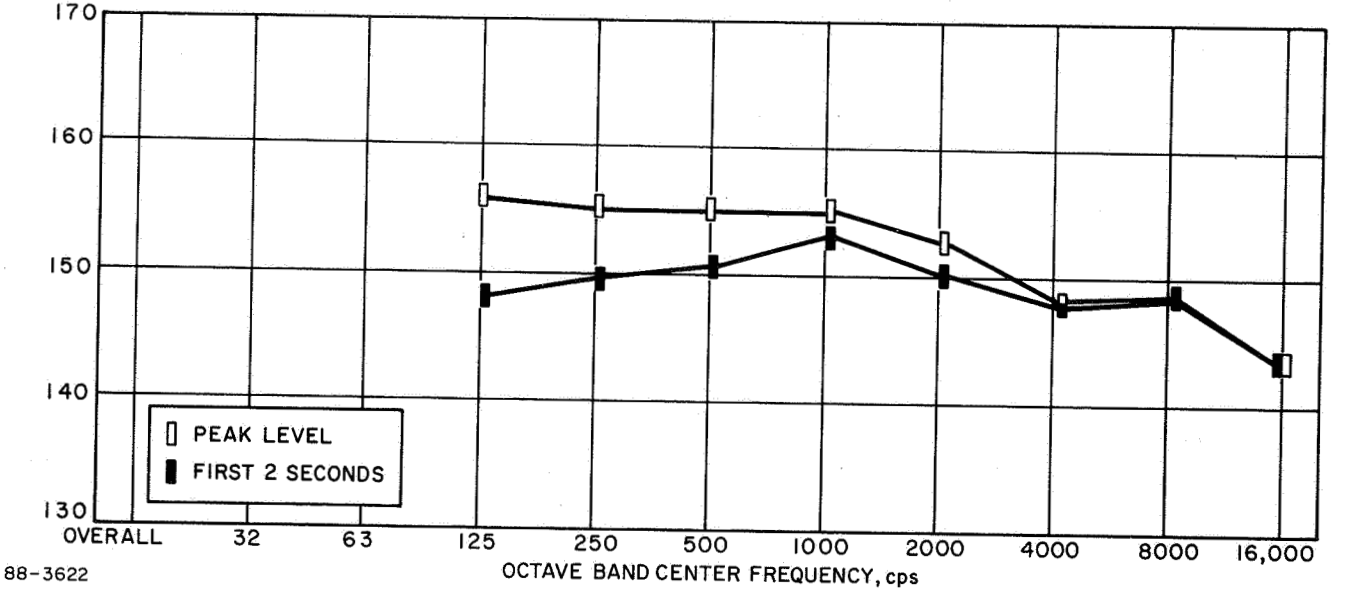

Figure V-33 ARC TEST OCTAVE BAND SPECTRA

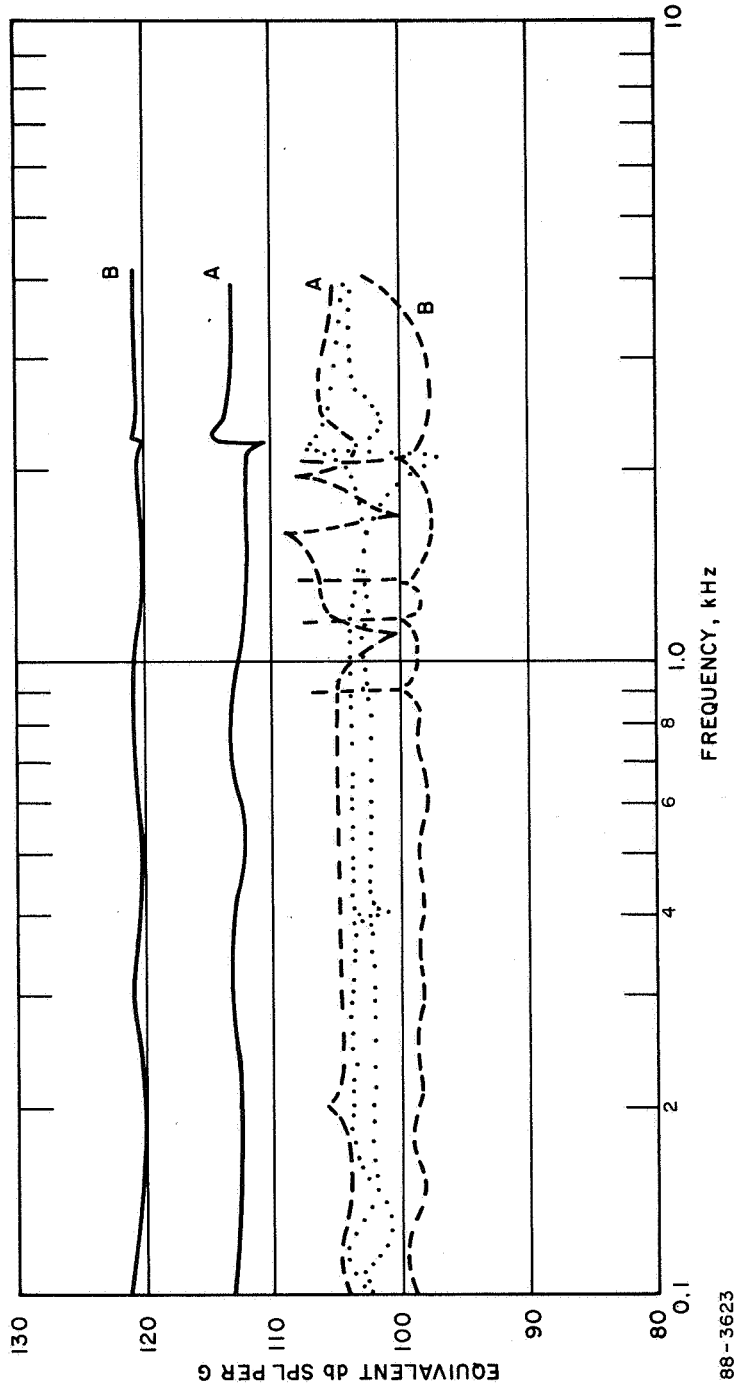

Figure V-34 VIBRATION RESPONSE OF TWO SAMPLES OF CT-4S

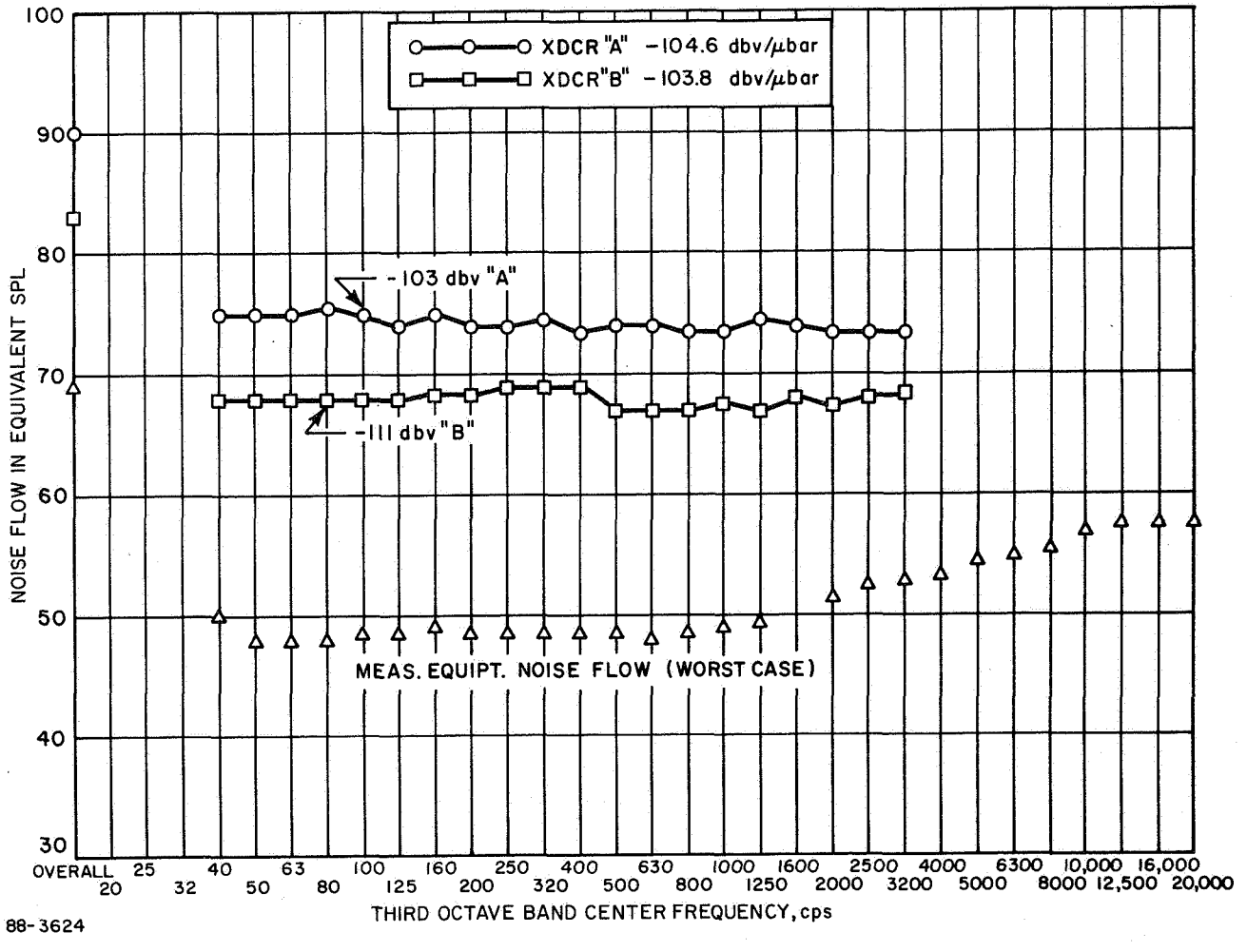

Figure V-35 ELECTRICAL NOISE FLOOR FOR TWO TRANDUCERS

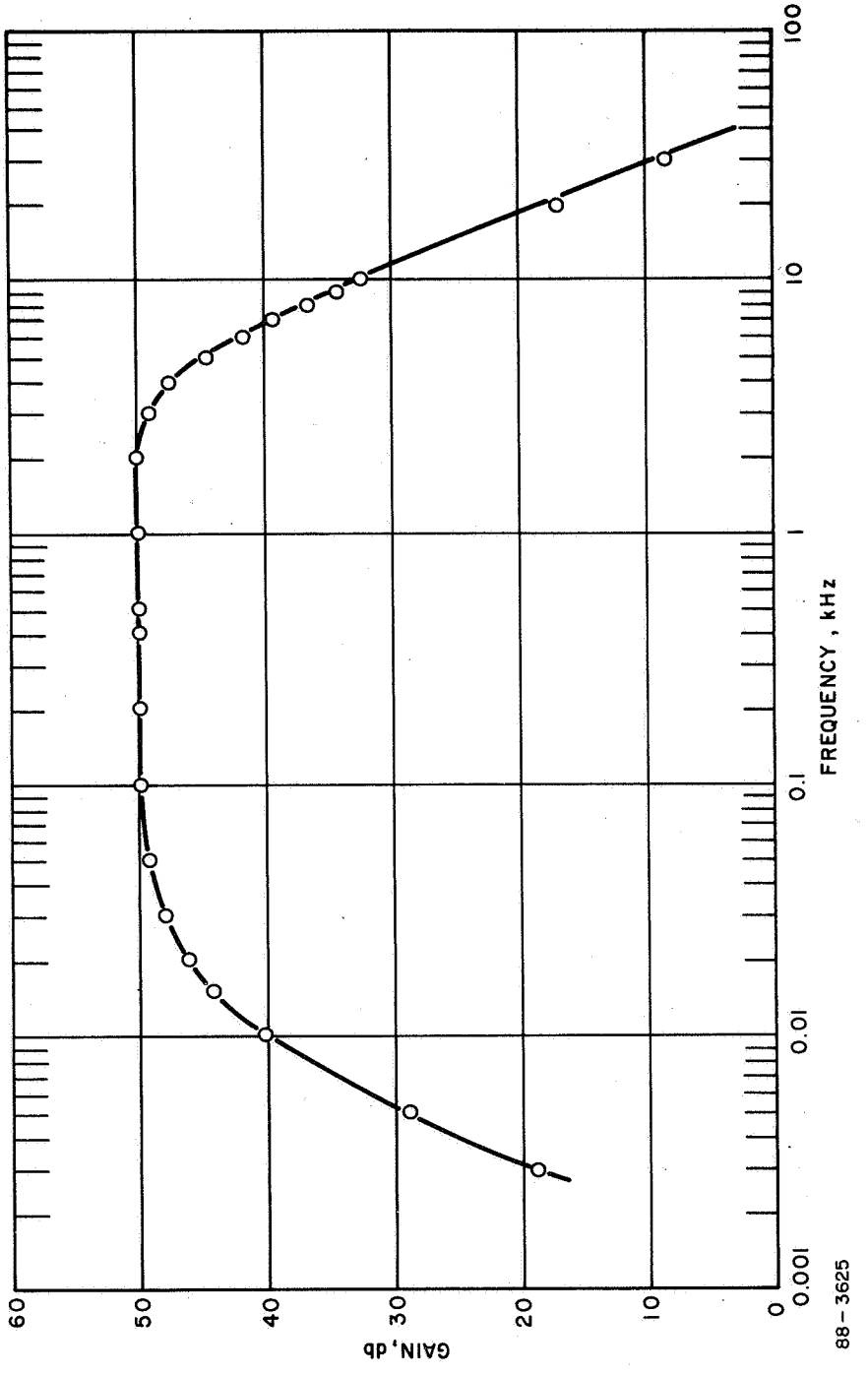

Figure V-36 TRANSITION DETECTOR 370A (BREADBOARD)
FREQUENCY RESPONSE

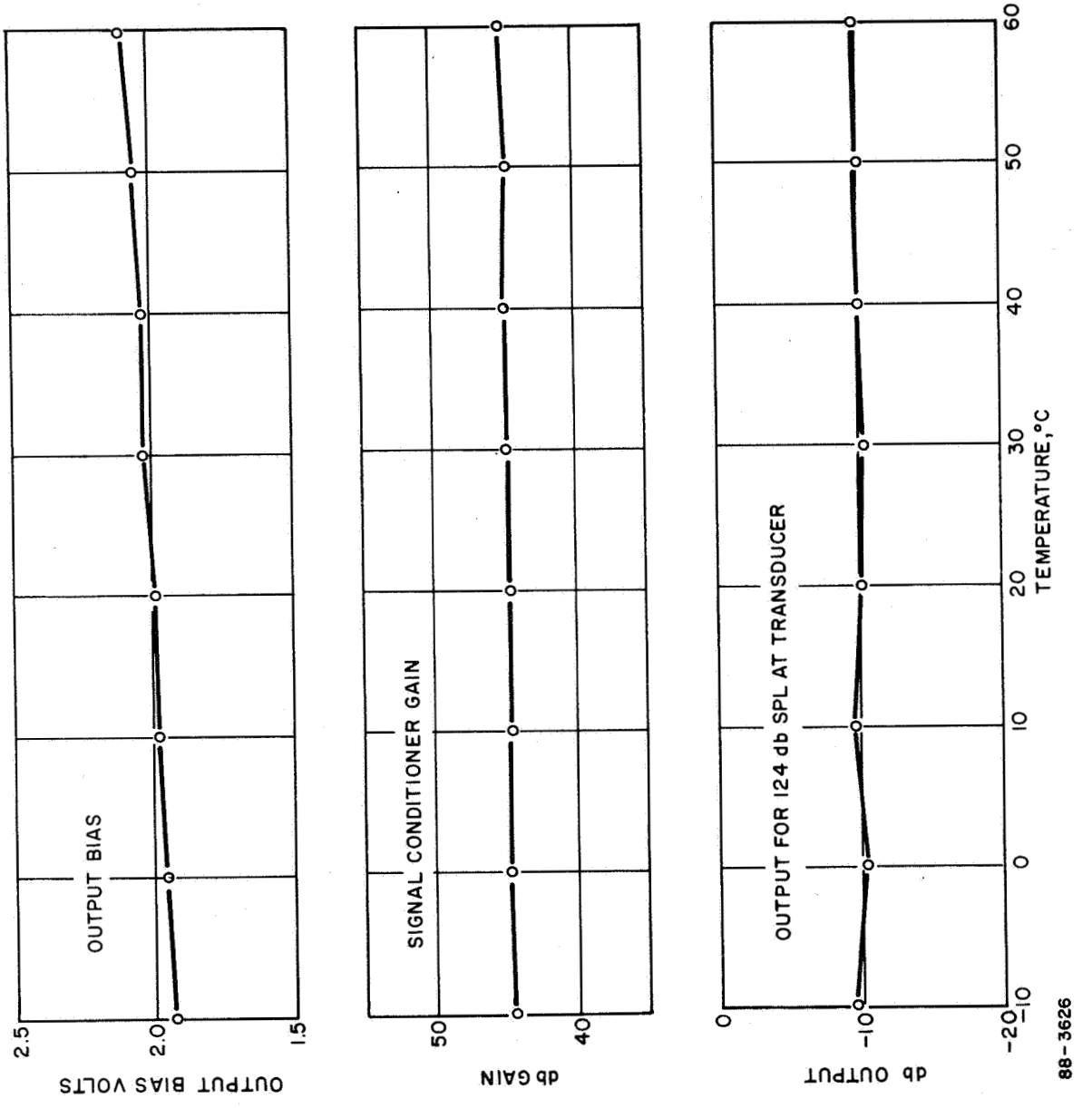

Figure V-37 SYSTEM TEMPERATURE TESTS

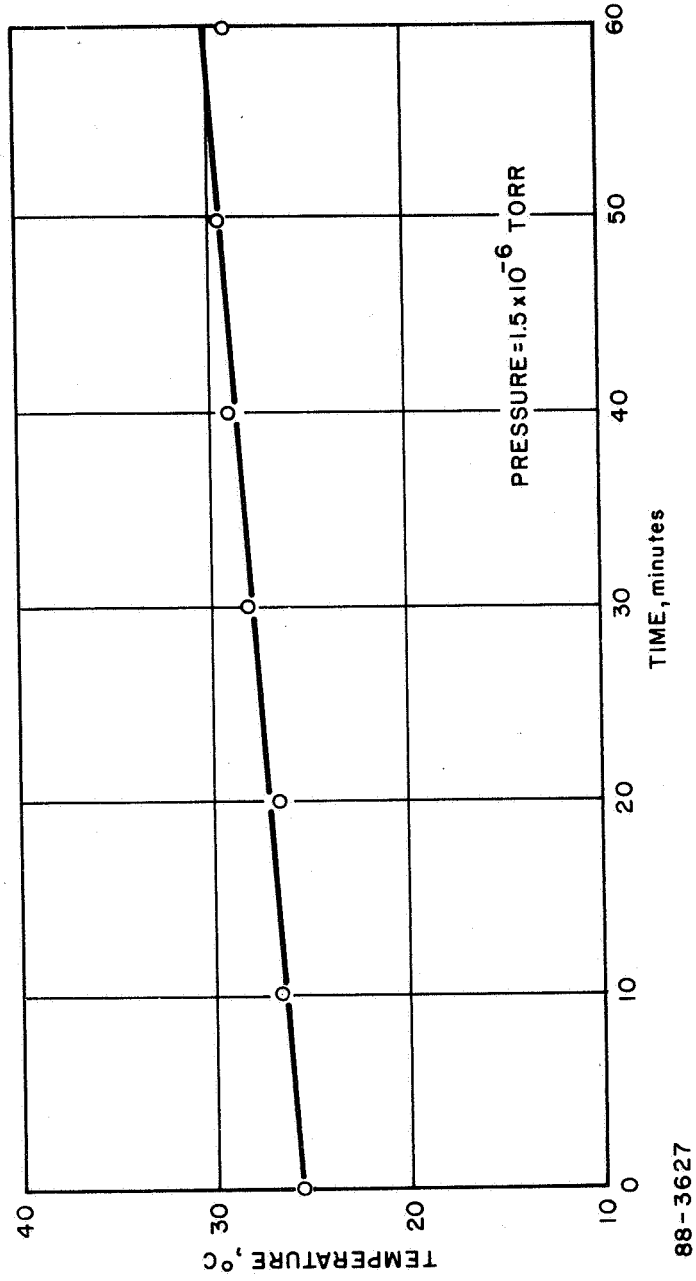

Figure V-38 CASE TEMPERATURE

VI. CONCLUSIONS AND RECOMMENDATIONS

The acoustic transition detector development has been successfully completed and the concept and hardware have been validated to the extent possible by laboratory and ground tests. The technical desirability and urgent requirement for such a measurement system has been demonstrated by the interest expressed by the scientific community and the concurrent flight hardware fabrication contract sponsored by the Air Force under Contract AF04(694)-932.

A. Conclusions

1) The concept of using a ported microphone to detect pressure fluctuations in the turbulent boundary layer of a body during reentry has been established to the extent possible in a wind tunnel.

2) A simple acoustic coupler consisting of a small diameter tube of constant cross-section with a 90 degree bend just forward of the microphone has been found adequate. This configuration is amenable to calculation of its acoustic characteristics and provides adequate protection of the transducer.

3) The port in the heat shield required to provide communication between the boundary layer and transducer did not disturb the laminar flow and cause premature turbulence during the wind tunnel tests.

4) The survey of available microphones has resulted in at least two units that are small (1/4 inch diameter) and have the performance characteristics required to accomplish the measurement.

5) The validity of the system design has been substantiated through the flight hardware phase by subjecting a packaged unit to rigorous performance and environmental tests.

B. Recommendations

It is recommended that:

1) The vibration sensitivity of the miniature microphone used as the transducing device be reduced to ensure that vibration does not mask the initial vorticity associated with transition onset.

2) The electronics required to condition the microphone output be fabricated using thick film techniques or integrated circuits to further miniaturize the system.

VII. REFERENCES

1. Reliability and Quality Assurance Plan for NAS 1-7439, Development of an Acoustic Flow Transition Detector for Reentry Spacecraft, Avco Corporation Report No. AVMSD-0113-68-CR, dated 22 January 1967 (U)

2. Boundary Layer Transition Study Group Meeting - Volume I, Opening Remarks, Keynote Address, Session on Flight Test Transition Data and Correlations, Aerospace Report No. TR-0158 (S3816-63)-1, Vol. I, dated August 1967 (S)

3. Boundary Layer Transition Study Group Meeting - Volume II, Session on Boundary Layer Stability, Aerospace Report No. TR-0158 (S3816-63)-1, Vol. II, dated August 1967 (U)

4. Boundary Layer Transition Study Group Meeting - Volume III, Session on Ground Test Transition Data and Correlations, Aerospace Report No. TR-0158 (S3816-63)-1, Vol. III, dated August 1967 (C)

5. Boundary Layer Transition Study Group Meeting - Volume IV, Session on Boundary Layer Transition Control and Panel Session, Aerospace Report No. TR-0158 (S3816-63)-1, Vol. IV, dated August 1967 (S)

6. Whittaker, R. L., Expected Aero-Thermo Environmental Parameters and Heat Shield Response for NASA Reentry Vehicle, Avco Corporation Report No. TR G600-67-909, dated 27 December 1967

7. Pappas, C. and A. Okuno, Heat Transfer Measurements for Binary Gas Laminar Boundary Layers with High Rates of Injection, NASA TN D-2473, dated September 1964

8. Leadon, B. M., C. Scott and G. Anderson, Mass Transfer Cooling of a 20^{o} Porous Cone at $M_{\infty} = 5$, University of Minnesota, Rosemount Aeronautical Laboratory RR 143, dated July 1957

9. Andrews, P., Revision of Program 1944-ADTECH III, Avco Corporation Report No. S210-TR-67-54

10. Zavasky, J. J., and J. R. Malone, Correlation of Boundary Layer Transition Data Based on Momentum/Displacement Thickness Reynolds Numbers and Local Mach Number, Avco Corporation Report No. TR G600-67-814, dated 9 November 1967 (S)

11. Bies, D. A., A Review of Flight and Wind Tunnel Measurements Boundary Layer Pressure Fluctuations and Induced Structural Response, BBN Report No. 1269, Contract NAS 1-5120, Langley Research Report, dated 28 January 1966 (U)

12. Widnall, S., Pressure Fluctuations on a Slender Cone at Mach 3, BBN Technical Memorandum, dated March 1968 (U)

13. Heller, H. H., A Supersonic-Wind-Tunnel Study of Flow Transition, BBN Report No. 1585, dated February 1968 (U)

14. Manning, J. E. and K. L. Chandiramani, Vibration Transmission in the RVTO Phase 1A Reentry Vehicles, BBN Report No. 1533, dated 15 March 1968 (U)

15. Nagamatsu, H. T., R. E. Sheer, Jr. and B. C. Graver, Hypersonic Laminar Boundary-Layer Transition, AIAA J. 5, No. 7, 1245-1252, dated July 1967 (U)

16. Braslow, A., A Review of Factors Affecting Boundary-Layer Transition, NASA TN D-3384, dated August 1966 (U)

17. O'Connor, T. J., E. H. Comfort and L. A. Cass, Turbulent Mixing of Axisymmetric Jets of Partially Dissociated Nitrogen with Ambient Air, Avco Corporation Report No. RAD-TR-65-18, dated 15 July 1965 (U)

18. Heller, H. H., Frequency Response of Acoustic Probes for Measuring Pressure Fluctuations on a Hypersonic Reentry Vehicle, BBN Report No. 1498, dated 3 May 1967.

A-1. Lighthill, M. J., Oscillating Airfoils at High Mach Number, J. Aeron. Sci. 20, No. 6, June 1953.

VIII. BIBLIOGRAPHY

1. Anderson, A., "Flow Characteristics of A 12-in. Intermittent Supersonic Tunnel," AEDC-TDR-63-203 (AD 418578) (1963).

2. Brinich, Paul F., "Effect of Leading-edge Geometry on Boundary-layer Transition at Mach 3.1," NACA TN 3659 (1956).

3. Brinich, Paul F. and Sands, Norman, "Effect of Bluntness on Transition for a Cone and a Hollow Cylinder at Mach 3.1," NACA TN 3979 (1957).

4. Brinich, Paul F., "Recovery Temperature, Transition and Heat Transfer Measurements at Mach 5," NASA TN D-1047 (1961).

5. Brinich, P. F., "Boundary Layer Transition at Mach 3.12 With and Without Single Roughness Elements," NACA TN 3267.

6. Coats, Jack D., "Flow Characteristics of a 40-in. Wind Tunnel at Mach Numbers 1.5 to 6," AEDC-TDR-62-130 (AD 277289) (1962).

7. Corcos, G. M., "Resolution of Pressure in Turbulence," J. Acoust. Soc. Am. 35, 192-199 (1963).

8. Fitzpatrick, H. M. "Spatial Resolution Effected by a Recesses Microphone," J. Acoust. Soc. Am. 40, 1247 (1966)(A).

9. Heller, H. H., "Frequency Response of Acoustic Probes for Measuring Pressure Fluctuations on a Hypersonic Reentry Vehicle," Bolt Beranek and Newman Inc. Rept. 1498 (1967).

10. Holloway, Paul F. and Sterrett, James R., "Effect of Controlled Surface Roughness on Boundary-Layer Transition and Heat Transfer at Mach Numbers of 4.8 and 6.0," NASA TN D-2054 (1964).

11. Kistler, A. L. and Chen, W. S., "The Fluctuating Pressure Field in a Supersonic Turbulent Boundary Layer," Jet Propulsion Laboratory Technical Report No. 32-277 (1962).

12. Kovasznay, Leslie, S. G., "Turbulence in Supersonic Flow," Fournal of the Aeronautical Sciences, 20, No. 10 (1953).

13. Laufer, J., "Factors Affecting Transition Reynolds Numbers on Models in Supersonic Wind Tunnels," JAS, vol. 21, no. 7, July 1964, pp. 497-498.

14. Laufer, John, "Sound Radiation from a Turbulent Boundary Layer," Jet Propulsion Laboratory Technical Report No.32-119, (1961).

15. Laufer, John, "Aerodynamic Noise in Supersonic Wind Tunnels," JPL Progress Report No. 20-378 (1959) and Journal of the Aerospace Sciences, 28, 685-692 (1961).

16. Laufer, John, "Some Statistical Properties of the Pressure Field Radiated by a Turbulent Boundary Layer," The Physics of Fluids, 7, No. 8 (1964).

17. Laufer, John and Marte, Jack E., "Results and a Critical Discussion of Transition Reynolds Number Measurements on Insulated Cones and Flat Plates in Supersonic Wind Tunnels," JPL Report No. 20-96 (1955).

18. Morkovin, M. V., "On Transition Experiments at Moderate Supersonic Speeds," JAS, vol. 24, no. 7, pp. 480-486, July 1957.

19. Morkovin, M. V., "On Supersonic Wind Tunnels With Low Free-Stream Disturbances," Journal of Applied Mechanics, Paper No. 59-APM-10, 26, 319-324 (1959).

20. Phillips, O. M., "On the Generation of Sound by Supersonic Turbulent Shear Layers," Journal of Fluid Mechanics, 9, 1-28 (1960).

21. Potter, J. L. and Whitfield, J. D., "Effects of Slight Nose Bluntness and Roughness on Boundary-Layer Transition in Supersonic Flow," U. S. Air Force, Arnold Engineering Development Center. AEDC-TR-60-5 (March 1960).

22. Rumsey, C. and Lee, D., "Measurements of Aerodynamic Heat Transfer and Boundary Layer Transition on a 10^{o} Cone in Free Flight at Supersonic Mach Numbers up to 5.2 NASA-TN-D-745, May 1961.

23. Schueler, C. J., "Comparison of the Aerodynamic Characteristics of AGARD Model A from Tests in 12-in. and 40-in. Supersonic Wind Tunnels," AEDC-TN-61-8 (AD 251477) (1961).

24. Schueler, C. J., "A Comparison of Transition Reynolds Numbers from 12-in. and 40-in. Supersonic Tunnels." AEDC-TDR-63-57 (AD 299290) (1963).

25. Sivells, J. C. and Payne, R. G., "A Method of Calculating Turbulent Boundary-Layer Growth at Hypersonic Mach Numbers," AEDC-TR-59-3 (AD 208774) (1959).

26. Staylor, W. F. and Morrisette, E. L., "Use of Moderate-Length Hot Wires to Survey a Hypersonic Boundary Layer," AIAA Journal, vol. 5, no. 9, September 1967, pp. 1698-1700.

27. Stetson, K., and Rushton, G., "A Shock Tunnel Investigation of the Effects of Nose Bluntness, Angle of Attack and Boundary Layer Cooling on Boundary Layer Transition at a Mach Number of 5.5," AIAA Paper 66-495.

28. Van Driest, E. R. and Blumer, C. B., "Boundary Layer Transition: Freestream Turbulence and Pressure Gradient Effects," AIAA J., vol. 1, no. 6, June 1963.

29. Vrebalovich, Thomas, Discussion on "On Supersonic Wind Tunnels with Low Freestream Disturbances," by M. V. Morkovin, Journal of Applied Mechanics (1960).

30. Whitfield, Jack D. and Potter, J. Leith, "The Influence of Slight Leading-Edge Bluntness on Boundary-Layer Transition at a Mach Number of Eight," AEDC-TDR-64-18 (AD 431533) (1964).

31. Whitfield, J. D. and Potter, J. L., "The Unit Reynolds Number as a Parameter in Boundary Layer Stability," AEDC-TN-58-77, Oct. 1958.

32. Willmarth, W. W. and Roos, F. W., "Resolution and Structure of the Wall Pressure Field Beneath a Turbulent Boundary Layer," J. Fluid Mech. 22, Pt. 1, 87-94 (1965).

APPENDIX

Dynamics of Ports for Measuring Pressure Fluctuations

The dynamics of the porting arrangement that comprises the acoustic coupler is central to the use of a ported microphone for study of fluctuating boundary layer pressure. Consequently, relatively extensive theoretical and experimental investigations have been accomplished to describe the behavior of ports subjected to acoustic excitation and both subsonic and supersonic flow. The frequency response of the porting arrangements studied was found to depend on both the interior geometry of the port and the physical characteristics of the flow. The most dramatic effect was found to be associated with changes of the impedance of the port opening under supersonic flow. Since the phenomena is difficult to grasp intuitively, we have included a theoretical discussion using piston theory aerodynamics as the flow model in an effort to describe the flow induced damping of a Helmholtz resonator (see figure A-1).

Using the model, we observe a pressure p=pc-v acting on the port, to which the system responds in addition to the actual signal pressure. When the external fluid is at rest or moves with subsonic flow speeds, the modification is slight. When the fluid moves at supersonic speeds, the modification is substantial.

The effect of the external fluid is modeled by considering the solution for a piston oscillating with velocity v in an infinite baffle. In this case, the pressure on the piston is not only the signal pressure p_a, but a contribution due to the motion of the piston. When the fluid is at rest, the pressure on the oscillating piston, including the effect of its motion, is

$$p_{port} = j\omega \frac{8}{3\pi} \rho r v + p_a , \qquad (1)$$

where r is the radius of the piston.

This essentially increases the effective mass of the system by a small amount, which is negligible for most applications. If the external flow is subsonic, the effective mass is reduced, raising the natural frequency slightly.

The presence of an external hypersonic flow, however, modifies the impedance of the opening in a manner that is not negligible. In the following discussion we show that the presence of an external hypersonic stream changes the p, v relation to

$$p = v \rho_e c_e + p_a , \tag{2}$$

where ρ_e and c_e are static properties outside the boundary layer. In addition, we will discuss a model for the effects of the boundary layer of thickness δ on Eq. (2).

Before discussing the effect of hypersonic flow on the impedance of the opening, let us examine the consequences of Eq. (2) upon the frequency response of a configuration with sufficient internal volume so that the Helmholtz resonator model is appropriate.

Comparing the transfer functions of a simple Helmholtz resonator with and without the ρ_c loading due to the external hypersonic flow, we have

without external flow

$$\frac{p_o}{p_a} = \frac{1}{1 - \dfrac{\omega^2 \cdot L \cdot V \cdot \rho}{c^2_o \cdot A \cdot \rho_o}} , \tag{3}$$

with external flow

$$\frac{p_o}{p_a} = \frac{1}{1 + \dfrac{j \omega V \rho_e c_e}{c^2_o A \rho_o} - \dfrac{\omega^2 L V \rho}{c^2_o A \rho_o}} , \tag{4}$$

where the subscript o refers to properties inside the port/volume combination and e refers to properties outside in the free stream, which may be different. L and A are the tube length and the tube cross-sectional area, respectively, and V is the effective total volume.

The system under the external hypersonic stream behaves as an overdamped second-order system. The break frequency occurs at

$$f_b = \frac{c_o^2 \, A \, \rho_o}{V \, \rho_e \, c_e}^{\frac{1}{2\pi}} \quad . \tag{5}$$

For operation under a boundary layer, the static pressure in the probe is equal to that of the free stream. Equation (5) can be written as

$$f_b = \frac{c_o^2 \, A}{V \, c_e} \left(\frac{c_e^2}{c_o^2} \right)^{\frac{1}{2\pi}} \quad , \tag{6}$$

since, assuming air in the cavity,

$$\frac{\rho_o}{\rho_e} = \frac{T_e}{T_o} = \frac{c_e^2}{c_o^2} \quad . \tag{7}$$

Thus,

$$f_b = f_b = \frac{C_e}{2\pi} \left(\frac{A}{V} \right) \tag{8}$$

where C_e is the external static speed of sound outside the boundary layer. C_e can be predicted from the shape of the vehicle in conjunction with the flight Mach number and altitude.

The remaining quantity A/V for the port/volume model can be determined from the natural frequency f_n measured at sea-level conditions in an anechoic chamber, since, from Eq. (3),

$$\frac{A}{V} = \frac{f_n^2{}_{\text{anechoic}} \cdot L \cdot 4\pi^2}{C^2{}_{\text{anechoic}}} \tag{9}$$

Thus, the theoretical prediction is that the effect of the external hypersonic stream will cause the Helmholtz resonator to respond as a highly damped second-order system with a break frequency that can be predicted from anechoic-chamber tests and predictable flight conditions.

We will now discuss a model which was used to evaluate the break frequency of the system, i. e., we will consider the effect of external hypersonic flow on the impedance of the port.

The calculation of pressures on a body in either steady or unsteady flow becomes greatly simplified for high Mach-numbers or hypersonic-flow regimes. As first pointed out by Lighthill,[A1] the gas flow may be treated as a series of one-dimensional vertical slabs moving rapidly past the body. The boundary condition of no flow through the body surface imposes a normal velocity at the base of each slab. The slab responds as an ordinary one-dimensional column of air when a piston moves into it with a given velocity.

The pressure on the body is given by

$$p = \rho c v_n \ , \tag{10}$$

where v_n is the normal velocity relative to the slab. This is the pressure on a piston moving into a gas of acoustic impedance ρ_c with velocity v_n.

Since the slab is moving relative to the body, the normal velocity at the base of the column is

$$v_n = \frac{\partial h}{\partial t} + V \frac{\partial h}{\partial x} \ , \tag{11}$$

where the shape of the body is given by h(x, t).

Piston-theory aerodynamics has found wide application in problems of wing and panel flutter at high Mach numbers. It is quite appealing because of its simplicity and seems accurate for M>3.

We use piston-theory aerodynamics to determine how external hypersonic flow modifies the dynamics of a Helmholtz resonator (see figure A-2) for the flow model.

We assume that the normal velocity at the opening on the plate is $v(x)\, e^{i\omega t}$. The pressure induced at this boundary by the oscillations of the column of air is

$$p = \rho_c \left[v(x) + \frac{V}{j\omega} \frac{\partial V(x)}{\partial x} \right] . \tag{12}$$

If we are concerned with the average pressure at the opening, we ignore the second term. This term is a local modification due to details of the profile of $v_n(x)$ at the opening on the plate and will certainly not modify the impedance as seen by the resonator.

The relation between the pressure induced by the motion of the air column to its velocity is then

$$p = \rho_c v \tag{13}$$

The consequences of this result on the dynamics of the pressure transducer have been previously discussed.

In reality, the fluid in a thin layer near the plate is at rest or moving slowly. This will modify the simple result of Equation 13.

As a model for the boundary layer, we consider a thin layer of incompressible (M=0) fluid, of height δ bounded below by the plate and above by the external hypersonic flow. The height δ is not the actual boundary layer, since most of the boundary layer has hypersonic flow speeds. It would be a measure of the incompressible or low Mach number part only. As an approximation, one could take as a value for δ, the distance to the sonic line.

We wish to calculate the pressure on a piston of area A, oscillating beneath these two fluid layers with velocity v_1. This will give us the modification to the system response caused by the boundary layer under the external hypersonic stream. A sketch of this model is shown in figure A-2.

For small δ, we set up a one-dimensional flow model for the dynamics of the two-fluid layer. Since this is the range of interest, these are the most useful results. The hypothesis is that v_δ would equal v_1 except for the fluid which escapes as u_r, tangentially. How much u_r is obtained for a given v_1 depends on the impedance of the layer to tangential velocities, p/u_r.

The pressure on the boundary is

$$p = \rho_e c \left(v_\delta + \left(\frac{V}{j\omega} \frac{\partial v_\delta}{\partial x} \right) \right) . \tag{14}$$

The second term, $\partial v_\delta / \partial x$, is an antisymmetric term and changes the impedance of the layer by a different amount in the upstream and downstream directions. The pressure on the piston should respond only to the average impedance of the layer.

Using one-dimensional flow concepts, we write a mass conservation equation for the thin layer:

$$v_\delta r + \delta \frac{\partial}{\partial r} (r u_r) = 0. \tag{15}$$

The r momentum equation is

$$\frac{\partial u_r}{\partial t} + j\omega u_r = - \frac{1}{\rho_\delta} \frac{\partial p}{\partial r} . \tag{16}$$

The relation between p and v_δ for the average impedance is

$$p = \rho_e c v_\delta . \tag{17}$$

Combining Equations (15), (16), and (17) gives

$$r^2 \frac{\partial^2 u}{\partial r^2} + r \frac{\partial u_r}{\partial r} - \left(1 - r^2 \frac{i\omega\rho_\delta}{c\rho_e \delta} \right) u_r = 0 . \tag{18}$$

In this section, we are using a time dependence $e^{-j\omega t}$ for convenience.

This is a form of Bessel's equation with outgoing wave solution

$$u_r \sim H_1^{(1)} \left(j^{1/2} \sqrt{\frac{\omega \rho_\delta}{\rho_e c \delta}} \; r \right) . \tag{19}$$

The pressure is found from

$$p = \rho c v_\delta = -\rho c \frac{\delta}{r} \frac{\partial}{\partial r} (r u_r) . \tag{20}$$

The tangential impedance is

$$\frac{p}{u_r} = -\rho \frac{c\delta}{r} i^{\frac{1}{2}} \sqrt{\frac{\omega \rho_\delta}{\rho_e c \delta}} \; r \frac{H_o^{(1)}\left(j^{\frac{1}{2}} \sqrt{\frac{\omega \rho_\delta}{\rho_e c \delta}} \; r \right)}{H_1^{(1)}\left(j^{\frac{1}{2}} \sqrt{\frac{\omega \rho_\delta}{\rho_e c \delta}} \; r \right)} . \tag{21}$$

The asymptotic relation for H_o/H_i is i or

$$\frac{p}{u_r} = \frac{1}{\sqrt{2}} \rho_e c \delta (1 + i) \sqrt{\frac{\omega \rho_\delta}{\rho_e c \delta}} . \tag{22}$$

As an approximation to the continuity of mass in the neighborhood of the piston, we write

$$v_\delta a = v_p a - 2\pi r_o \delta u_r , \tag{23}$$

where r_o is the radius of the piston.

Assuming the pressure in the region is constant and equal to $\rho c v_\delta$, we may write for the final relation

$$p = \rho c v_p \frac{1}{\left[1 + \sqrt{2} \frac{(1-i)}{r_o} \sqrt{\frac{\rho_e c \delta}{\omega \rho_\delta}} \right]} . \tag{24}$$

This relation reduces to $p = \rho_e c v_p$ for $\delta = 0$, and gives a first-order correction for small δ/r_o. The value of δ/r_o expected on typical reentry vehicles is small, so the simpler expression is expected to be accurate for most purposes.

MEDIUM AT REST

M = 0

HYPERSONIC FLOW

M >> 1

HELMHOLTZ RESONATOR

TYPICAL RESPONSE

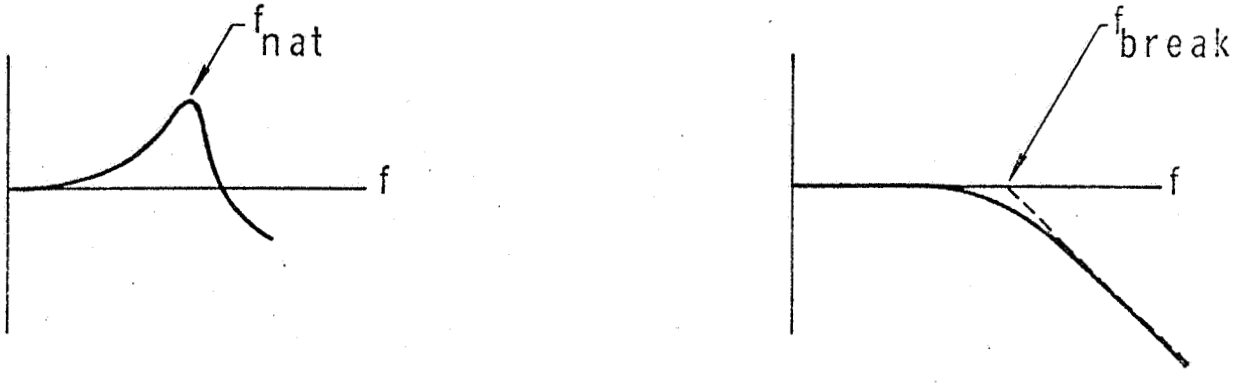

$$f_{nat} = \frac{c_o}{2\Pi}\sqrt{\frac{A}{V\ell}}$$

$$f_{break} = \frac{c_e}{2\Pi}\,\frac{A}{V}$$

FIGURE A-1

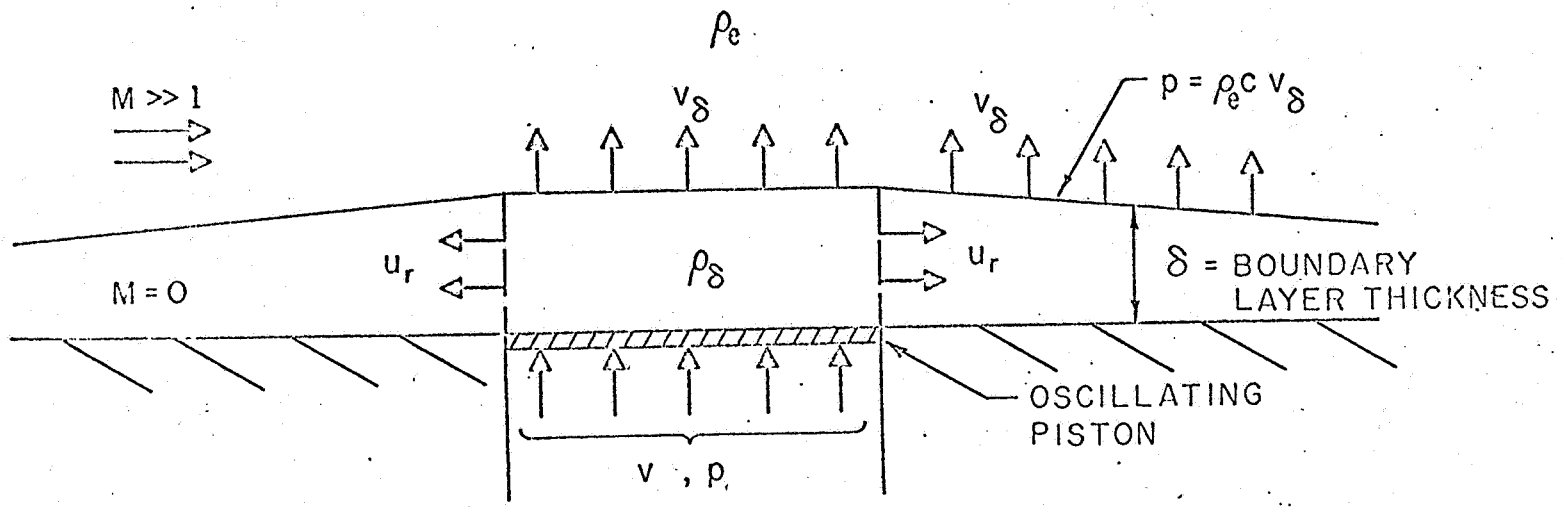

FIGURE A-2 MODEL FOR OPERATION UNDER A THIN BOUNDARY LAYER

DISTRIBUTION

Addressee	No. of Copies
NASA Langley Research Center Langley Station Hampton, Virginia 23365	
Attention: Contracting Officer, Mail Stop 126	1
Research Reports Division, Mail Stop 122	1
R. L. Zavasky, Mail Stop 117	1
A. G. Beswick, Mail Stop 477	12
C. A. Sandahl, Mail Stop 215	1
R. L. James, Jr., Mail Stop 215	1
R. P. Rhinehart, Mail Stop 215	1
E. M. Sullivan, Mail Stop 214	1
R. L. Wright, Jr., Mail Stop 214	1
R. N. Hopko, Mail Stop 215	1
B. J. O'Hare, Mail Stop 215	1
F. L. Staggs, Mail Stop 488	1
C. S. Laird, Mail Stop 488	1
R. R. Nelms, Mail Stop 488	1
M. J. Long, Mail Stop 315	1
F. M. Ballentine, Jr., Mail Stop 334	1
C. S. Gilliland, Mail Stop 334	1
R. W. Lovelady, Mail Stop 477	1
T. E. Walton, Mail Stop 215	1
W. G. Witte, Jr., Mail Stop 215	1
D. V. Maddalon, Mail Stop 163	1
R. D. Wagner, Mail Stop 163	1
W. J. Tuovila, Mail Stop 165	1
W. H. Mayes, Mail Stop 239	1
R. W. Hess, Mail Stop 340	1
J. C. Emery, Mail Stop 164	1
E. L. Morrisette, Mail Stop 164	1
J. R. Sterrett, Mail Stop 164	1
A. Henderson, Jr., Mail Stop 163	1
P. C. Stainback, Mail Stop 161	1
W. V. Feller, Mail Stop 161	1
NASA Ames Research Center Moffett Field, California 94035	
Attention: Library, Stop 202-3	1
NASA Flight Research Center P. O. Box 273 Edwards, California 93523	
Attention: Library	1

DISTRIBUTION (Cont'd)

Addressee	No. of Copies
Jet Propulsion Laboratory 4800 Oak Grove Drive Pasadena, California 91103 Attention: Library, Mail 111-113	1
NASA Manned Spacecraft Center 2101 Webster Seabrook Road Houston, Texas 77058 Attention: Library, Code BM6	1
NASA Marshall Space Flight Center Huntsville, Alabama 35812 Attention: Library	1
NASA Wallops Station Wallops Island, Virginia 23337 Attention: Library	1
NASA Electronics Research Center 575 Technology Square Cambridge, Massachusetts 02139 Attention: Library	1
NASA Lewis Research Center 21000 Brookpark Road Cleveland, Ohio 44135 Attention: Library, Mail Stop 60-3	1
NASA Goddard Space Flight Center Greenbelt, Maryland 20771 Attention: Library	1
NASA John F. Kennedy Space Center Kennedy Space Center, Florida 32899 Attention: Library, Code IS-CAS-42B	1
National Aeronautics and Space Administration Washington, D. C. 20546 Attention: Library, Code USS-10 NASA Code RV	1 1

DISTRIBUTION (Concl'd)

Addressee	No. of Copies
NASA Scientific and Technical Information Facility P.O. Box 33 College Park, Maryland 20740 (+ 1 Reproducible)	22
Bolt, Beranek and Newman	25
Attention: Russell Meyers	1
Research Library - Wilmington	3
Research Library - Lowell	1
Reports Distribution Center	60